

CLOUD PHYSICS organized convection

13 - 23 FEBRUARY 1030-1130

- Monday 13      Structure of cumulus clouds (P R Jonas)  
Drop size and liquid water distribution.  
Updraught structure.  
Turbulence structure and entrainment processes.  
Calculations of development of droplet spectra.  
Homogeneous and inhomogeneous mixing.
- Tuesday 14     Radiation and clouds (R Brown)  
Interaction of clouds with longwave and shortwave radiation.  
Influence of microphysical structure on radiative properties.  
Effects of radiation on individual droplet growth.
- Wednesday 15   Physics of fog (R Brown)  
Processes influencing formation, growth and dissipation of radiation fog.  
The roles of radiation and turbulence.  
Effects of soil heat flux and cloud top radiative cooling.  
Formation of advection fog.
- Thursday 16    Physics of stratiform cloud (S Nicholls)  
Climatology of stratiform cloud.  
Physical properties of stratocumulus.  
Factors influencing cloud structure and evolution.  
Models of stratiform cloud.
- Friday 17      Cloud Physics Instrumentation (S Nicholls)  
Impact of new techniques on observational studies.  
Nucleus counters.  
Microphysical instruments for particle sizing and counting.  
Microphysical instruments for thermodynamic parameters and velocity components.  
Discussions of instrument and sampling problems, frequency response etc.

Monday 20

Cumulonimbus clouds and organised convection  
(D A Bennetts)

Review of parcel theory and CAPE.  
Structure of single cell clouds.  
The development of the downdraught and gust front.  
Multi-celled storms and squall lines.

Tuesday 21

Cumulonimbus clouds and organised convection  
(D A Bennetts)

Supercells.  
Merging clouds.  
The effects of vertical wind shear on precipitation production.  
Efficiency of precipitation production.

Wednesday 22

Electrification and lightning (P R Jonas)

Electrical structure of clouds.  
Requirements of a theory of electrification.  
Charge separation mechanisms.  
The properties of lightning.  
Initiation of lightning.  
Effects of lightning.

Thursday 23

Weather modification (P R Jonas)

Physical basis for precipitation enhancement.  
Warm cloud modification by salt particle seeding.  
Cold cloud seeding for microphysical effects.  
Cold cloud seeding for dynamic effects.  
Dissipation of fog.  
Hail suppression.

Monday 24

Tuesday 25

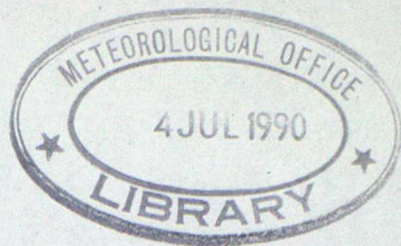
Wednesday 26

Thursday 27

For each of these the structure and possible origins will be described. An indication will be given of the simple models used to gain insight into the basic physics of the processes involved. Finally there will be a description of how more sophisticated models have been used to simulate the detailed structure of the disturbances.

Dr. P. R. Jonas

London



## Radiation and Clouds

by R Brown

### 1. Introduction

The purpose of this lecture is to give an introduction to the ways in which electromagnetic radiation interacts with clouds. The discussion will concentrate on the shortwave and longwave properties of liquid water clouds. There will be little discussion of the mathematical formalism of radiative transfer or the general theory of the interaction of radiation with spherical particles, first published by G Mie in 1908. Instead the results of such calculations will be presented and compared with observations. It is intended to give a general indication of the magnitude and relative importance of the various processes such as absorption and scattering. Some of the consequences of the cloud - radiation interaction will be discussed further in the lectures on the physics of stratiform cloud and fog.

### 2. Basic Definitions

A cloud of droplets can scatter, absorb and emit electromagnetic radiation. All three processes occur in the longwave region whilst in the shortwave region there is negligible emission and only scattering and absorption need be considered. A parallel beam of radiation of initial intensity  $I_0$  will be attenuated to  $I$  after passing a distance  $L$  through such a cloud, according to the equation;

$$I = I_0 \exp \left\{ - \int_0^L \beta_{ed} dl \right\} \quad (1)$$

where  $\beta_e$  is known as the volume extinction coefficient, with units  $\text{length}^{-1}$ . It is convenient to summarize here the definitions of quantities basic to the subject of radiative transfer.  $\int_0^L \beta_{ed} dl$  is known as the

optical depth ( $\mathcal{V}$ ). The optical depth, being dimensionless, is very useful in the theory of radiative transfer allowing the equations to be written in a non-dimensional form. Another quantity used is the transmissivity  $T = e^{-\mathcal{V}}$ . The volume extinction coefficient is composed of the volume absorption and scattering coefficients ( $\beta_a, \beta_s$ ) i.e.

$$\beta_e = \beta_a + \beta_s \quad (2)$$

The relative importance of scattering and absorption is generally expressed in terms of the single scattering albedo ( $\bar{W}_0$ ) which for a population of drops is given by:-

$$\bar{W}_0 = \frac{\beta_s}{\beta_s + \beta_a} \quad (3)$$

i.e. for pure scattering  $\bar{W}_0 = 1$ , for pure absorption  $\bar{W}_0 = 0$ . Finally  $\beta_e$  is related to the drop-size distribution by

$$\beta_e = \pi \int_0^{\infty} n(r) r^2 Q_e(r) dr \quad (4)$$

where  $n(r)$  is the concentration of drops with radii between  $r, r+dr$  and  $Q_e(r)$  is the extinction efficiency factor of a drop of radius  $r$ . Similar expressions can be written for  $\beta_s, \beta_a$  with  $Q_e(r)$  replaced by the scattering efficiency factor  $Q_s(r)$  and the absorption efficiency factor  $Q_a(r)$  respectively. The efficiency factors are dimensionless numbers defined as follows: the energy removed from an incident wave by a drop of radius  $r$  is  $\pi r^2 Q_e(r) I_0$ , the energy which reappears as scattered energy is  $\pi r^2 Q_s(r) I_0$ , the energy absorbed is  $\pi r^2 Q_a(r) I_0$ .

In summary the attenuation of radiation by cloud depends upon  $\beta_e$  which can be calculated from the drop-size distribution and the extinction efficiency factor. The latter is calculated from Mie theory.

### 3. Mie theory

Mie theory provides the general solution to the problem of the interaction of a plane electromagnetic wave with a spherical dielectric of arbitrary size. The solutions are obtained by a straightforward application of Maxwell's equations with the appropriate spherical boundary conditions. For details refer to the books by van de Hulst and Deirmendjian. These constraints provide solutions containing Legendre polynomials and Bessel functions, they are complicated series and will not be reproduced here. In general the solutions depend upon the size parameter  $\chi = \frac{2\pi r}{\lambda}$  and the complex refractive index of the sphere. Since the Mie solution is exact it reduces to other simpler solutions in the limit of small and large  $\chi$ .

$$\begin{array}{ll} r \ll \lambda & \text{Rayleigh scattering (scattered intensity } \propto \frac{r^6}{\lambda^4} \text{ )} \\ r \gg \lambda & \text{Geometrical optics} \end{array}$$

However for cloud droplets  $r \sim 10 \mu\text{m}$ .

Longwave	$\lambda \sim 10 \mu\text{m}$	$\chi \sim 6$	} Require Mie solutions
Shortwave	$\lambda \sim 1 \mu\text{m}$	$\chi \sim 60$	

The number of terms required in the series solutions is generally larger than the numerical value of the size parameter. It is only in the last decade or so that routine Mie theory calculations have become possible, because of the large CPU time required. The very complexity of the solutions can often be a hindrance because it is not possible to identify each term with a recognisable physical effect. Even when presented graphically the solutions contain intricate details which are not assimilated quickly. A good description of the gross overall behaviour of the solutions is contained in the book on Atmospheric Aerosols by Twomey (1977). The problem for the meteorologist interested in radiative transfer is to pick out the important features of the solutions from the irrelevant detail.

Besides giving the amount of radiation scattered by a drop, the Mie solutions also predict the angular distribution of the scattered intensity. Figure 1 illustrates the polar diagrams of the scattered intensity for a single drop as the size parameter is increased from about unity. The polar diagram is initially nearly symmetric, as in Rayleigh scattering, but as  $\chi$  increases a strong forward peak appears, which becomes sharper and more intense and subsidiary maxima appear at other angles. The forward peak is caused mainly by small angle diffraction around the edge of the drop. The small backscatter peak and other features are due to rays which penetrate the sphere and those which creep around the edge as surface waves. If for a given drop size the imaginary part of the refractive index is increased (i.e. more absorption) the forward peak is not greatly affected since the diffracted light has not actually passed through the particle. However the intensity scattered into the backward hemisphere is significantly reduced.

In practice the Mie scattering properties have to be calculated for a drop-size distribution, this results in many of the detailed features being averaged out but the principle features are retained. An example is shown in Figure 2 using a drop-size distribution measured in Sc during the JASIN project. In this figure the relative intensity scattered at angle  $\theta$  (defined in Figure 1) is plotted. This is the more normal presentation because the scattering is symmetric about the direction of  $I_0$ . Clearly the large forward peak and the subsidiary backward peak are retained as important features. For radiative transfer calculations the minimum information required about the angular distribution of the scattered radiation is contained in the asymmetry factor ( $g$ ) defined by:-

$$g = \frac{1}{2} \int_0^\pi P(\theta) \sin \theta \cos \theta \, d\theta \quad (5)$$

This is the average value of the cosine of the scattering angle, weighted by  $P(\theta)$  and approximately indicates the difference between the flux scattered into the forward and backward hemispheres. For isotropic scattering  $g = 0$  and for complete scatter into the forward direction  $g = +1$ .

The specification of  $\beta_e$ ,  $N_0$  and  $g$  for a cloud allow accurate radiative transfer calculations, including multiple scattering, to be performed. The mathematical details will not be pursued further here.

#### 4. Longwave Radiative Properties

Figure 3 shows an example of the variation of  $Q_e(r)$ ,  $Q_s(r)$  and  $Q_a(r)$  with radius, for  $\lambda = 8 \mu\text{m}$ . It can be seen that  $Q_a(r)$  increases with radius and asymptotes to a value of one. This means that the larger cloud drops absorb and emit as black bodies. Since  $Q_s(r) > Q_a(r)$  scattering would appear to be an important process for longwave transfer. However it is possible to ignore scattering in longwave transfer calculations and still compute heating rates with an error of less than 10%, Paltridge and Platt (1976). There are two reasons for this, first much of the radiation is scattered into the forward direction and secondly the drops are strong absorbers in the longwave region and hence only a small fraction of the radiation is backscattered. In fact the reflectivity of clouds for longwave radiation is only a few percent. The increase of  $Q_a(r)$  with radius indicates that the longwave radiative properties of clouds are insensitive to variations in the drop-size distribution. For example as a crude approximation write  $Q_a(r) = cr$  where  $c$  is a constant, then:-

$$\beta_a = \pi C \int_0^{\infty} n(r) r^3 dr$$

But liquid water content  $w = \frac{4}{3} \pi \rho_L \int_0^{\infty} n(r) r^3 dr$

$$\beta_a = \frac{3cw}{4\rho_L} \quad (5)$$

With an appropriate choice of  $C$ , (5) has been found to be a useful approximation in the atmospheric window where most of the radiative cooling takes place, Chylek and Ramaswamy (1982). The insensitivity to drop-size distribution is indicated in Figure 4 where the flux emissivity is plotted

against liquid water path for three different clouds, whose mode radius varied from about 5 to 8  $\mu\text{m}$ . The flux emissivity plotted in Figure 4 is defined by

$$F\downarrow(Z) = [1-\epsilon] F\downarrow(0) + \epsilon \sigma T^4 \quad (7)$$

where  $F\downarrow(0)$ ,  $F\downarrow(Z)$  are the downward fluxes at cloud top and distance  $Z$  beneath cloud top and the cloud is assumed to be isothermal. The plotted points result from the application of a longwave transfer scheme due to Roach and Slingo (1979), using drop-size distributions measured in  $S_C$ . The line represents a parametrization of the results of calculations carried out by Stephens (1979b). Figure 4 indicates that liquid water clouds become black in the longwave region when the liquid water path reaches about  $90 \text{ gm}^{-3}$  (eg a vertical depth of 60m for a cloud LWC of  $0.5 \text{ gm}^{-3}$ ). Finally note that if the mode radius varied over a much greater range, particularly towards larger values, some dependence on drop-size would be found because of the constancy of  $Q_a(r)$  for larger drops.

#### 5. Longwave Flux Profiles and Heating Rates

Figure 5 shows theoretical and observed flux profiles through a sheet of  $S_C$ . The measurements were made from the C-130 of the Meteorological Research Flight during the Joint Air-Sea Interaction Project (JASIN, August 1978) to the NW of Scotland, Slingo et al (1982). The extent of the cloud sheet is shown by the vertical bar. The dashed lines show the theoretical profiles. The main features of interest are:-

(i) The upward longwave flux from the surface ( $L\uparrow$ ) decreases markedly above cloud base as result of the absorption of the 8-13  $\mu\text{m}$  'window' radiation from the surface. Less radiation is re-emitted by the cloud drops because the cloud base temperature is several degrees lower than the surface temperature.

(ii) The downward flux ( $L\downarrow$ ) at cloud top is about  $100 \text{ } \mu\text{m}^{-2}$  less than the upward flux because of the lack of emission in the atmospheric window. However emission from the cloud drops in the atmospheric window causes a rapid increase in  $L\downarrow$  beneath cloud top. Eventually  $L\downarrow = L\uparrow$  as the cloud is optically thick.

(iii) At the surface the net longwave flux ( $L_{\text{net}} = L\uparrow - L\downarrow$ ) is about  $20 \text{ } \mu\text{m}^{-2}$  because of the temperature difference between the surface and cloud base. Above cloud base the net flux falls to zero within the body of the cloud and then within 50m of cloud top rises rapidly to about  $80 \text{ } \mu\text{m}^{-2}$ . The failure of the observed net flux to fall to zero is believed to represent experimental error, since it is a difference of two large fluxes measured by independent upward and downward facing radiometers.

(iv) The radiative heating rate is given by:

$$\frac{\partial T}{\partial t} = -\frac{1}{\rho_a c_p} \frac{\partial F_N}{\partial z} \quad (8)$$

where  $\rho_a$ ,  $c_p$  are the density and thermal capacity of air and  $F_N$  represents the net longwave or shortwave flux. The decrease in  $L_N$  at cloud base represents a warming of about  $1/2^\circ\text{C/hr}$  whilst the large increase at cloud top indicates a local cooling of up to  $8^\circ\text{C/hr}$ . (See also Figure 9). Clearly such cooling at cloud top will rapidly destabilize the atmosphere, leading to the generation of convective motions. This topic will be discussed in more detail in subsequent lectures.

## 6. Effect of longwave loss on Droplet growth

Radiative cooling at cloud top is mainly due to longwave loss from the individual drops. This cools the drops below the ambient air temperature and hence the air cools by molecular conduction to the drops. Without radiative loss the classical theory of droplet growth by diffusion predicts that a growing drop is warmer than its environment because of the release of latent heat. The cooling of a drop by radiative loss can have a

significant effect on its growth rate. Roach (1976) calculated the effect for a clear sky radiation field and produced a modified form of the droplet growth equation:-

$$\frac{dr}{dt} = \frac{1}{A} \left[ \frac{G}{r} - \frac{B}{r^2} + \frac{C_{ln}}{r^4} - D Q_a(r) F \right] \quad (9)$$

where A, B, C, D are constants, G is the supersaturation and  $F = \frac{1}{2} (L\uparrow + L\downarrow) - \sigma T_D^4$ .  $T_D$  is the droplet temperature which is within a few  $\frac{1}{100}^\circ\text{C}$  of the air temperature. (NB if the cloud is radiating as a black body  $F \approx -\frac{1}{2} L_{net}$ ). The radiative term becomes relatively more important with increasing dropsize since  $Q_a(r)$  increases with r then becomes constant, all the other terms decrease with increasing radius.

Equation (9) shows that it is possible for drops to grow in a slightly undersaturated environment if F is sufficiently large. It is also possible for the larger nuclei to be activated in slightly undersaturated air. The exact importance of the radiative loss term is difficult to establish because it depends upon the lifetime of the droplet in the radiatively active region close to cloud top. It is believed to have a significant effect on the growth of fog droplets because the ambient supersaturation is very low (Brown 1990). The long lifetime of some ice crystals falling from Cirrus clouds may also be due to radiative loss. However in this case it is also possible for the crystals to experience a net radiative gain, enhancing evaporation. This can happen if the cloud is very cold so that  $\sigma T_D^4$  is small and also optically thin (or there is no cloud beneath) so that the crystals receive the window radiation from the warmer surface.

## 7. Shortwave Radiative Properties

Figure 6 shows the solar spectrum at the top of the atmosphere and at the ground. The main features of the latter are the absorption by  $O_3$  at wavelengths  $< 0.3 \mu\text{m}$ , depletion by Rayleigh scattering up to  $0.7 \mu\text{m}$  and the marked absorption bands. The feature at  $0.76 \mu\text{m}$  is caused by oxygen absorption whilst the rest are water vapour absorption bands.

Figure 7 shows the single scattering albedo as a function of wavelength (computed for several drop-size distributions). It can be seen that there is negligible droplet absorption ( $\bar{W}_0 = 1$ ) out to  $1 \mu\text{m}$  and that the regions of absorption roughly coincide with the water vapour absorption bands. These two features result in a theoretical maximum absorption of about 20% of the downward flux. Some observational studies eg Reynolds et al (1975) have obtained absorptions well in excess of the 20% theoretical maximum. The presence of absorbing aerosol, observational error and finite cloud geometry have all been invoked to explain this discrepancy. Welch et al (1980) suggest that the excess heating may be caused by a secondary drop population up to precipitation size (ie the clouds may be close to, or actually, raining), which it is known have a much higher absorption optical depth in the visible than smaller drops, for the same liquid water content.

For shortwave radiation and cloud drops the size parameter  $x \gg 1$  and the extinction coefficient approaches a value of 2, independent of radius. Substituting  $Q_e = 2$  in (4) produces

$$\beta_e = \frac{3w}{2r_e \rho_L} \quad (10)$$

where  $\rho_L$  is the density of water and  $r_e$  is known as the equivalent radius

$$r_e = \frac{\int_0^\infty n(r) r^3 dr}{\int_0^\infty n(r) r^2 dr} \quad (11)$$

Equations (10) and (11) show that the shortwave properties of clouds are dependent upon the drop-size distribution and that variations in the latter can be taken into account using one variable,  $r_e$ . Figure 6 also shows  $\beta_e$  as a function of  $\lambda$  for three different drop-size distributions (with different  $r_e$  and  $w$ ). The bars to the left of this diagram indicate the value of  $\beta_e$  from equation (10), this is seen to be a very good approximation.

## 8. Shortwave Flux Profiles

The observed flux profiles through a sheet of Sc obtained during the JASIN project are shown in Figure 8. Also shown are the predictions of the shortwave radiative transfer schemes of Slingo and Schrecker (1982) and Schmets et al (1981). The extent of the cloud layer is marked by a vertical bar. The downward flux  $S_{\downarrow}$  is depleted by scattering and some absorption, most of the radiation reaching the sea is absorbed (sea surface albedo  $\approx 0.05$ ), hence the small upward flux from the surface. The upward flux increases through the cloud since it mainly comprises backscattered radiation from the droplets. For this cloud (LWC max =  $0.7 \text{ gm}^{-3}$ ) the albedo ( $S_{\uparrow}/S_{\downarrow}$  at cloud top) is 65 to 70% whilst about 6% of the incident flux is absorbed.

Figure 9 shows the computed shortwave heating rates for the same cloud sheet, the solid histogram. The maximum heating rate is about  $2^{\circ}\text{C/hr}$ . Also shown is the longwave heating rate and to the right of the diagram the net heating rate resulting from the addition of the shortwave and longwave contributions. It can be seen from the inset figures that the net longwave loss from the cloud sheet is comparable to the shortwave absorption. However the shortwave absorption is more evenly distributed through the cloud so that it only partially offsets the intense longwave cooling at the cloud top.

## 9. Influence of Cloud structure on shortwave properties

Some of the more important papers on the shortwave properties of clouds are those by Lacis and Hansen (1974), Zdankowski and Davis (1974), Twomey (1976), Welch et al (1976), Stephens (1979), Liou and Wittman (1979) and Welch et al (1980). The broadband reflectivity or albedo  $R$ , flux transmissivity  $T_p$  and absorption  $A$  depend in a complex way on a number of parameters but the main results of these studies may be summarised as follows:-

a) As liquid water path increases

$R \uparrow$   
(max  $\simeq$  80%)

$T_F \downarrow$

$A \uparrow$   
(max  $\simeq$  20%)

b) As solar zenith angle increases

$R \uparrow$

$T_F \downarrow$

$A \downarrow$  (complex dependence)

c) As mean drop radius increases at constant liquid water content

$R \downarrow$

$T_F \uparrow$

$A \uparrow$

An example of the latter dependence is shown in Figure 10 from Slingo and Schrecker (1982). The albedo and percentage absorption are computed as a function of  $r_e$  for three model clouds. As  $r_e$  increases the cloud absorbs more and transmits more (reflects less) radiation, the latter indicates more absorption at the underlying surface. Thus the total absorption by the cloud/surface system is quite sensitive to variations in  $r_e$ . Figure 10 also shows the values of cloud absorption when the absorption by the drops is suppressed (excluding the Arctic case). These values are much smaller than the previous ones and show clearly that for such boundary layer clouds it is the drops themselves that are responsible for the bulk of the absorption and not the water vapour. Welch et al (1990) agree with this but Stephens (1978) finds water vapour absorption to be more important. The different conclusions are believed to be due to the different relative amounts of water vapour and liquid in the model clouds. Finally the horizontal bars on the cloud absorption graph indicate the absorption in the cloud layer when no cloud is present (ie just due to the water vapour). The values are seen to be higher than in the case of a cloud with no droplet absorption. This is because a significant fraction of the incident radiation is scattered back to space in the latter case, this more than offsets the increased path length for radiation in the cloud due to multiple scattering.

## 10. Future Research

This presentation has concentrated on the radiative properties of layer clouds composed of water drops. Under such conditions radiative transfer schemes, which assume a horizontally homogeneous atmosphere, have been shown to be in good agreement with observations. In reality clouds are inhomogeneous and measurement programs are now under way, eg at the Meteorological Research Flight, to study the radiation field associated with broken cloud. There is also much interest in the radiative properties of Cirrus clouds because of the possible effect of variations in cloud amount on the earth's radiation budget, Freeman and Liou (1979). This requires computation of the scattering properties of ice crystals. Exact solutions to this problem are not available from Mie theory but a variety of approximate methods have been devised, Schuerman (1980), Mugnai and Wiscombe (1980). In general non-spherical particles scatter more radiation to the side than equi-volumed spheres.

### Figure Legend

- Figure 1. Scattering polar diagrams for  $\lambda = 0.55 \mu\text{m}$  and size parameters  $\chi$  ( $= \frac{2\pi r}{\lambda}$ ) in the range 1 to 17. The direction of the incident radiation  $I_0$  is also indicated.
- Figure 2. Relative intensity (as defined by the phase function  $p(\theta)$ ) vs. scattering angle  $\theta$ , for the drop-size distribution shown on the inset.  $\theta$  is the angle between the incident and scattered radiation as shown on Figure 1.
- Figure 3. Efficiency factors  $Q_e$ ,  $Q_a$ ,  $Q_s$  as a function of  $\chi$  for  $\lambda = 8 \mu\text{m}$ .
- Figure 4. Downward emissivity  $\epsilon$ , defined in the text, as a function of liquid water path. The plotted points refer to calculations for three different Sc sheets using the longwave scheme of Roach and Slingo (1979). The curve represents an approximation derived by Stephens (1978).
- Figure 5. Observed ——— and theoretical - - - - profiles of upward, downward and net longwave flux through a sheet of Sc. The vertical bar indicates the position of the cloud.
- Figure 6. The spectrum of direct solar radiation at the top of the atmosphere (upper curve) and at the ground (lower curve).
- Figure 7. Single scattering properties for three drop-size distributions as a function of wavelength. The bars to the left of the upper diagram indicate the value of  $\beta_0$  assuming  $Q_e = 2$ .
- Figure 8. Upward  $S\uparrow$ , downward  $S\downarrow$  shortwave flux profiles, ——— observed, and the theoretical profiles of Slingo and Schrecker (1982) - - - - and Schmetz et al. (1981) - . - . - .

Figure 9. Theoretical longwave (unshaded), shortwave (shaded) and net heating rates for the Sc sheet observed during JASIN. The extent of the cloud is shown by the vertical bar.

Figure 10. Cloud absorption and albedo for three different atmospheric profiles as a function of equivalent radius. The clear sky absorptions are shown by the horizontal bars. The lower two absorption curves, not joined by a line, represent the case of no droplet absorption, i.e. the cloud droplets just scatter the radiation and the absorption is due to the water vapour.

## References

### General Textbooks

- Deirmendjian D. 1969 Electromagnetic scattering of spherical polydispersions. Elsevier, New York.
- van de Hulst H.C. 1957 Light scattering by small particles. John Wiley & Sons, New York.
- Paltridge G H and Platt C H R 1976 Radiative processes in meteorology and climatology. Developments in atmospheric Science, 5. Elsevier, Amsterdam.
- Twomey S 1977 Atmospheric Aerosols. Developments in atmospheric Science 7. Elsevier, Amsterdam.

### Other References

- Brown R. 1980 A numerical study of radiation fog with an explicit formulation of the microphysics. Quart. J.R. Met. Soc. 106, 781-802.
- Chylek P and Ramaswamy V 1982 Simple approximations for the emissivity of water clouds. J. Atmos. Sci., 39, 171-177.
- Freeman K P and Liou K N 1979 Climatic effects of Cirrus cloud. Advances in Geophys., 21, 231-284.
- Lacis A A and Hansen J E 1974 A parametrization for the absorption of solar radiation in the earth's atmosphere J. Atmos. Sci., 31, 118-133.

- Liou K N and Hittman G D 1979 Parametrization of the radiative properties of clouds. *J. Atmos. Sci.*, 36, 1261-1273.
- Mugnai A and Niscombe H J 1980 Scattering of radiation by moderately non-spherical particles. *J. Atmos. Sci.*, 37, 1291-1307.
- Reynolds D H, 1975 The effect of solar radiation absorption  
von der Haar T H in the tropical troposphere.  
and Cox S K *J Appl. Met.*, 14, 433-444.
- Roach W T 1976 On the effect of radiative exchange on  
the growth by condensation of a cloud or  
fog droplet. *Quart. J. R. Met. Soc.*,  
102, 361-372.
- Roach W T and Slingo A 1979 A high resolution infrared radiative  
transfer scheme to study the interaction  
of radiation and cloud. *Quart J.R. Met.  
Soc.*, 105, 603-614.
- Schmetz J., Raschke E 1981 Solar and thermal radiation in Maritime  
and Fimpel H stratocumulus clouds. *Contrib. Atmos.  
Phys.*, 54, 442-452.
- Schuerman D H (Ed) 1980 Light scattering by irregularly shaped  
particles. Plenum Press, New York,  
334pp.
- Slingo A 1982 On the shortwave radiative properties of  
and Schrecker H H stratiform water clouds. *Quart. J.R.  
Met. Soc.*, 108, 407-426.

- Slingo A, Nicholls S and Schmetz J. 1982 Aircraft observations of marine strato-cumulus during JASIN. *Ibid.*, 103, 833-856.
- Stephens G L 1978 Radiation profiles in extended water clouds.  
I Theory  
II Parametrization Schemes  
*J. Atmos. Sci.*, 95, 2111-2122, 2123-2132.
- Twomey S 1976 Computations of the absorption of solar radiation by clouds. *J. Atmos. Sci.*, 33, 1087-1091.
- Welch R, Geleyn J F, Zdunkowski H G and Korb G. 1976 Radiative transfer of solar radiation in model clouds:  
*Beitr. z. Phys. der. Atmos.*, 49, 128-146.
- Welch R H, Cox S K, and Davis J M 1980 Solar radiation and clouds.  
*Met. Monograph 17, No. 39, Amer. Met. Soc.*
- Zdunkowski H G and Davis C T 1974 Radiative transfer in vertically inhomogeneous layer clouds. *Beit. z. Phys. der. Atmos.* 47, 187-212.

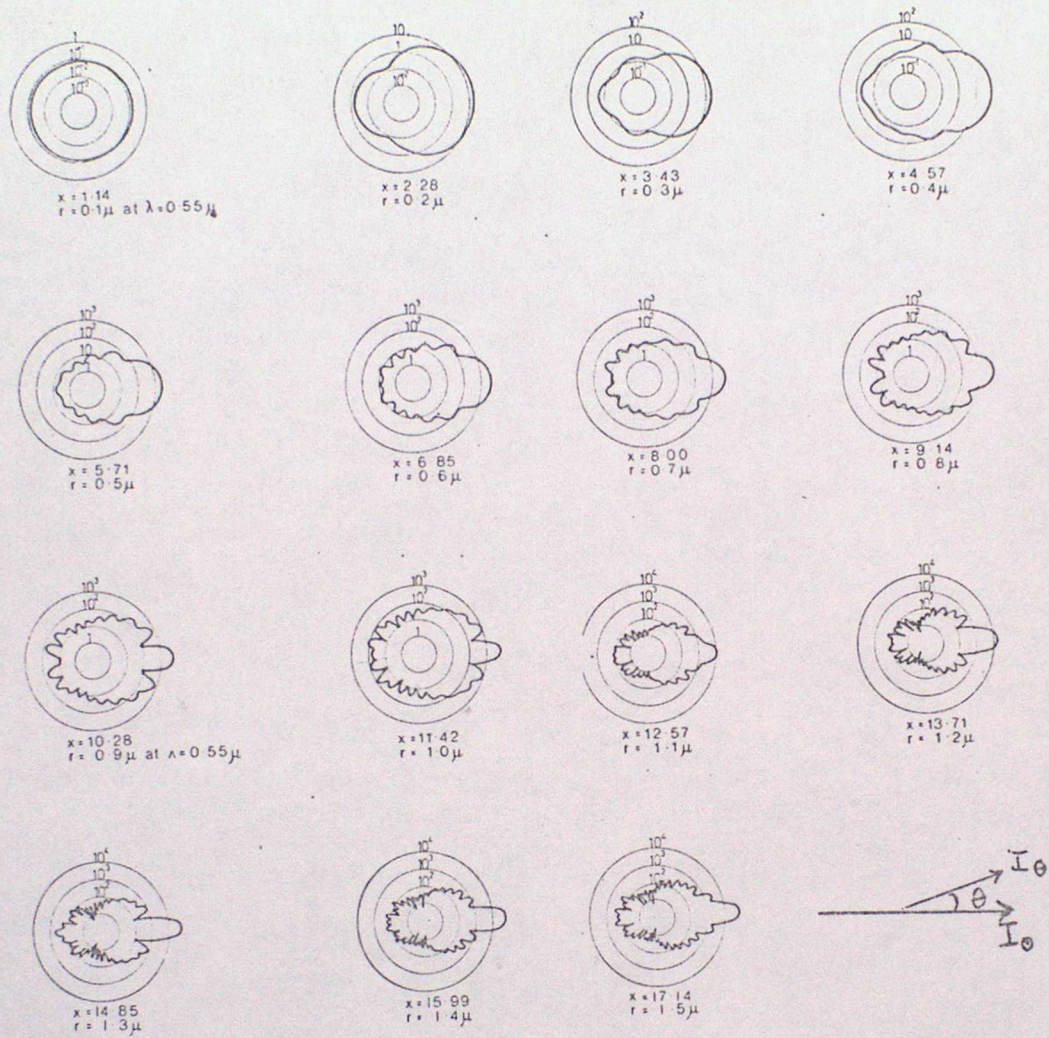


Fig. 1 Scattering polar diagrams. The size parameter  $2\pi r/\lambda$  is indicated on the individual diagrams.

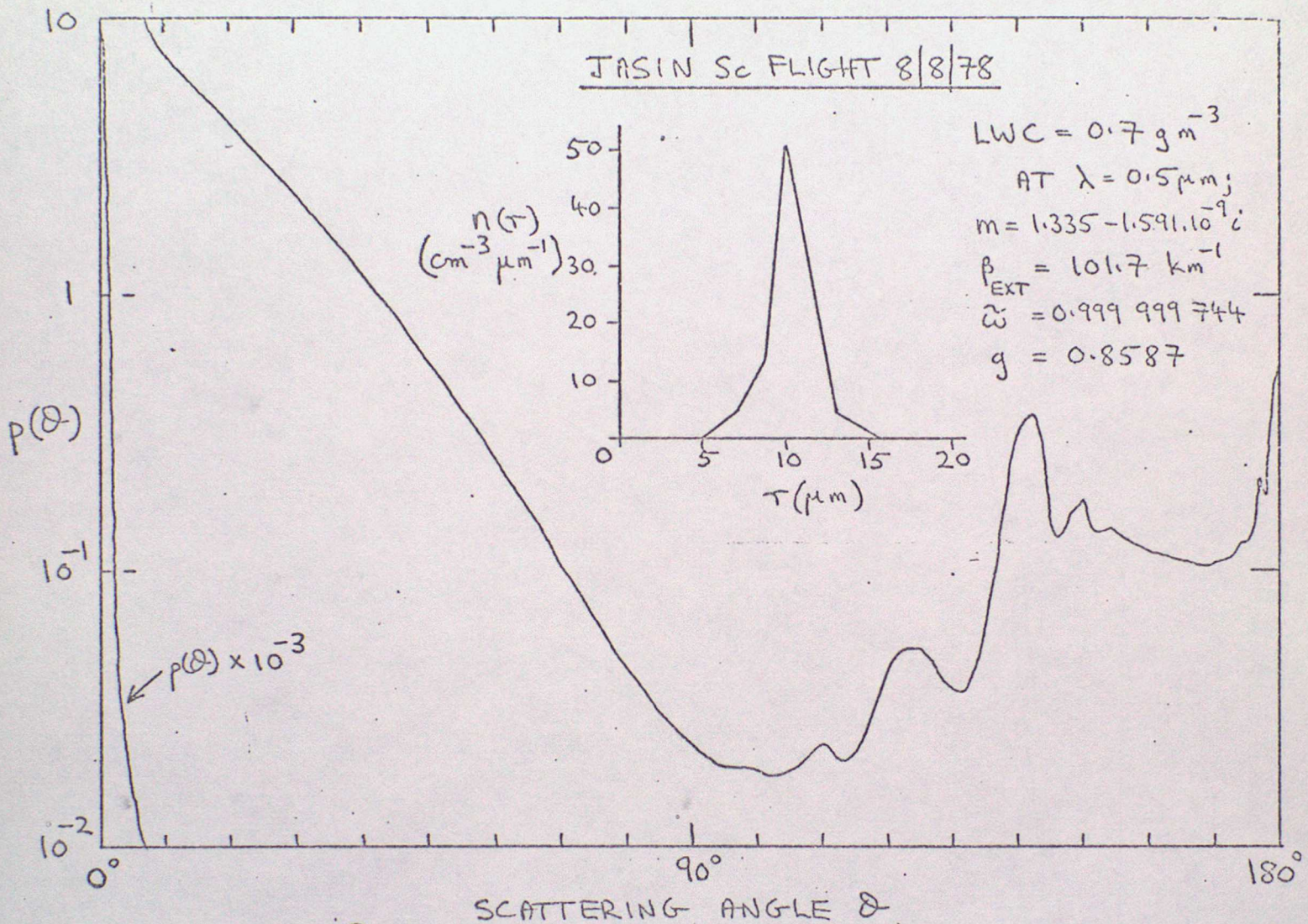
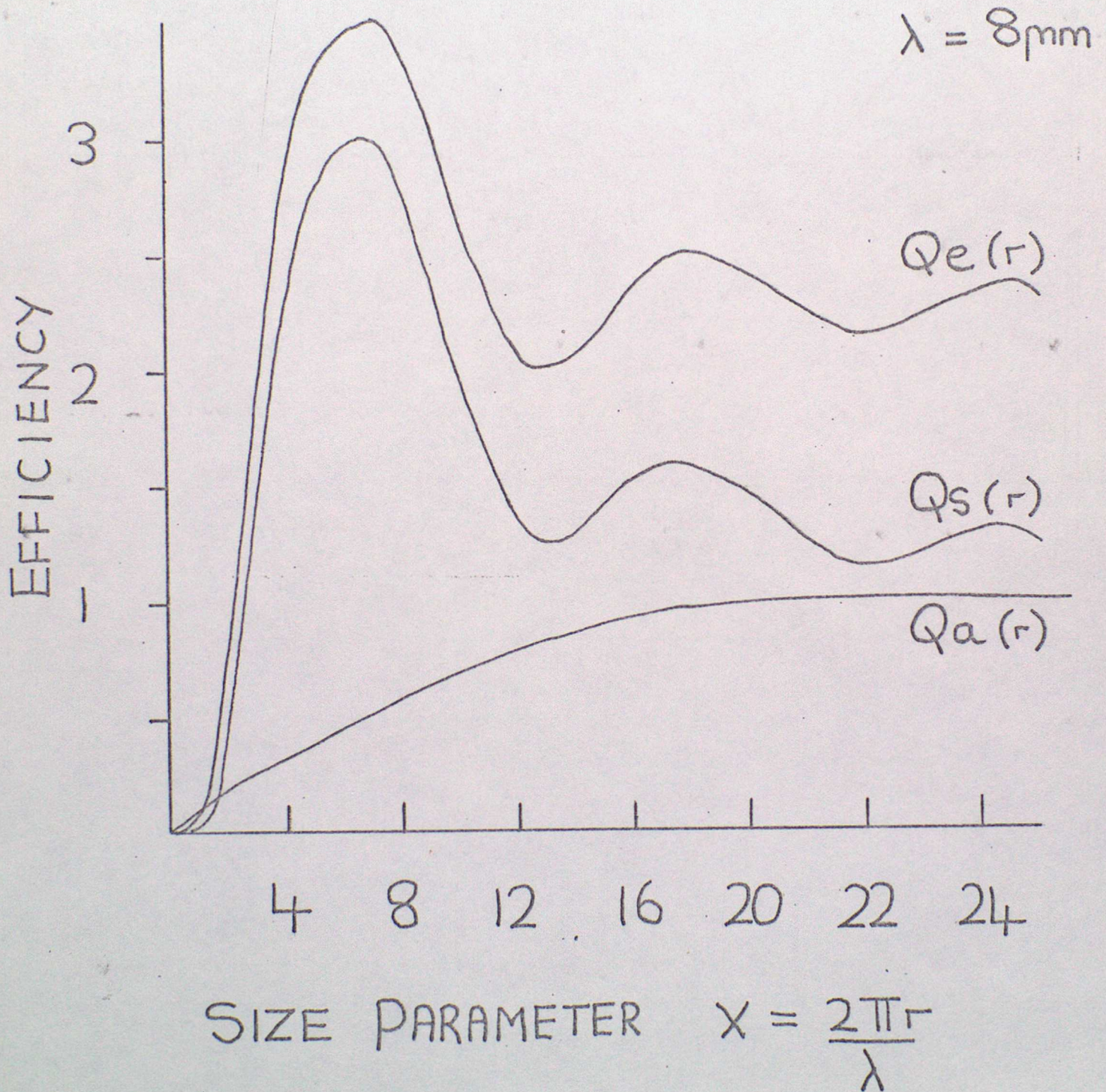


Fig. 2 Phase function for stratocumulus at  $\lambda = 0.5 \mu\text{m}$

FIGURE 3



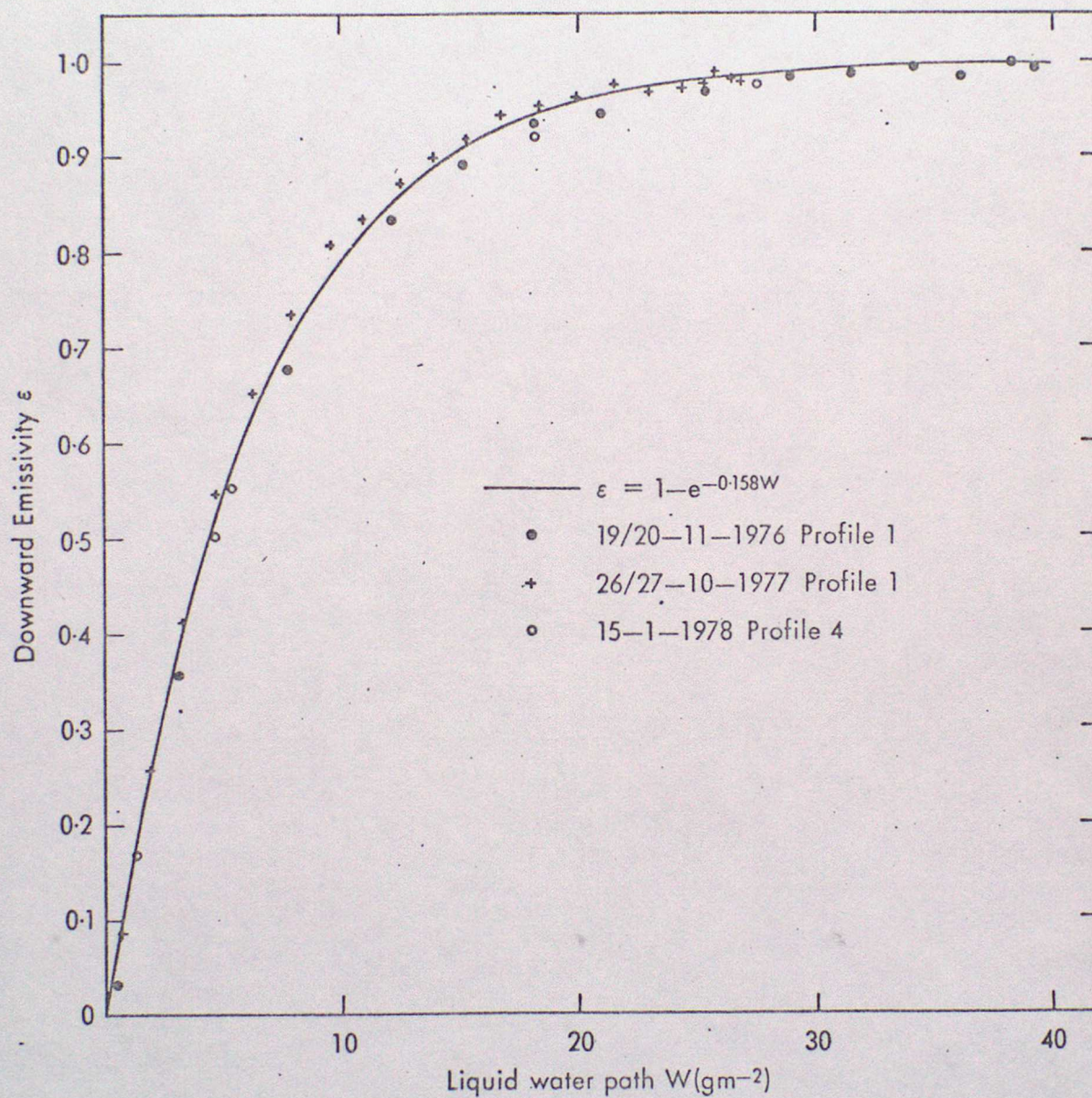


Figure 4

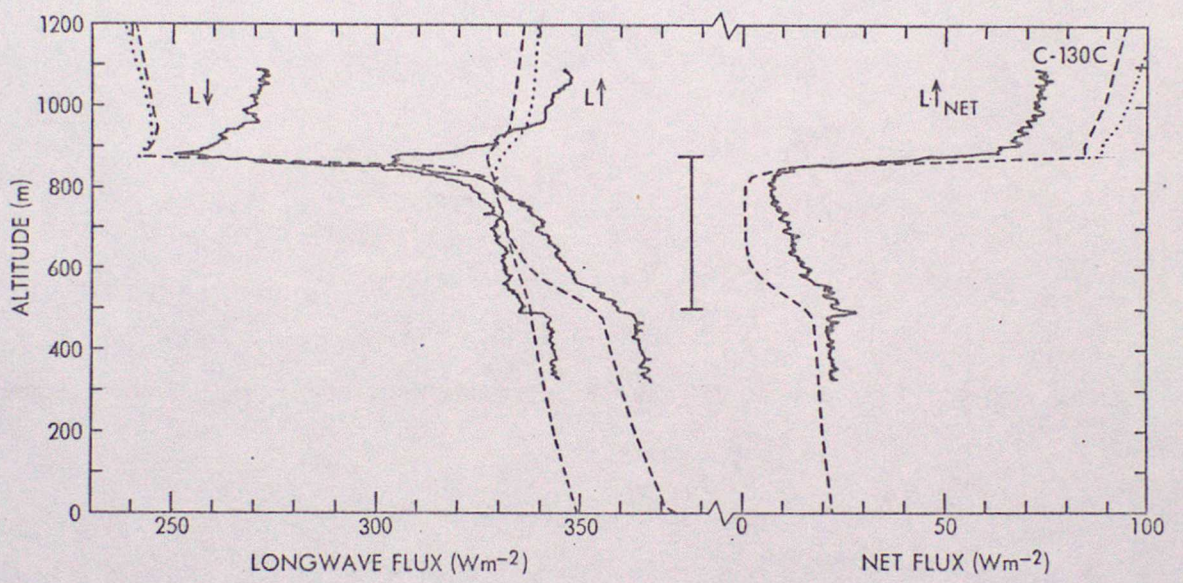


FIGURE 5

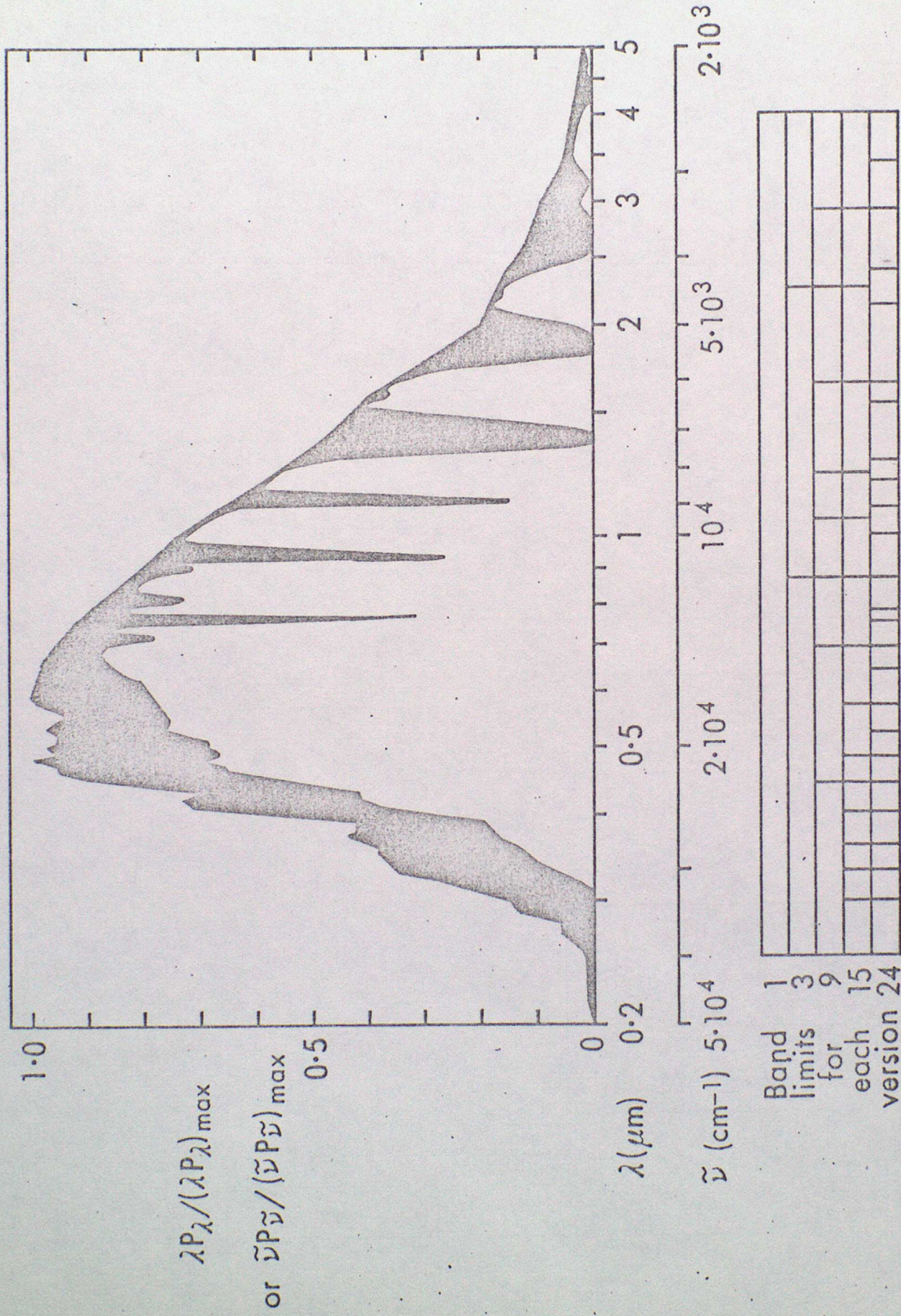
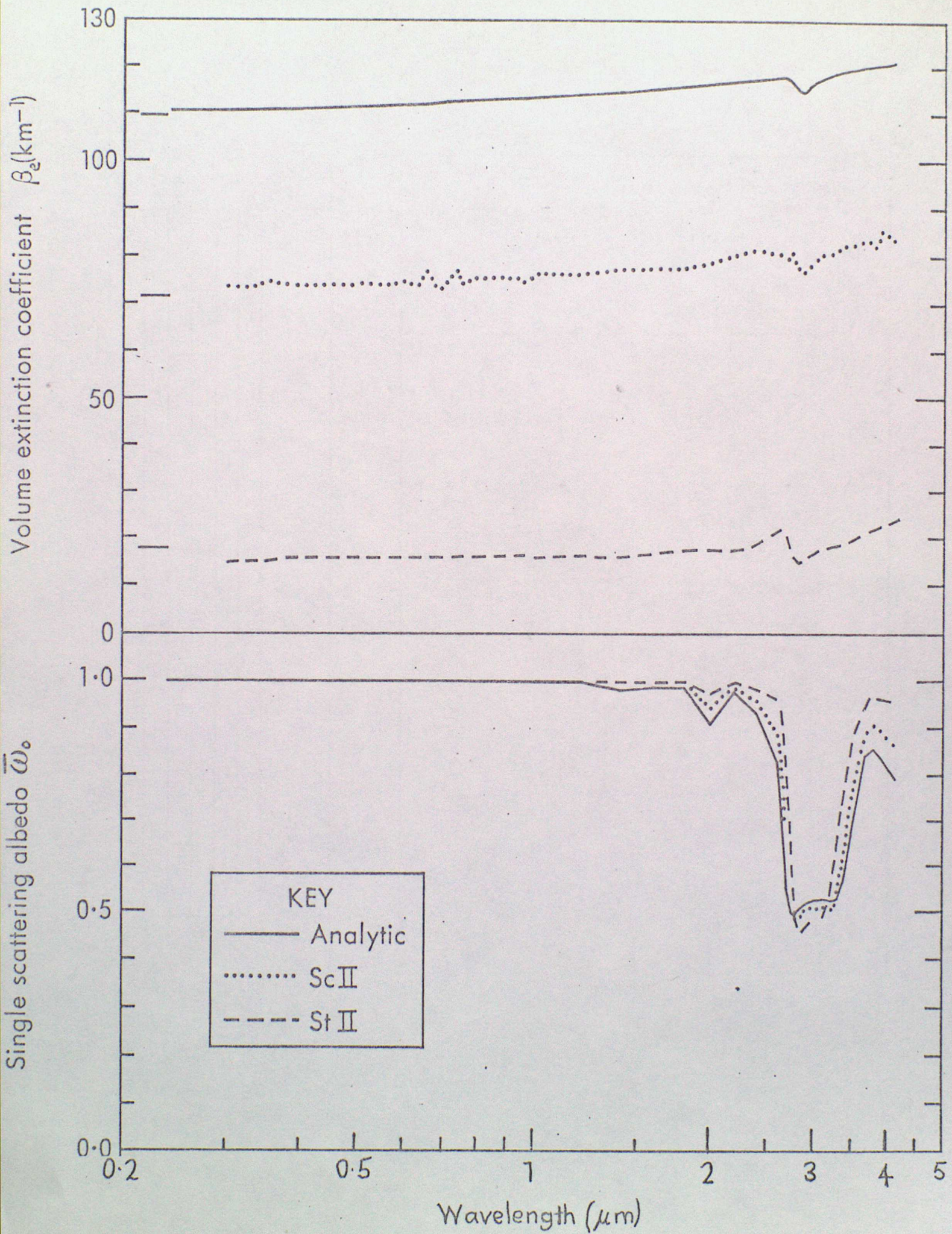


Figure 6

FIGURE 7



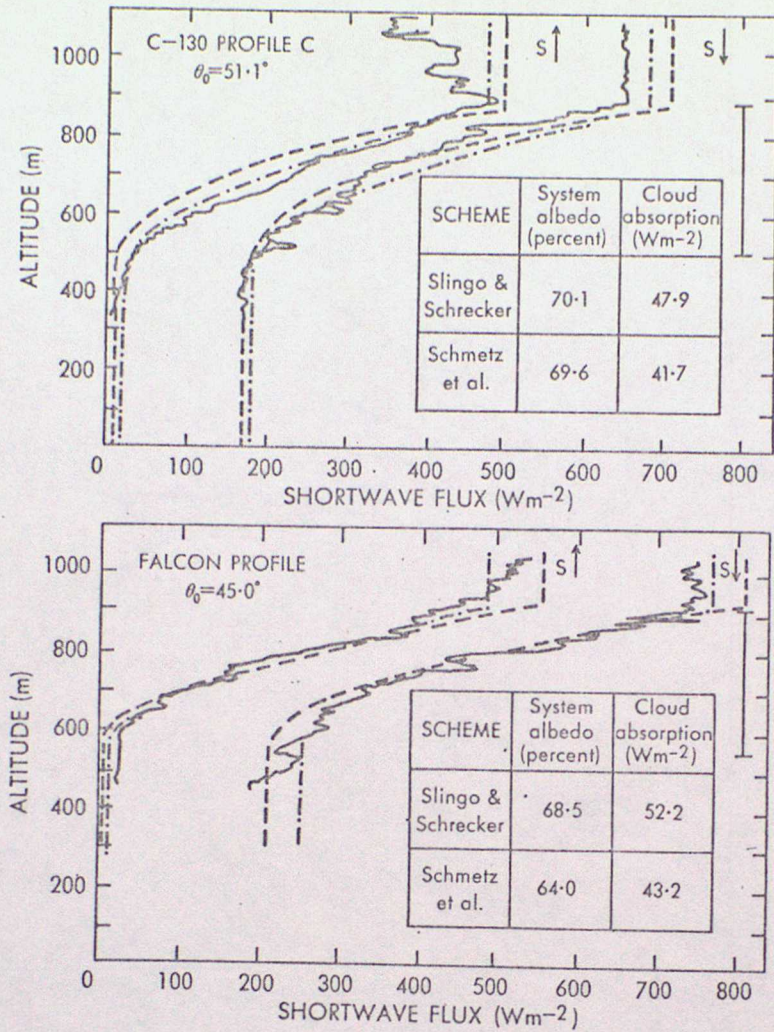


FIGURE 8

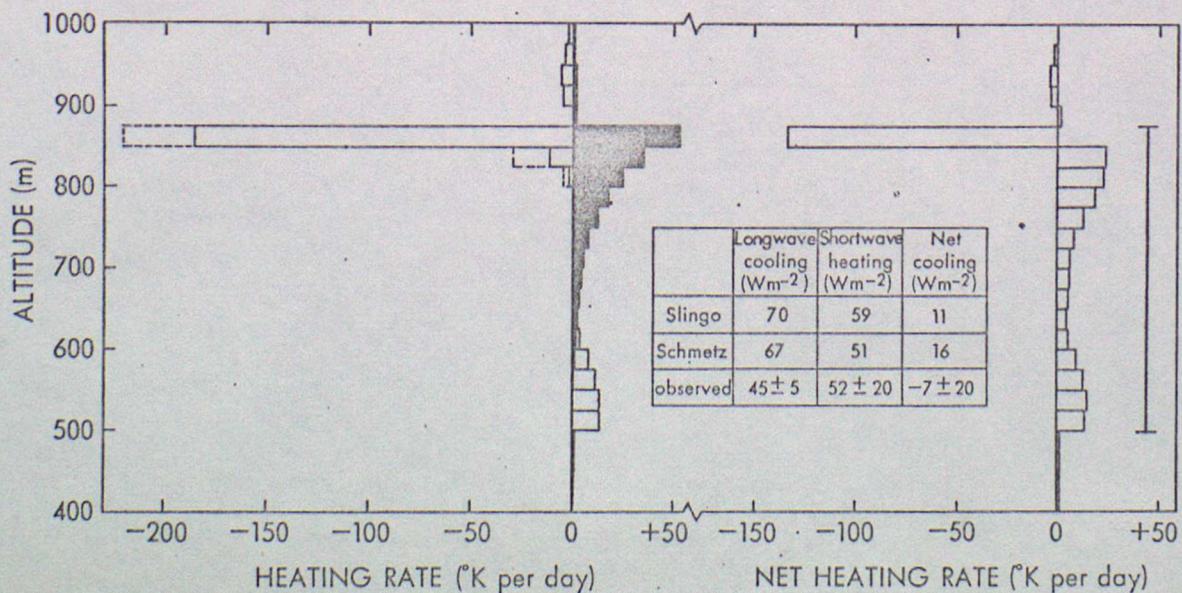
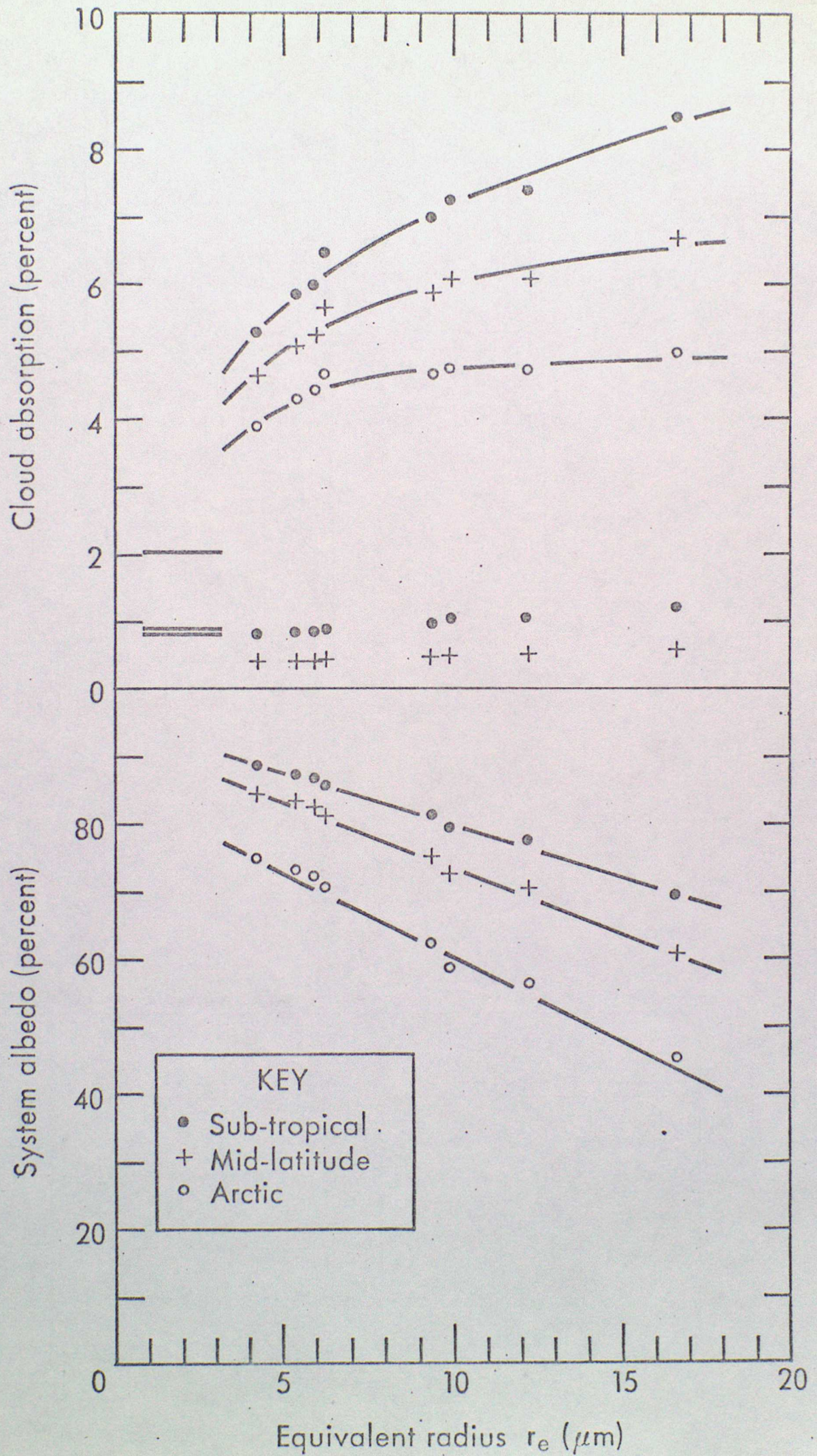


FIGURE 9

FIGURE 10



The Physics of Fog

by

R Brown

1. Introduction

Jiusto (1980) suggests that up to 15 types of fog have been described in the literature. However there are basically three physical mechanisms for the formation of fog:

- i. Cooling of the air to its dew point (by radiative cooling, turbulent diffusion or ascent).
- ii. Addition of water vapour to the air e.g. the evaporation of rain.
- iii. Vertical mixing of moist air parcels at different temperatures.

Radiation fog is generally associated with type (i) mechanism, with radiative cooling providing the driving force, frontal fog with type (ii) and advection fog with type (iii). Radiation fogs typically occur inland whereas advection fogs generally form over open water or coastal locations. In reality the situation is not so clear cut as suggested by these simple classifications. For example there is still some controversy over the relative importance of radiative cooling and turbulent mixing during the formation of radiation fog. Also a variety of mechanisms have been suggested for the formation of fog at sea and some of these will be mentioned briefly later.

Before discussing in detail the physical processes involved in the formation, growth and dissipation of fog, some comments on the definition of fog are required. The standard meteorological definition associates visibilities of less than one Kilometer with fog. However a fog with visibility exceeding 500m will be comprised of unactivated droplets (haze droplets) whose equilibrium size is tied to the ambient relative humidity ( $r < 2\mu\text{m}$ ). Once the visibility falls below 500m there is often a rapid descent into a dense fog (visibility  $\leq 200\text{m}$ ), which indicates that the air has become supersaturated and that some of the haze droplets have been activated and grown into fog droplets (2 - 20 $\mu\text{m}$  radius). In the discussion presented here the term fog will indicate that the visibility is less than a few hundred metres and activated fog droplets are present.

2. Formation of Radiation Fog

The following picture of the formation and growth of radiation fog has emerged from a combination of observations and modelling eg Stewart (1955), Roach et al (1976), Brown and Roach (1976), Lala et al (1975). On a radiation night the ground cools by radiating to space mainly through the atmospheric window, a typical value of the surface net longwave flux being 55-75W m<sup>-2</sup> in the United Kingdom. The surface temperature initially falls rapidly but then more slowly as the radiative loss is partially offset by heat conducted upwards through the soil as a result of the temperature gradient established within the top few centimetres. A typical value for this soil heat flux, measured at a depth of 4 cm is 20 - 30W m<sup>-2</sup>. The turbulent fluxes of sensible and latent heat only make a small contribution to the surface energy balance because of the low level of mixing with light winds and a strong inversion.

As the surface cools the air in the lowest few metres radiates directly to the colder ground. The radiative cooling rate in this region can reach 1 or 2°C hr<sup>-1</sup> compared to a typical value well removed from the surface of 0.1-0.2°C hr<sup>-1</sup>. Once the air at the surface becomes saturated, further cooling leads to dew deposition and hence a drying of the air. Whether fog now forms depends upon a balance between radiative cooling leading to saturation of the air and turbulent

diffusion which although it may be cooling the air is also drying it. Both model results and observations show that radiation fog forms more readily with a low level of turbulent mixing. This is illustrated in Figure 1 by results from a numerical model. At the top are the exchange coefficient profiles associated with the model I-IV temperature and liquid water content profiles presented beneath. Model IV used only molecular diffusion and fog formed earliest in this case. The model results of Brown and Roach and of Lala et al agree that  $K \sim 0.01 \text{ m}^2 \text{ s}^{-1}$  for fog formation on a realistic time scale. The field studies of Roach et al suggested that fog formed when the air was close to saturation and the surface wind fell below  $1 \text{ m s}^{-1}$ . This ties in with the observations of Monteith (1957) that on a radiation night if the  $2 \text{ m}$  wind fell below  $0.5 \text{ m s}^{-1}$  there was an abrupt decrease in the rate of dew deposition. He suggested this was caused by the virtual cessation of turbulent transfer under these conditions. Since radiative cooling of the air will continue, condensation must eventually take place directly into the air.

The above description is based upon work published up to 1976 and since then it has been subject to some criticism. In particular Jiusto and Lala (1983), in discussing the preliminary results from a continuing radiation fog field project at the State University of New York, suggest that it mainly applies early in the night. They believe that as the nocturnal inversion deepens and the relative humidity rises the atmosphere becomes conditioned for fog formation. At this stage, between midnight and sunrise, they suggest that turbulent mixing can intensify fog, although their evidence is not particularly clear. In fact they state:- 'One of the fundamental elusive questions is the exact sequence of events leading to sudden onset of dense fog formation'. Gerber (1981) has developed a saturation hygrometer to measure relative humidities in the range 95 to 105%. From measurements on one night, when shallow fog formed intermittently, he concluded that turbulent mixing of nearly saturated eddies was the cause of fog formation and the broadening of the droplet size distribution. However he made no turbulence or wind measurements and based his conclusion on the fact that the peak supersaturation was higher and the development of the fog more rapid than suggested by the predictions of radiative conductive models. An interesting feature of his observations is that periods of supersaturation are associated not only with a decrease in temperature but with a marked reduction in temperature fluctuations. They are therefore open to the interpretation that a reduction in turbulence was associated with the formation of the fog.

Met 09 are currently involved in making a limited series of measurements in fog at RAE Bedford. They are measuring the wind at  $2 \text{ m}$  with a sensitive Porton-type anemometer, in order to try and establish more firmly the proposed link between wind-lulls and fog formation. Observations from two nights have shown that fog developed during a lull in the  $2 \text{ m}$  windspeed. Furthermore during the wind lull the chart trace showed a marked reduction in the variance of the horizontal windspeed, indicating a reduction in the level of turbulence.

The model of Brown and Roach has been extended to include the 1-D momentum equations with the exchange coefficients made functions of the local Richardson number ( $Ri$ ). Although the model was extended originally in order to better simulate the mature fog, it has been used to examine again the development stage, by comparison with detailed observations made at Cardington. The comparisons indicate that the model windspeed is too high near the surface, leading to an overestimate of the intensity of the surface turbulence and the partial destruction of the large temperature gradients which are a feature of the observations. This in turn reduces the radiative cooling of the air close to the surface and inhibits fog formation there. Eventually fog develops aloft, at  $50$  to  $100 \text{ m}$ , and descends to the surface about an hour later. Jiusto and Lala (1983) have observed fog to form in this manner. If a wind lull is introduced into the model fog develops at the surface on a realistic time scale, but not if radiative cooling of the air is removed. The formation of fog aloft in the model is only delayed by two hours if gaseous radiative cooling is removed, thus it appears to be predominantly a mixing phenomenon.

In summary the current position appears to be that theoretically fog can form at the surface without turbulent mixing. Observations and numerical experiments associate fog formation with wind lulls and a reduction in turbulent mixing but later in the night fog may form without a lessening of mixing.

One problem with the elementary theory whereby mixing of two saturated parcels at different temperatures produces fog is that large temperature differences are required to produce a reasonable fog liquid water content eg  $5^{\circ}\text{C}$  to produce  $0.1 \text{ g m}^{-3}$ . Although such temperature differences are found at the surface it must be remembered that water vapour is not conserved because of dew deposition. The more sophisticated mixing theories eg Rodhe (1962), Oliver et al (1978) do not explicitly consider the mixing of individual parcels but establish expressions for the equilibrium profiles of temperature and humidity mixing ratio, produced by mixing. Fog is predicted to form if the actual mixing ratio decreases less rapidly with height than the saturation mixing ratio. Both references agree that mixing alone cannot produce the observed fog liquid water contents ( $0.1$  to  $0.3 \text{ g m}^{-3}$ ) and that radiative cooling from the droplets must play an important role.

### 3. Development of the Mature Fog

As the fog increases in depth and liquid water content radiative cooling by the fog drops becomes dominant in the upper part of the fog. With the increasing optical depth of the fog the radiative loss from the surface is reduced to a value below that of the soil heat flux and the surface temperature starts to rise. The inversion then lifts from the surface where it is replaced by a superadiabatic lapse rate. This process is illustrated by the model III and IV numerical simulations shown in Figure 1. Both model results and observations show that the inversion starts to lift from the surface when the fog is 20 to 50 m deep.

Figure 2 shows the observed temperature and net longwave flux profile through a deep mature fog. The inversion has lifted to become almost coincident with the fog top, although it is not as sharp as at the top of stratocumulus. The radiative cooling rate calculated from the net flux profile is also shown. This is lower than that observed in stratocumulus because of the lower liquid water content typical of radiation fog. However the cooling at the fog top combined with the warming at the surface produces weak convection and Figure 2 shows a wet adiabatic lapse rate throughout most of the fog.

The original fog model with specified exchange coefficients eventually produced unrealistically large superadiabatic lapse rates throughout the fog. The revised model, in which the exchange coefficients respond to changes in stability, develops a wet adiabatic lapse rate in the mature fog. Observations made in mature fog at Cardington and RAE Bedford using a tethered balloon or minisonde have shown that the temperature can remain constant for many hours, despite the longwave loss from the fog top. About 50% of the longwave loss is offset by latent heat release, the rest must be balanced by weak convection from the surface and entrainment of warmer air from above the fog top. The model fog continues to cool which suggests that the turbulence scheme is underestimating mixing at the fog top.

Besides having a significant effect on the thermal structure of the boundary layer, a mature fog can also modify the windfield. Figure 3a shows a time-height cross-section of the windspeed on a radiation night when fog did not form. The windshear is mainly concentrated at the surface. Figure 3b shows a similar cross-section (on a different night) through a deep fog. The windshear is concentrated through the fog top and appears to move upward with it during the night. Figures 3c and 3d show cross-sections from the extended fog model. These are qualitatively similar to the observed cross-sections and confirm the influence of the fog on the windfield. The weak convective regime within the mature fog is responsible for this

phenomenon. This enhances the transport of momentum to the surface, especially from higher levels, where without fog the turbulence would be decaying after sunset. This leads to the momentum deficit beneath the fog top, especially if the pre-fog inversion has caused the cessation of turbulent transport from levels above the fog top.

#### 4. Dispersal of Radiation Fog

Radiation fog may be dispersed by increasing gradient wind, by the advection of cloud cover and by solar radiation.

Analysis of the Cardington fog project data suggests that increasing gradient wind causes an increase in windshear through the fog top. This enhances the mixing of drier air into the fog and in the limited number of cases analysed led to the dispersal of the fog from the top first.

Saunders (1960) has drawn attention to the effectiveness of the advection of a cloud sheet in dispersing an existing radiation fog. He found that the lower the cloud the more rapid was the fog clearance. The ability of clouds to clear fog also seemed related to the soil-air temperature gradient with large gradients enhancing fog clearance. This latter result was related by Saunders to the role of the soil heat flux in dispersing the fog. The mean dispersal time from all Saunders observations was 2.2 hours.

Figure 4 shows the temperature and liquid water content profiles from a numerical simulation of the clearance of fog by cloud. A cloud sheet more than a few hundred metres thick will have an emissivity approaching unity and so will produce a downward flux in the atmospheric window approximately equal to the black body flux at the cloud base temperature. The cloud has been introduced into the model at time  $t$  by increasing the downward flux in the atmospheric window from above the top boundary of the model. This significantly reduces the net longwave loss from the fog. For example in the model integration illustrated in Figure 4 the radiative cooling near the fog top was reduced from  $5^{\circ}\text{C hr}^{-1}$  to  $0.3^{\circ}\text{C hr}^{-1}$  by the appearance of cloud. However the surface continued to be warmed by the soil heat flux and the upward diffusion of heat from the surface warmed the air and reduced the fog liquid water content. In the example illustrated in Figure 4 the fog has nearly cleared two hours after the appearance of cloud. Note that a net input of heat of  $10 \text{ w m}^{-2}$  into a fog of depth 50 m and liquid water content  $0.2 \text{ g m}^{-3}$  will evaporate it in about 40 minutes.

Solar radiation is generally less effective at dispersing fog than cloud because the fog top net longwave loss continues undiminished. During the United Kingdom fog season direct absorption of solar radiation in the fog will be small compared to the longwave loss. Although accurate calculations have yet to be performed for radiation fog, the direct absorption is unlikely to exceed 2-3%. The maximum downward solar flux in the United Kingdom in early December is  $\sim 300 \text{ w m}^{-2}$ , giving a figure for the direct absorption around  $10 \text{ w m}^{-2}$ , but only several hours after sunrise. Thus the fog can continue to grow upwards after sunrise, driven by the longwave loss. The mode of clearance is by heating of the surface by absorption of the solar radiation and turbulent transport of the heat to the air. This suggests that clearance will commence at the surface and this is often observed to happen.

It is commonly believed that fog thickens around sunrise because of enhanced turbulence. The classical mixing mechanism is generally assumed to be responsible. It is likely that the release of water vapour from the warming surface is an important factor.

## 5. Radiation Fog Microphysics

The pre-fog radiative cooling rates of  $1-2^{\circ}\text{C hr}^{-1}$  are equivalent to very low ascent rates of  $5 \text{ cm s}^{-1}$ . Thus the peak supersaturation in radiation fog is believed to be low  $\sim 0.05 - 0.1\%$  eg Brown (1980), Meyer et al (1980). For a given CCN distribution a lower concentration of nuclei will be activated in fog than in stratocumulus or cumulus.

The visibility in fog is influenced by the CCN concentration and the model results of Brown (1980) have shown that the minimum visibility  $\propto \frac{1}{\sqrt[3]{n}}$

where  $n$  is the CCN concentration. The CCN concentration influences the visibility by its effect on the drop-size distribution. As the CCN concentration is increased a higher concentration of activated drops are formed and competition for the available water reduces the mean drop radius. This is illustrated by the model results shown in Figure 5. The drop-size distributions are shown which result from increasing the basic CCN concentration by a factor of  $2^{\frac{1}{2}}$  and 5. These have a higher drop concentration and lower mean radius. The effect on visibility ( $V$ ) can be demonstrated by a simple calculation assuming a monodisperse drop-size distribution. From Koschmeider's theory

$$V = \frac{3.0}{2\pi N r^2} \quad (1)$$

The liquid water content is given by

$$W = \frac{4}{3}\pi \rho_L N r^3 \quad (2)$$

where  $N$  is the drop concentration and  $\rho_L$  the density of water.

Combining (1) and (2)

$$V = \frac{2\rho_L r}{W} \quad (3)$$

For a given liquid water content reducing  $r$  decreases the visibility.

The microphysical fog model tends to give a mean radius which is larger than that shown by the majority of the observations. This is probably because the model underestimates the mixing at the top of a mature fog since it uses exchange coefficients which are constant in time. This implies that the entrainment of drier air and fresh nuclei at the fog top can lead to a reduction in the mean drop radius.

There does not appear to be a consensus opinion about the variation of liquid water content and drop-size distribution with height in radiation fog. Jiusto (1980) reports observations which show liquid water content decreasing

with height in shallow fogs but increasing with height in deep fogs. The Cardington observations have generally shown no trend or a decrease of liquid water content and mean drop radius with height, even in deep fogs. It is necessary to explain these differences before it can be claimed that the physics of radiation fog is completely understood.

Roach (1976) has shown that the net radiative loss from the drops, besides cooling the drops and hence the air by conduction, also fundamentally alters their growth rate. This led him to modify the classical growth equation by the addition of a term representing radiative exchange with the atmosphere. Whilst all other terms in the growth equation decrease with increasing drop radius, the radiative term increases becoming roughly constant at  $15 \mu\text{m}$  radius. Thus radiative exchange dominates the growth of the larger drops in layer cloud and fog.

The importance of this term has been examined using a fog model containing explicit microphysics. The results are shown in Figure 6 for a low and high nucleus concentration (nucleus spectrum B and E). A significant effect is found using a low nucleus concentration, the drops grow larger and thus are lost from the fog more rapidly by gravitational settling. The radiative term has very little influence with a very high nucleus concentration. This is because the drops only experience a radiative loss over a small distance beneath the fog top due to the large opacity of the fog.

### Sea Fog

Judging by the relative number of publications, sea fog has been a neglected area relative to radiation fog in recent years. Most of the work has originated from the United States and much of this has concerned the formation of fog and low stratus off the coast of California. Sea fog is generally considered to be an advection fog but several other mechanisms have been suggested for its formation and these are mentioned briefly later.

Warm advection fog forms when warm air flows over a colder surface. It generally has a high liquid water content (up to  $1 \text{ g m}^{-3}$ ), can cover large areas and is stable. Barker (1973) has described a detailed study of warm advection fog using a two-dimensional radiative-conductive model. The fog generally formed aloft and descended to the surface downstream. At low geostrophic wind-speeds the cloud descended to the surface almost immediately. He found that gaseous radiative cooling was required to make fog form using his 'normal' geostrophic windspeed of  $4 \text{ ms}^{-1}$ . Radiative cooling from the fog top played an important role in developing the fog, as in radiation fog. The radiative loss from the mature fog was mainly balanced by latent heat release and advection. Heat loss to the sea was small and the model turbulence scheme produced negligible entrainment.

Cold advection fog forms when cold air flows over a warmer sea surface. According to Lee (1975) it has a low liquid water content ( $0.01 \text{ g m}^{-3}$ ), short duration (2-3 hours) and is shallow. He studied its formation using a two-dimensional model, if the sea-air temperature difference was less than  $1^\circ\text{C}$  he obtained a shallow steam fog but when the temperature difference exceeded  $4^\circ\text{C}$  stratus formed. Pilie et al (1979) have summarized the results of seven field expeditions to study the formation of marine fog along the California coast. Fog was often found to be associated with warm water patches. From their observations they have built up the following picture of its formation:-

i. Upwind, warm air flowing over a colder sea surface is cooled and moistened in a layer close to the surface. The stability of the surface-based inversion which develops inhibits the turbulent transfer of moisture to higher levels.

ii. When a warm water patch is encountered the stability of the surface layer is destroyed. The resultant mixing of the newly formed warm surface air with the near saturated cool air produces condensation.

iii. Radiative cooling from the fog top and warming from the surface drives the inversion to the fog top. The air is cooled further enhancing the evaporation from the warm sea surface.

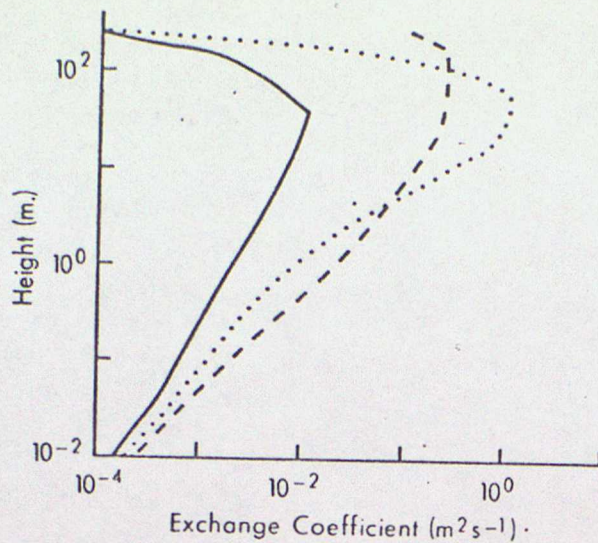
The model of Oliver et al (1978) has been found to realistically simulate this formation process.

Pilie et al also observed fog to form offshore in a region of low-level convergence, produced by the interaction of the windfield with the coastal topography. Although the mean undraught was computed to be  $1-2 \text{ cm s}^{-1}$  they postulate that an organized pattern of stronger updraughts and downdraughts persisted, with a net updraught of  $1 \text{ cm s}^{-1}$ . Fog forms in the updraughts and is prevented from evaporating in the downdraughts by the extra condensation generated by radiative cooling. Fog was also observed to form from the lowering of stratus, especially at night when the longwave cooling is no longer partially offset by solar absorption. This process was also modelled by Oliver et al. who found that the lowering process can only produce fog at the surface if the cloud top inversion is below 350 m, which is in excellent agreement with the observations.

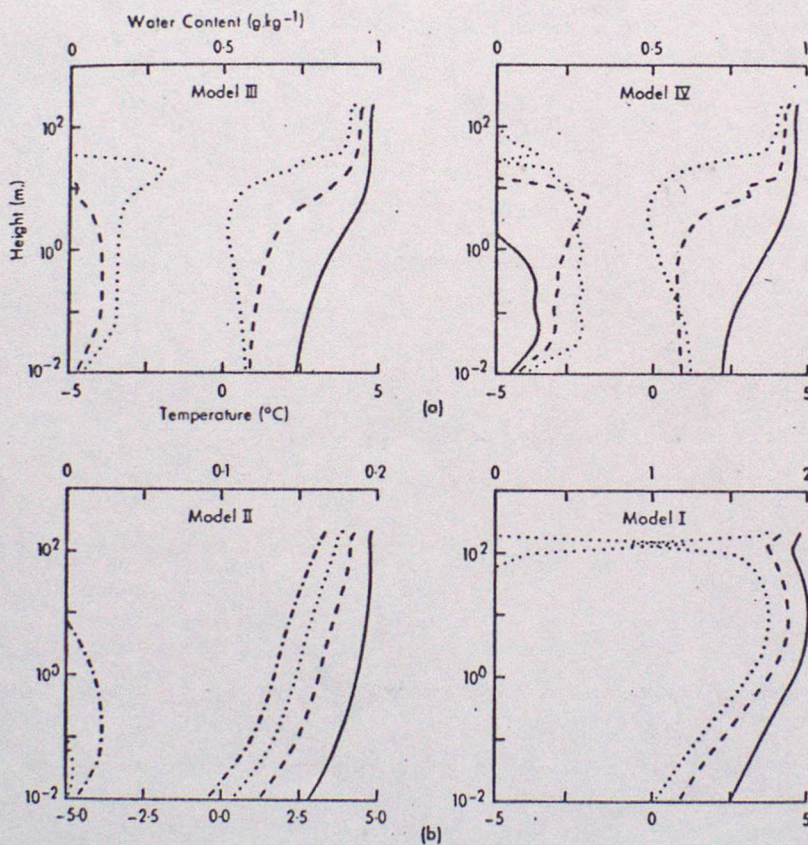
## References

- Barker E H 1973 Oceanic fog - a numerical study. Monterey Cal. Nav. Postgrad. School. Environment Prediction Research Facility, Tech. Pap. 6-73.
- Brown R 1980 A numerical study of radiation fog with an explicit formulation of the microphysics. Quart.J.R.Met.Soc., 106, 781-802.
- Brown R and Roach W T 1976 The physics of radiation fog: II - a numerical study. Ibid., 102, 335-354.
- Gerber H E 1981 Microstructure of a radiation fog. J.Atmos.Sci., 38, 454-458.
- Jiusto J E 1980 Fog structure. Atmos.Sci.Res.Centre, New York Cloud Physics Lab., Pub. No. 745.
- Jiusto J E and Lala G G 1983 Radiation fog field programs - recent studies. Ibid., Pub. No. 869.
- Lala G G, Mandel E and Jiusto J E 1975 A numerical evaluation of radiation fog variables. J.Atm.Sci., 32, 720-728.
- Lee S C 1975 Marine Fog Studies. Univ. Missouri, Tech.Rep. No. N00014-75-C-0180.
- Meyer M B, Jiusto J E and Lala G G 1980 Measurements of visual range and radiation fog (Haze) Microphysics. J.Atm.Sci., 37, 622-629.
- Monteith J L 1957 Dew. Quart.J.R.Met.Soc., 83, 322-341.
- Oliver D A, Lewellen W S, and Williamson G G 1978 The interaction between turbulent and radiative transport in the development of fog and low-level stratus. J.Atm.Sci., 55, 301-316.
- Pilie R J, Mack E J, Rogers C W, Katz U and Kockmond W C 1979 The formation of marine fog and the development of the fog-stratus system along the California coast. J.Appl.Met., 18, 1275-1286.
- Roach W T 1976 On the effect of radiative exchange on the growth by condensation of a cloud or fog droplet. Quart.J.R.Met.Soc., 102, 361-372.
- Roach W T, Brown R, Caughey S J, Garland J A and Readings C J 1976 The physics of radiation fog: I - a field study. Ibid., 102, 313-333.

Saunders W E	1960	The clearance of water fog following the arrival of a cloud sheet during the night. Met.Mag., <u>89</u> , 8-10.
Stewart K H	1955	Radiation fogs: 'Investigations at Cardington 1951-54 Air Ministry Met. Research Committee' MRP 912.



Exchange coefficient regimes ——— Model III; ..... Model I; - - - - Model II; - · - · - Model IV.



(a) Temperature and liquid water profiles obtained from integrations with model III and model IV exchange coefficient regimes. The profiles are presented at three times from the start of the integration: ——— one hour; - - - - three hours; ..... five hours. (b) Temperature and liquid water profiles obtained from integrations with model I and model II exchange coefficient regimes. The profiles are presented at four times from the start of the integration: ——— one hour; - - - - four hours; ..... seven hours; - · - · - ten hours.

FIGURE 1.

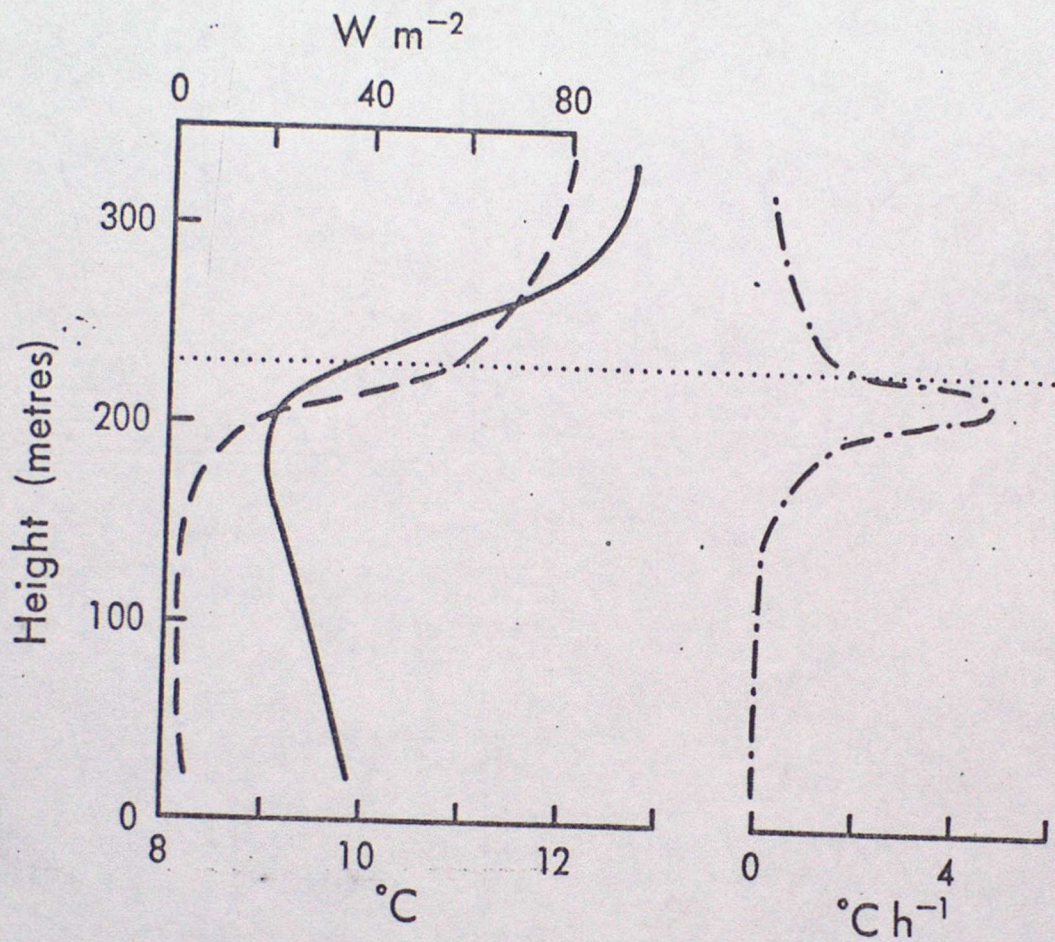
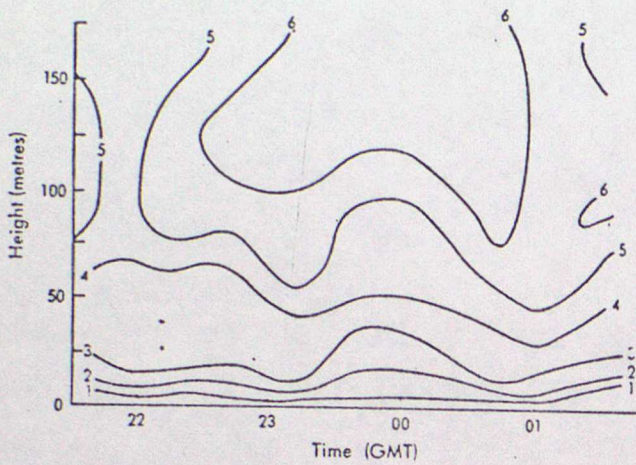
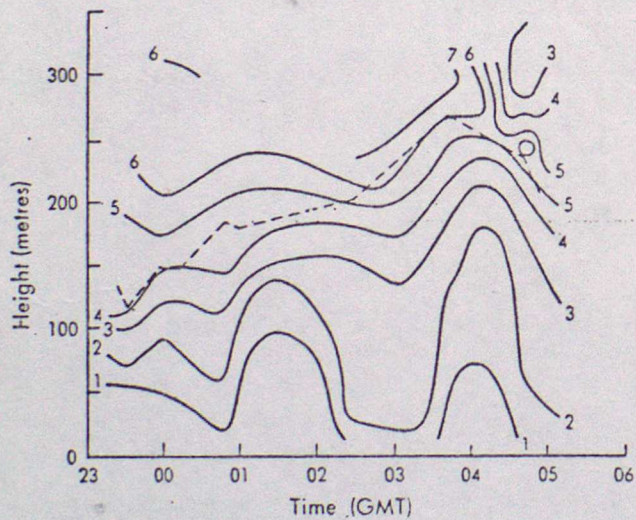


FIGURE 2 Observed profiles of temperature ,  
 net long wave flux   
 and derived radiative cooling rate ,  
 ..... FOG TOP



**Figure 3a** Cross-section of the windspeed ( $\text{ms}^{-1}$ ) on a radiation night with no fog (3/4 November 1976).



**Figure 3b** Cross-section of the windspeed ( $\text{ms}^{-1}$ ) through the deep fog of 17/18 October 1977. --- Fog top.

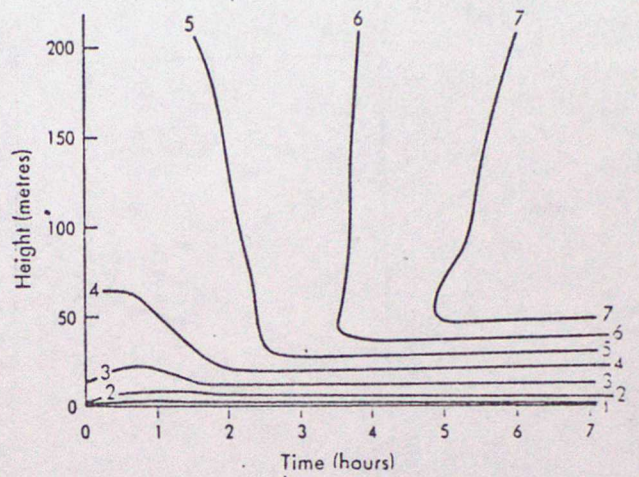


**Figure 3c** Cross-section of the model predicted windspeed ( $\text{ms}^{-1}$ ) on a radiation night with no fog.

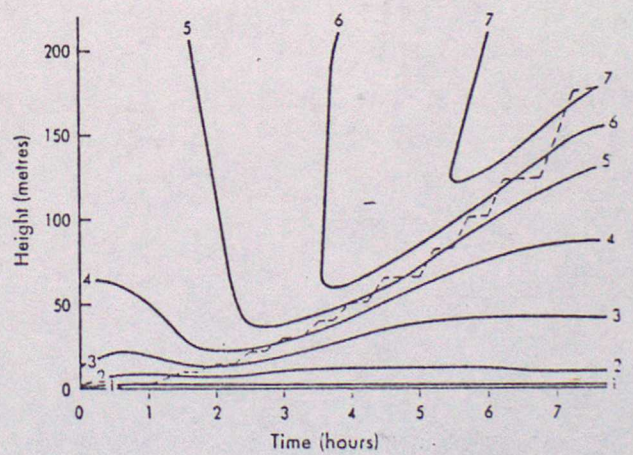
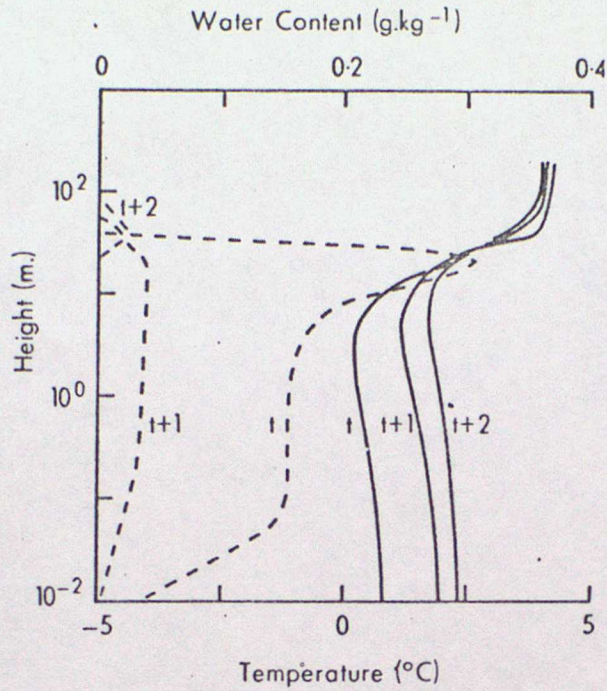


**Figure 3d** Cross-section of the model predicted windspeed ( $\text{ms}^{-1}$ ) through a developing fog. --- Fog top.



Liquid water content and temperature at times  $t + x$  hours where  $t$  is the time of advection of cloud cover: - - - liquid water content; — temperature.

FIGURE 4 Model simulation of the clearance of radiation fog by cloud.

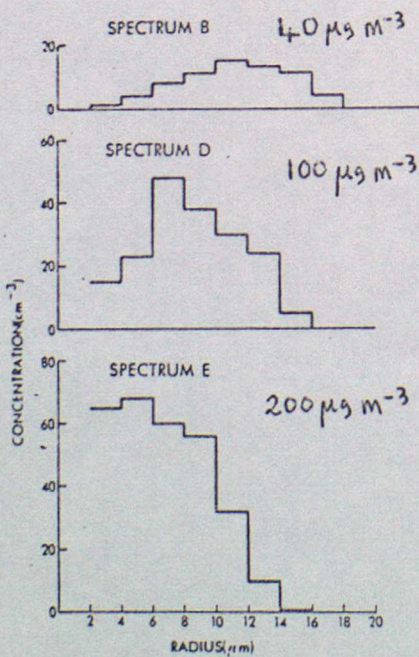


Figure 5. Drop size distribution at 2m after 4 hours integration as a function of nucleus concentration.

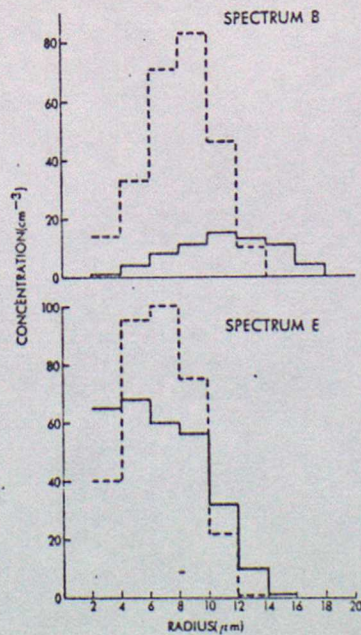
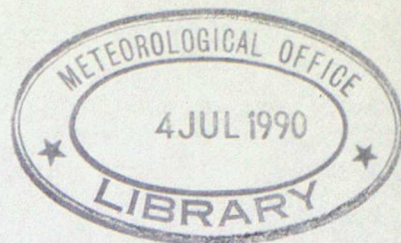


Figure 6. Drop size distribution at 2m after 4 hours integration — with radiative term, - - - without radiative term in eq (1).

# THE PHYSICS OF STRATIFORM CLOUD

by S Nicholls



## 1. INTRODUCTION

Although stratiform cloud is observed at all levels in the troposphere, we will concentrate here in low level layer cloud i.e. Sc and St. The complications of the ice phase will be ignored although many of the concepts may be usefully generalised to deal with As or Cs.

Sc is a very common phenomenon around the UK (see Fig 1), is horizontally extensive (often covering areas greater than  $10^6 \text{ km}^2$ ) and in certain parts of the world is very persistent, especially around the edges of subtropical anticyclones where strong subsidence and cool ocean currents exist (Fig 2). Its importance lies in the changes in the radiation balance which accompany it. This drastically alters the energy transfers within, and therefore the structure of, the boundary layer and the surface energy balance. Forecasts of boundary layer phenomena e.g. fog formation and dispersal, max. and min. temperatures, surface conditions etc. are therefore highly sensitive to the presence of layer cloud. On a different timescale, large semi-permanent areas of low level layer cloud over the oceans may markedly affect the heat input to the oceanic boundary layer with consequences for coupled atmosphere-ocean climate simulations. However, as the important physical processes occurring in such clouds involve interactions between cloud microphysics, radiation and turbulence, they are not well understood and forecasting cloud evolution is particularly uncertain.

## 2. PHYSICAL PROCESSES OCCURRING IN STRATOCUMULUS

### 2.1 General features

In order to simplify the discussion only a single cloud layer will be considered. The formation of stratocumulus is associated with the cooling or moistening of the boundary layer or the spreading out of cumulus beneath an inversion. The general features are best illustrated by examples (Fig 3). Here cloud has formed at the top of a well-mixed boundary layer (one in which conservative quantities, e.g.  $\theta$ ,  $q_t$ : see 3.1 below for definition, are nearly constant with height) underneath a marked inversion and hydrolapse. The mixed layer is turbulent while the air above cloud top is not, due to the strong static stability. The relatively large density difference keeps local perturbations of the interface small so cloud top is quite flat although small amplitude gravity waves can often be observed. The combined effects of turbulence and radiation keep the interface sharp. The local interface between cloudy mixed layer and inversion air (up to several degrees warmer) has been observed to be as little as a few metres thick (Ref 2). In contrast, cloud base is quite diffuse due to inhomogeneities resulting from turbulent motion. In a well mixed boundary layer without entrainment the humidity mixing ratio above cloud base would be constrained to be the saturation value at the local temperature. It would therefore decrease with height at a rate determined by the wet adiabatic lapse rate. The total water content  $q_t$  would be independent of height, since it is a conservative quantity. Therefore the liquid water content  $q_l$  would increase roughly linearly with height at the adiabatic value of about  $1 \text{ g m}^{-3} \text{ Km}^{-1}$ . Observations show that in stratocumulus  $q_l$  does increase roughly linearly with height but at a somewhat

smaller rate (see Fig 3). This is probably caused by entrainment of drier air at cloud top. Windshear within the body of the cloud is generally small unless the cloud is close to the surface but may be large at cloud top and within the inversion layer.

## 2.2 Microphysical structure

The increase in  $q_1$  with height is generally observed to be due to an increase in mean drop size. On any particular occasion there is normally little variation of droplet concentration with height (see Fig 4) although this value may vary considerably between occasions reflecting the different aerosol properties of the mixed layer air. This is consistent with the peak supersaturation being attained near cloud base. The concentration of activated drops is established close to cloud base and the increase of  $q_1$  with height is achieved by condensation on the pre-existing drops. As soon as sufficient numbers of large drops are formed (drops  $> 20 \mu\text{m}$  radius in concentration exceeding  $10^{-4} \text{ cm}^{-3}$  according to Ref 3), a process obviously favoured in thicker clouds, coalescence begins to transfer water into precipitation sized drops ( $> \sim 100 \mu\text{m}$ ). An example is shown in Fig 5. Even though this cloud was only 450 m thick, significant concentrations of drops radii up to  $\sim 100 \mu\text{m}$  were observed within and beneath cloud in drizzle. Note that the concentration of drops  $< 20 \mu\text{m}$  increased downwards through the cloud while the opposite is true for smaller drops, illustrating the size ranges over which condensation and coalescence are dominant. Almost all of the liquid water is contained in the small ( $< 20 \mu\text{m}$ ) drops ( $q_1 \propto nr^3$ ) but the water flux due to gravitational settling (ie, rainfall) is proportional to  $\text{wt.} q_1$  where  $\text{wt}$  is the droplet terminal velocity. Since  $\text{wt} \propto r^2$  ( $r < 50 \mu\text{m}$ ) with a slightly decreasing power of  $r$  at larger radii (Ref 4),  $\text{wt.} q_1 \propto nr^5$ , so is much more sensitive to larger drops. This is shown in Fig 6 which shows the contribution of larger drops ( $> 24 \mu\text{m}$ ) to the rainfall rate increasing downwards, although the much greater concentration of smaller drops near cloud top compensates for their smaller fallspeeds. The water flux within the cloud due to rainfall is therefore approximately constant in this case although decreasing in the unsaturated subcloud layer due to evaporation. This process is less important in clouds with high particle concentrations than in maritime clouds where this water flux may be as large as the turbulent water vapour flux. Evaporation of precipitation beneath the cloud may also have dynamical effects by cooling the subcloud layer.

## 2.3 Cloud radiative properties:

As we are dealing with a situation whose horizontal scales are large compared to the vertical ones, the radiative properties may be discussed in terms of two streams: hemispherically integrated upward and downward fluxes. The detailed radiative properties have been discussed in other lectures, here we are interested in the net heating effects, so only the broadband fluxes will be considered: insolation ( $0.3-3 \mu\text{m}$ ) and long wave fluxes ( $4-40 \mu\text{m}$ ). A typical value for the net longwave radiative loss from the cloud top, is  $60-100 \text{ Wm}^{-2}$ , if there is clear sky above. The resultant divergence of net longwave flux, occurring typically over a few tens of metres beneath cloud top, leads to radiative cooling rates of  $5$  to  $10^\circ\text{C hr}^{-1}$  (Fig 7). Note also that there is a slight warming at cloud base due to

absorption of 8-13  $\mu\text{m}$  window radiation from the warmer surface. The long wave radiative cooling rate is a function of cloud liquid water content but is fairly independent of the drop-size distribution.

It is more difficult to summarise the role of solar radiation because of the variation of the incident intensity with zenith angle (ie time of day, latitude, season). Typical values for the downward flux are  $1000 \text{ Wm}^{-2}$  with sun overhead,  $800 \text{ Wm}^{-2}$  UK June midday,  $400 \text{ Wm}^{-2}$  UK October midday. The albedo of layer cloud (ie percentage of the incident flux which is reflected back to space) is in the range 40-90% whilst 3-15% of the incident flux is absorbed in the cloud. The absorption increases with cloud thickness but reaches a limiting value of about 20% if precipitation is absent. As the zenith angle increases (ie low sun) the albedo increases and the percentage absorption decreases. There is also some dependence on drop size. With increasing drop size the cloud reflects less and absorbs more solar radiation. Note that the depth over which insolation is absorbed is much greater than the depth of strong long wave cooling although the net gain (ie flux divergence across the whole cloud layer) may be about the same. Although this warming is a maximum at cloud top, it is still insufficient to cancel the long wave cooling so that the net flux (Fig 8) still shows marked cooling near cloud top with warming beneath. On this occasion the net flux divergence in the cloud layer is nearly zero, but the distribution of heating and cooling (ie  $\partial R/\partial z$ ) remains a strongly destabilising influence. The magnitude of the solar absorption ( $\sim 70 \text{ Wm}^{-2}$ ) suggests that thick clouds may display significant diurnal changes. This effect is likely to be less important in thin clouds since the net shortwave flux divergence will be disproportionately reduced.

#### 2.4 Turbulence and entrainment

The distribution of radiative heating and cooling would, by itself, promote an unstable density profile, so turbulent motions are generated to compensate. These are observed to take the form of relatively cold, negatively buoyant downdraught descending from the vicinity of cloud top with associated warm compensating updraughts between (Fig 9a). Such motions therefore comprise an upward heat flux balancing the radiative cooling: thus the temperature at cloud top does not decrease at a rate of several degrees per hour. Radiative cooling therefore generates a positive buoyancy flux or a source of turbulent kinetic energy (TKE) near cloud top. The downdraughts penetrate deep into the cloud, losing their buoyancy deficit by a variety of mechanisms in a very similar way to positively buoyant plumes generated in clear boundary layers by a heated surface. The degree of penetration of these elements depends upon the details of the energy balance within the cloud. The vertical velocities are therefore often greatest just below cloud top (Fig 9b). Of course there are other sources of TKE besides that due to radiative effects: surface fluxes, latent heat release and generation by shear may also be important. This may provide a distinction between stratocumulus and stratus: in Sc generation of TKE by buoyancy is important while in St, shear generation dominates. As the two processes generally display different characteristic length scales (Ref 5), this could account for their different appearance.

An important consequence of the cloud being turbulent is that warm, dry air from the inversion is entrained into the cloud. This maintains the very sharp interface at cloud top. This is a difficult process to observe directly since the zone in which significant contrasts between the two fluids

remain before becoming mixed appears to be only a few tens of metres deep. This is of the same order as local cloud top fluctuations unconnected with this process. The entrained air, being warmer than the cloud, represents a downward flux of sensible heat into the cloud. However this is partially offset by the latent heat of evaporation required to saturate the dry entrained air. The predominant effect can be determined from the cloud top step in any variable which is conserved during evaporation eg. wet bulb or equivalent potential temperature ( $\theta_w, \theta_e$ ). Under certain conditions, the evaporative cooling might outweigh the higher temperature of the entrained parcel so that the resultant mixture becomes denser than its surroundings. If the mixture remains saturated, a condition for this occurrence (Refs 6, 7) is that

$$\beta \Delta \theta_e < \theta \Delta q_T \quad (1)$$

where  $\Delta =$  (value above cloud - in cloud) and  $\beta$  is a clearly varying function of temperature (typically 0.5-0.6). Entrainment then acts as a source of TKE (positive buoyancy) rather than a sink and will augment that produced by radiative processes. It has been suggested (Ref 8, 9) that such a situation would be unstable: turbulence promoting entrainment, increasing TKE production, increasing turbulence etc. resulting in the rapid dispersal of the cloud. This is known as entrainment instability and it has been hypothesised (Ref 8) to be the cause the break-up of subtropical Sc into the Cu-form trade wind regime. However, a more careful appraisal of the TKE balance within the cloud is required before such a mechanism is accepted.

Energy is extracted by entrainment in a number of ways:

- i) against the buoyancy of the entrained air,
- ii) to give TKE to the previously quiescent entrained air,
- iii) against viscous dissipation and
- iv) by generation of gravity waves.

This is usually supplied by transport of TKE from beneath, but on other occasions local generation e.g. by shear across the interface may also be important.

As entrainment proceeds, the mixed layer must deepen unless there is subsidence:

$$\frac{dh}{dt} = w + w_e \quad (2)$$

where  $\frac{dh}{dt}$  is the rate of change of height of the mixed layer top,  $w$  is the large scale vertical velocity and  $w_e$  is the 'entrainment velocity'. Thus  $w_e = dh/dt$  in the absence of mean vertical motion or the mixed layer top remains at the same height if the subsidence rate exactly matches  $w_e$ .  $w_e$  is always positive.

With stratocumulus  $w_e \approx 0.5 \text{ cm s}^{-1}$  is typical (Refs 10, 11). (Note this may be up to 30 times larger than the corresponding value for a clear boundary layer with the same surface fluxes. This is due to the additional sources of TKE near the interface). Thus  $w_e \sim w$  and is very difficult to measure experimentally.

## 2.5 Summary

The important processes operating in Sc are illustrated schematically in Fig 10. Note that the flux gradients associated with these processes suggest they alter the cloud on a timescale of a few hours. Advective effects controlled by the synoptic scale flow will therefore be equally important in general in determining cloud evolution, due both to the mean vertical motion and advection over different surfaces changing the boundary fluxes. For this reason alone, instantaneous mean cloud structure is very unlikely to be determined solely by local conditions.

## 3. STRATOCUMULUS MODELS

Modelling cloud topped boundary layers has received much attention in recent years (Ref 9, 12-19) although the two main approaches are extensions of models originally designed for the cloud free case.

### 3.1 Mixed layer or slab models

These are fairly simple in concept although the effects of most of the physical processes listed above can be included. They require little computational effort yet allow the interaction of different processes to be investigated. In the situations to which they are applicable, they produce very similar results to those from the much more complex simulations mentioned in 3.2.

The central assumption of this class of models is that internal mixing is sufficiently thorough that vertical gradients of conserved quantities are negligibly small. Profiles of conserved quantities (which may be defined in a number of ways e.g.  $\theta_w$ ,  $\theta_e$ ,  $\theta_l$ ,  $h$  etc see Refs 12-19) therefore appear as shown in Fig 11. Here we shall consider  $\theta_e$  and  $q_T$  defined to sufficient approximation (in the absence of ice) by

$$\theta_e = \theta + \frac{L}{C_p} q \quad ; \quad q_T = q + q_1 \quad (3)$$

with  $L$  and  $C_p$  assumed constant. The  $q_1$  profile is therefore forced to be adiabatic (eg<sup>p</sup> Fig 3). If horizontal advection may be neglected (e.g. small horizontal gradients or windspeeds) or by following the motion along trajectories, the conservation laws may be written as

$$\frac{dq_T}{dt} = - \frac{\partial}{\partial z} (\overline{w'q'_T}) \quad (4)$$

$$\frac{d\theta_e}{dt} = - \frac{\partial}{\partial z} (\overline{w'\theta'_e}) - \frac{\partial R}{\partial z} \quad (5)$$

where the flux of total water is expanded to include transport by gravitational settling (or rainfall, denoted  $\widetilde{w_T q_1}$  and defined in Fig 6).

$$\overline{w'q'_T} = \overline{w'q'} + \overline{w'q'_1} + \widetilde{w_T q_1} \quad (6)$$

(Note that  $q_T = q + q_1$  remains a good approximation at all levels: the large drops make a large contribution to the water flux but carry a negligible fraction of the total water substance). By assumption the LHS

of eqns. (4) and (5) are constant with height in the mixed layer, so integration across the depth of this layer yields the height variation of  $\overline{w'q'_T}$  and  $\overline{w'\theta'_e}$  given values at the boundaries and  $R$  and  $\overline{w_T q_1}$  as a function of height.

At cloud top, the fluxes are related to the jumps  $\Delta\theta_e$ ,  $\Delta q_T$  occurring at the upper boundary (e.g. Ref 18)

$$-\overline{w'\theta'_e} = w_e \Delta\theta_e \quad ; \quad -\overline{w'q'_T} = w_e \Delta q_T \quad (7)$$

where  $w_e$  is the entrainment velocity. An extra condition is required to compute the other fluxes ( $\overline{w'\theta'_v}$ ,  $\overline{w'q'_1}$ ,  $\overline{w'\theta'_v}$ ,  $\overline{w'q'_1}$  etc) from  $\overline{w'\theta'_e}$  and  $\overline{w'q'_T}$ . This is important because the generation of TKE by buoyancy is proportional to  $\overline{w'\theta'_v}$ .  $\theta_v (= \theta(1 + \epsilon q - q_1))$ , where  $\epsilon = 0.61$ ) is not conserved during phase changes, but  $\overline{w'\theta'_v}$  may be diagnosed if it is assumed that the cloud remains exactly saturated.

With this type of model, the equations must be closed by specifying  $w_e$ . Unfortunately, there is presently no satisfactory way of doing this although several formulations have been proposed based mainly on simplified TKE balance arguments, which is why  $\overline{w'\theta'_v}$  is so important. This is currently an active research area.

Examples of the results which such models can produce are illustrated in Fig 12 which shows the predicted variation of the fluxes with height using initial conditions shown in Fig 3, net radiation flux from Fig 8 and the rainfall rate from Fig 6. These values and that of  $w_e$  (set at  $0.71 \text{ cm s}^{-1}$ ) were obtained from aircraft measurements. The results display characteristics typical of this type of model:

- i) Discontinuities in fluxes of non-conserved variables at cloud base are due to the simplified model geometry. In reality cloud base is distributed across a range of heights and gradients are consequently less severe.
- ii) Double jumps at cloud top in fluxes of variables explicitly dependent on  $R$ . The upper part of the jump represents entrainment fluxes (assumed to take place within cloud), the lower part reflects the strong radiative cooling.

The buoyancy flux maximum just below cloud top is largely controlled by the combined effects of radiative cooling (promoting a positive  $\overline{w'\theta'_v}$ ) and entrainment (promoting negative  $\overline{w'\theta'_v}$  in this case, although if eqn (1) were satisfied, this would be reversed). In the absence of other TKE sources, buoyancy drives the mixed layer from the top and the bottom. Note that cloud top fluxes are as large or larger than those at the surface and must therefore be modelled carefully.

These models generally suggest that processes tending to cool and moisten the mixed layer e.g. radiative cooling, surface evaporation, small entrainment fluxes, are associated with thickening cloud while absorption of insolation, large surface heat and entrainment fluxes tend to have the opposite effect. But since, say, increased radiative cooling tends to promote greater entrainment, the balance of these processes in particular situations is not at all obvious. However, the models show a strong sensitivity to the radiative fluxes so strong diurnal effects might be anticipated.

The predicted cloud evolution due to the fluxes shown in Fig 12 is shown in Fig 13. Over the  $1\frac{1}{2}$  period the fluxes only change a little, their effect being to warm and dry the mixed layer, so the cloud thins from the

bottom as the rate of change of the lifting condensation level exceeds the entrainment rate.

The main limitation of these models is the well-mixed assumption. Elevated, detached cloud layers cannot be successfully handled and it is not always clear that turbulent mixing will maintain well-mixed profiles. For example Fig 12 shows large negative buoyancy fluxes below cloud base. Can these be maintained? Also, the methods used to specify  $w_e$  remain controversial.

### 3.2 Higher Order Closure Models

These have included 1-D models which use prognostic equations for higher order turbulence statistics with a closure supplied at some level (Ref 16, 20) and 3-D large eddy simulations (Ref 9 ) which use a very small grid spacing (e.g. 50m) and explicitly calculate motions down to these scales so that the parametrization of sub-grid scale motions can then be placed on a surer base. However, with the extremely strong stability and consequently very small length scales at cloud top, it is not clear that even these models can resolve the motions sufficiently well.

These models have the advantage of considerable flexibility gained at the expense of considerable complexity and computational requirements. The TKE balance is usually properly accounted for and non-well-mixed layers can be simulated. Although the turbulence schemes are quite sophisticated radiation and cloud microphysics are often treated inadequately or not at all. Despite these shortcomings, these models have provided a number of useful insights. In conditions where mixed layer models are applicable, the results are often very similar although an additional wealth of information concerning detailed turbulence structure is also produced. Results pertaining to more complex situations may be found in Refs 9, 16, 20.

### 4. REFERENCES

- 1 Davies, H E 1972 Frequency of occurrence of different types of cloud in the British Isles. I.D.M No 107 London Met Office 31pp.
- 2 Caughey, S J, 1982  
B A Crease &  
W T Roach A field study of nocturnal stratocumulus: II. Turbulence structure and entrainment. Quart.J.R.Met.Soc., 108, 125-144.
- 3 Jonas P R 1974  
& Mason B J The evolution of droplet spectra by condensation and coalescence in cumulus clouds. Quart. J.R.Met.Soc., 100, 286-295.
- 4 Beard, KV 1976 Terminal velocity and shape of cloud and precipitation drops aloft. J.Atmos.Sci. 33, 851-864.
- 5 Nicholls, S 1981  
& Readings C J Spectral characteristics of surface layer turbulence over the sea. Quart.J.R.Met.Soc., 107, 591-614.

- 6 Randall, D A 1980b Conditional instability of the first kind upside down. J.Atmos.Sci., 37, 125-130.
- 7 Deardorff, J W 1980b Cloud top entrainment instability. J.Atmos.Sci., 37, 131-147.
- 8 Randall, D A 1980a Entrainment into a stratocumulus layer with distributed radiative cooling. J.Atmos.Sci., 37, 148-159.
- 9 Deardorff, J W 1980a Stratocumulus-capped mixed layers derived from a three-dimensional model. Boundary Layer Met., 18, 495-521.
- 10 Nicholls, S 1984 The dynamics of stratocumulus: aircraft observations and comparisons with a mixed layer model. Submitted to Quart.J.R. Met.Soc.
- 11 Roach, W T, 1982  
R Brown,  
B A Crease  
& Slingo A. A field study of nocturnal stratocumulus I. Mean structure and budgets. Quart.J.R.Met.Soc., 105, 603-614.
- 12 Stage, S A & 1981  
Businger JA A model for entrainment into a cloud-topped marine boundary layer. Part I: Model description and application to a cold-air outbreak episode. J.Atmos.Sci., 38, 2213-2229.
- 13 Schubert, W H 1979  
Wakefield J S  
Steiner, EJ &  
Cox S K Marine stratocumulus convection. Part I and II. J.atmos.Sci., 36, 1286-1324
- 14 Schubert, W H 1976 Experiments with Lilly's cloud topped mixed layer model. J.Atmos.Sci., 33, 436-446.
- 15 Schaller E & 1981  
Kraus H. The role of radiation in an inversion capped planetary boundary layer. Part I and II. Boundary Layer Meteor, 20, 485-513.
- 16 Oliver, D A 1978  
Lewellen W S  
G G Williamson The interaction between turbulent and radiative transport in the development of fog and low level stratus. J.Atmos.Sci. 35, 301-316
- 17 Fravalo C, 1981  
Y Fouquart &  
R Rosset The sensitivity of a model of low stratiform clouds to radiation. J.Atmos.Sci., 38, 1049-1062.
- 18 Lilly, D K 1968 Model of cloud topped mixed layers under a strong inversion. Quart.J.R.Met.Soc., 94, 622-634.
- 19 Deardorff J W 1976 On the entrainment rate of a stratocumulus topped mixed layer. Quart.J.R.Met.Soc., 102, 563-582.
- 20 Chen, C and 1983  
Cotton, W R A one dimensional simulation of the stratocumulus-capped mixed layer. Boundary Layer Meteorol., 25, 289-321.

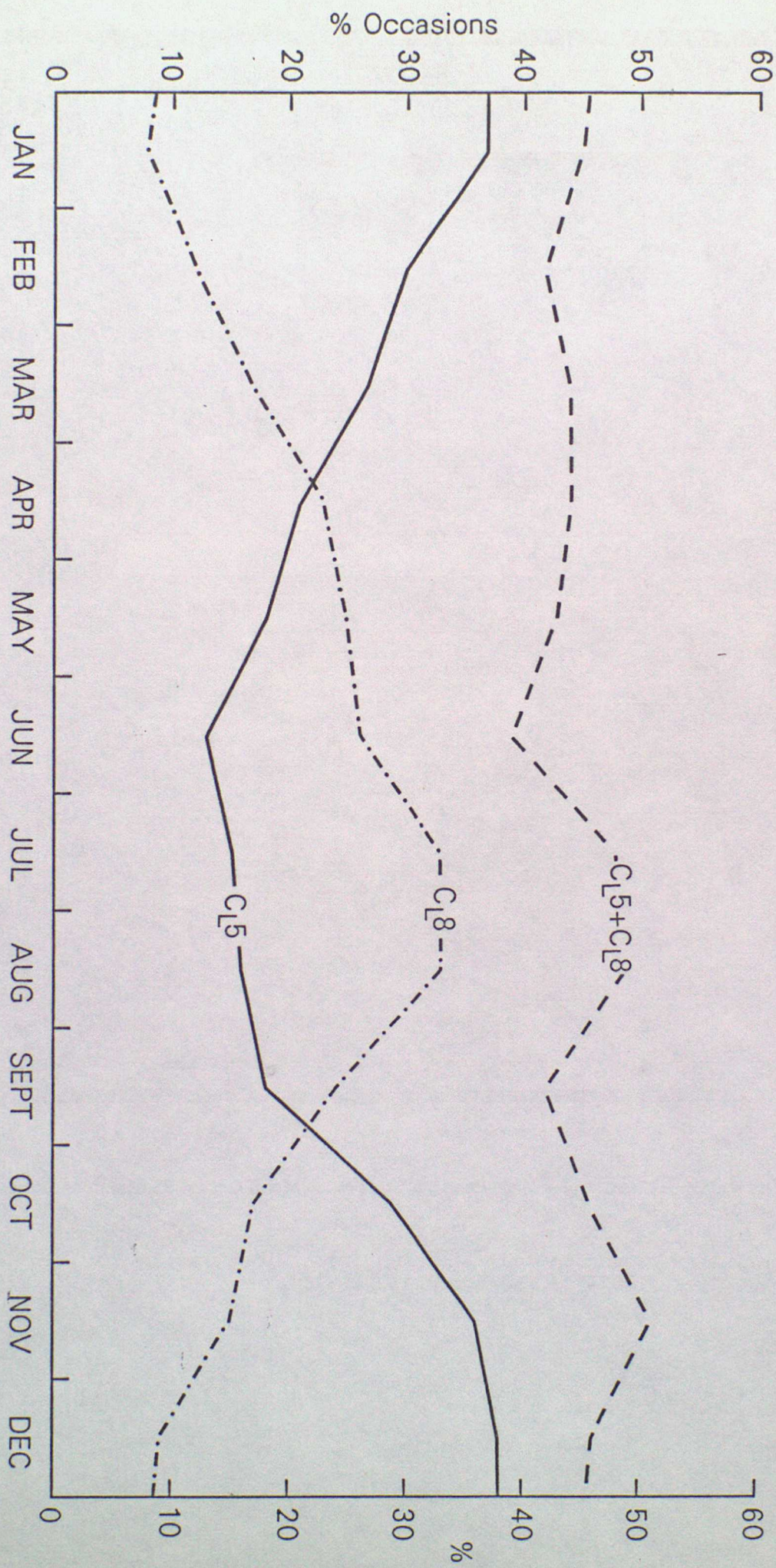


Fig 1 Frequency of occurrence of low cloud types  $C_{L5}$  (stratocumulus) and  $C_{L8}$  (cumulus rising into stratocumulus) in daytime observations at a typical UK station. Data are monthly averages taken from Ref1.

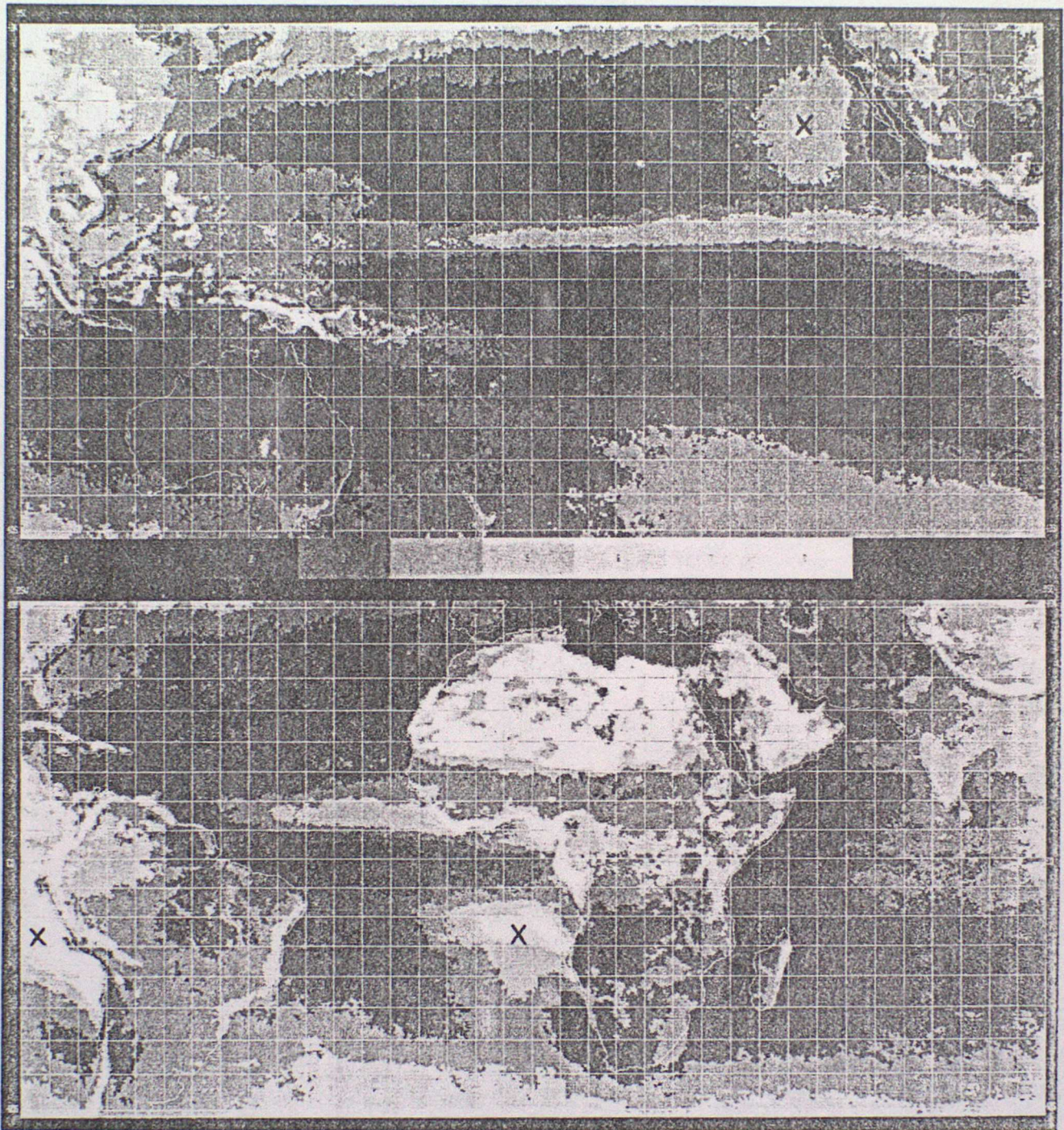


Fig 2

Mercator Satellite Relative Cloud Cover, 1400 Local, 40° N to 40° S, Mean Octas, Semiannual, June through November 1967-1970.

Areas of stratiform cloud denoted X. Taken from 'Global Atlas of Relative Cloud Cover 1967-70', NOAA and AWS (1971).

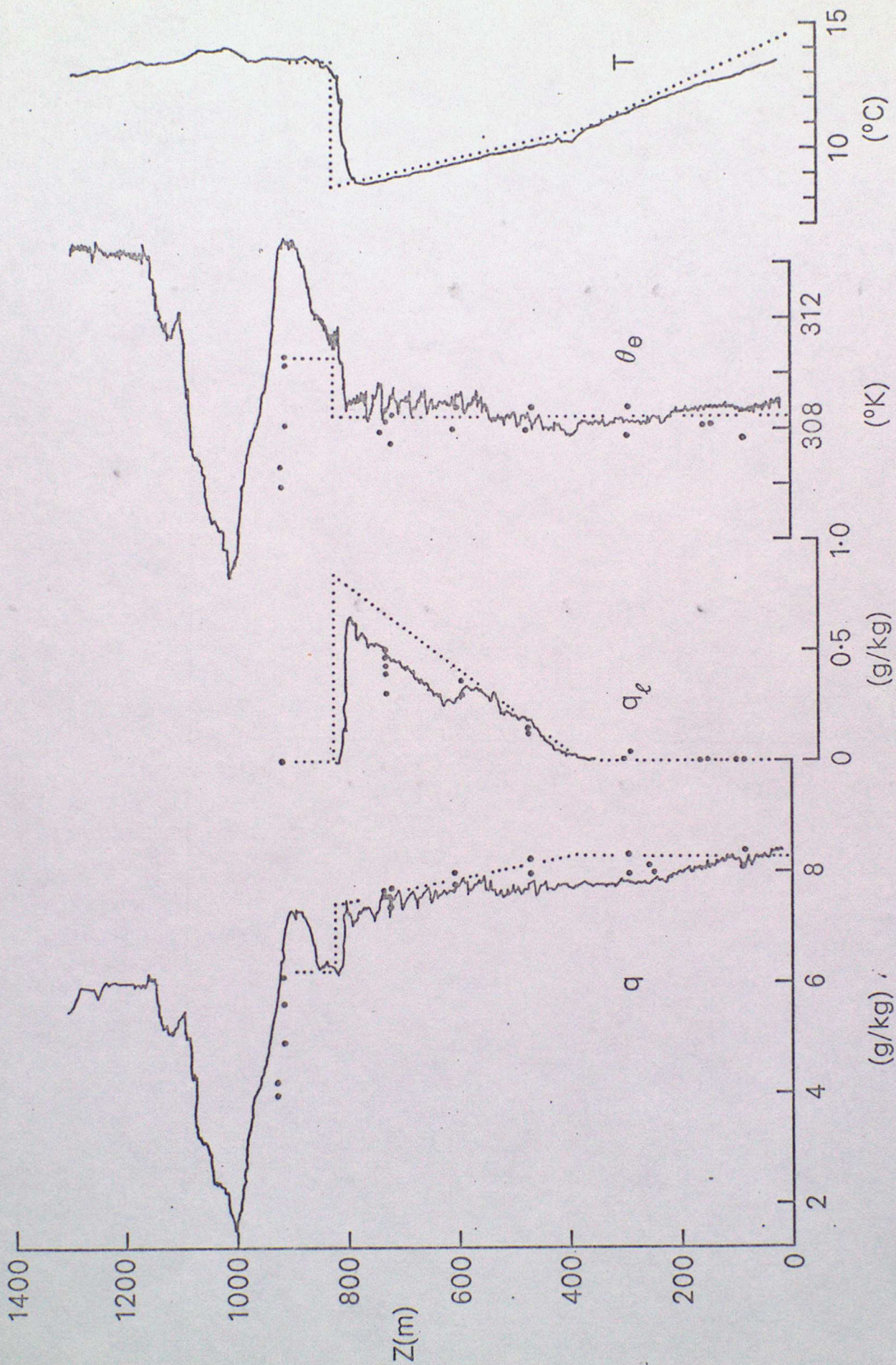


Fig 3 Vertical structure measured by the MRF C130 on a slow descent at 1100 GMT on 22 July 1982 (solid lines) together with horizontal run averages ( $\bullet$ ) and the representation used in a mixed layer model (dotted).

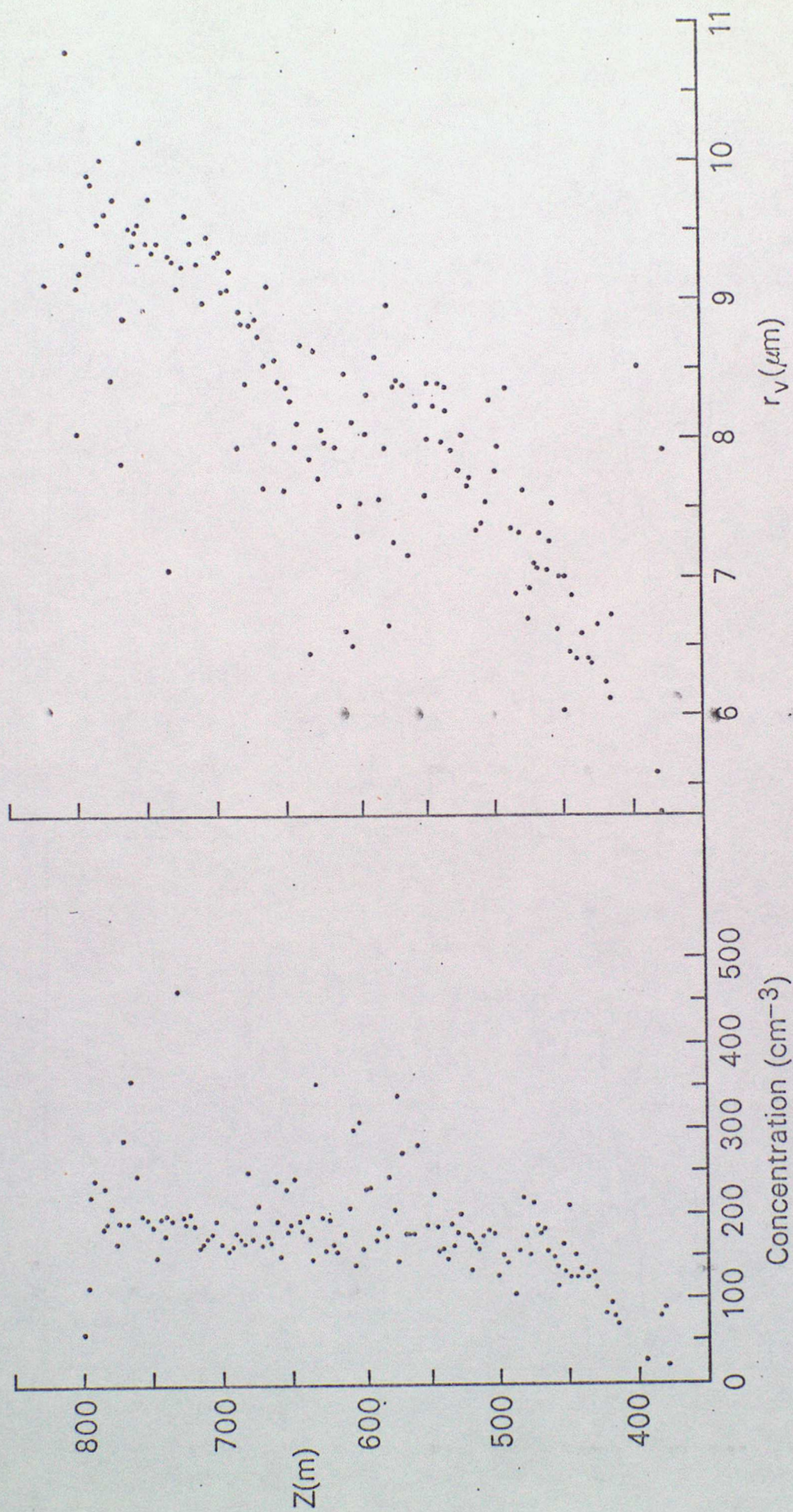
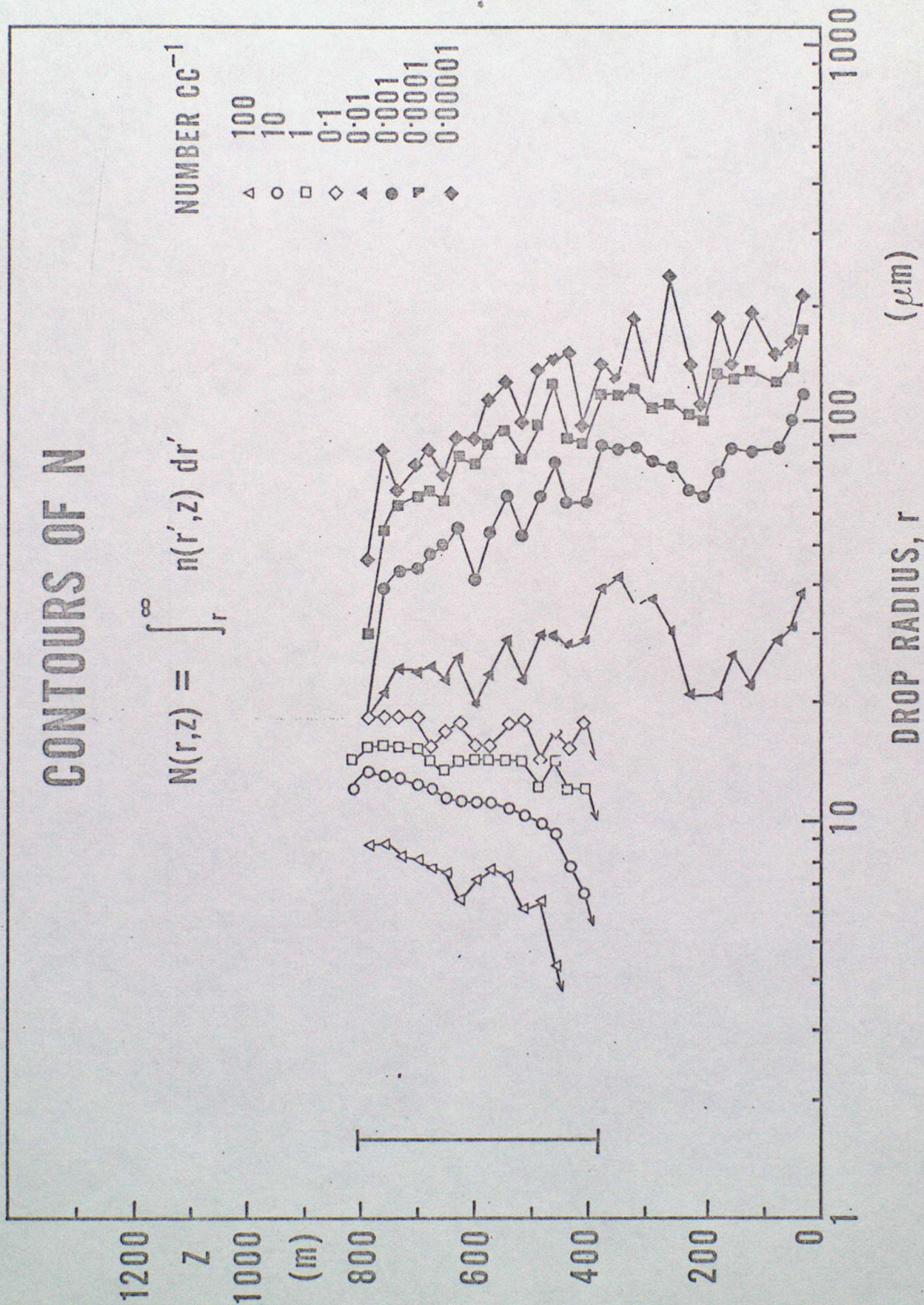


Fig 4 Variation of droplet concentration and mean volume radius,  $r_v$ , with height on the same descent as Fig 3. Each point is a 1s average.

Fig 5 Contours of the cumulative number distribution  $N(r, z)$  from the same descent as Fig 3. The vertical extent of the cloud layer is indicated by the bar.



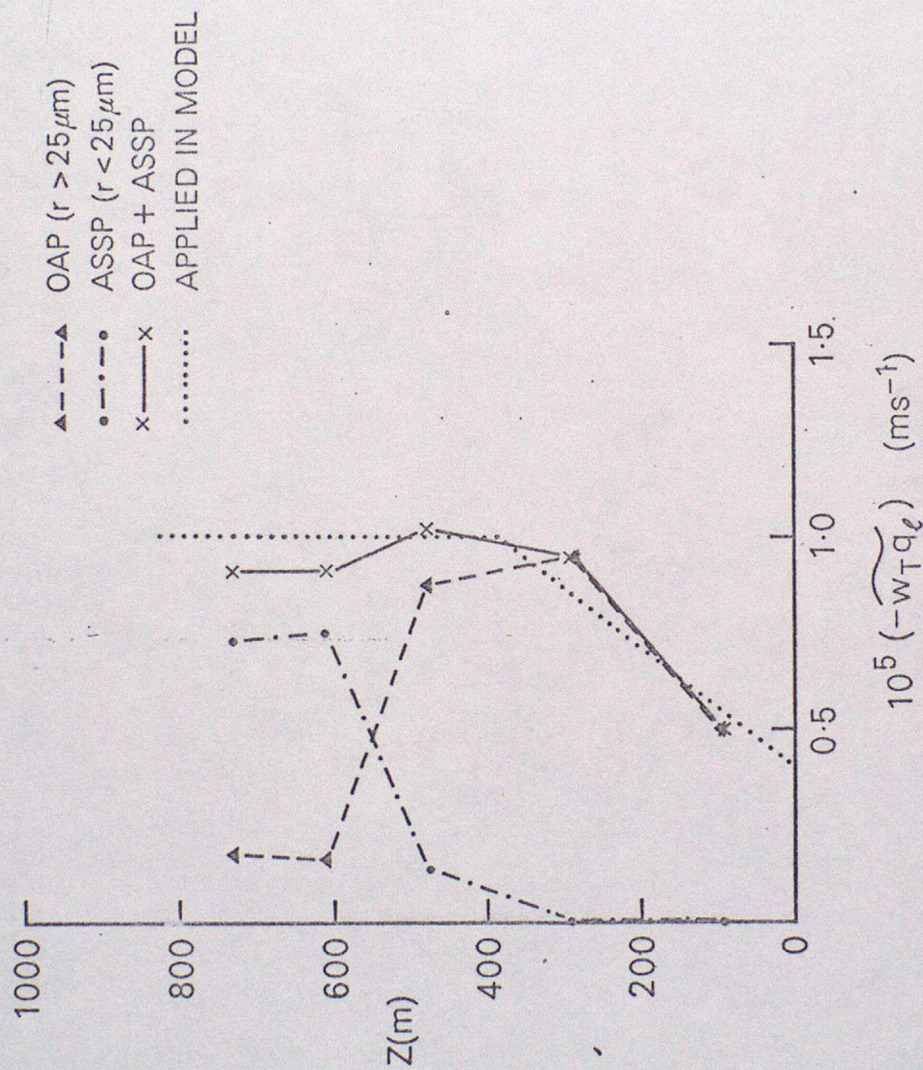


Fig 6 Mean rainfall rates for each level computed from the expression

$$\overline{w_T q_l} = \frac{4\pi}{3} \frac{\rho_w}{\rho} \int_0^\infty w_T(r) r^3 n(r) dr$$

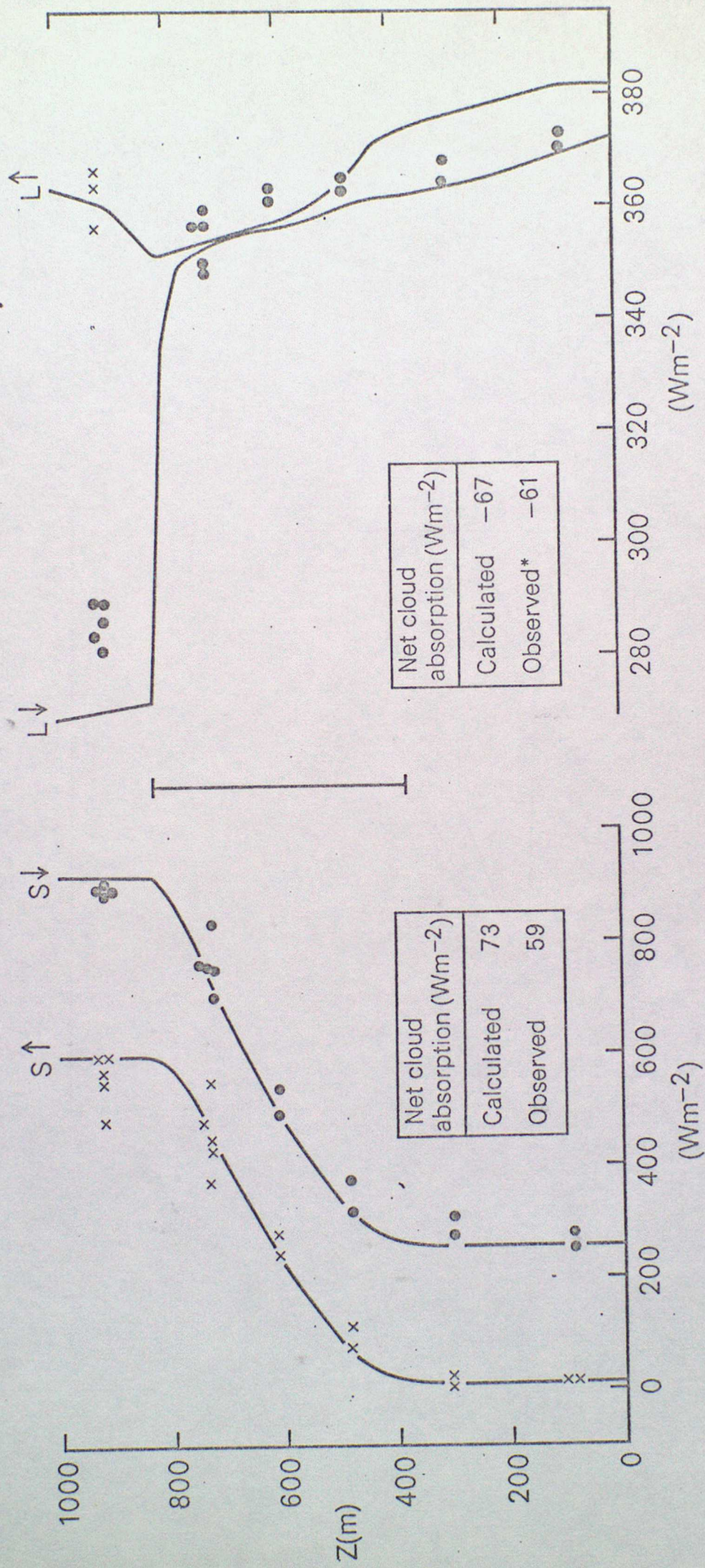


Fig 7 Measured average radiation fluxes from horizontal runs,  $\bullet$  ( $S\downarrow, L\downarrow$ ) and  $x$  ( $S\uparrow, L\uparrow$ ) with theoretical solutions shown by the curves. The extent of the cloud layer is shown by the vertical bar. \* In calculating this value,  $L\uparrow$  beneath cloud is assumed equal to the computed value.

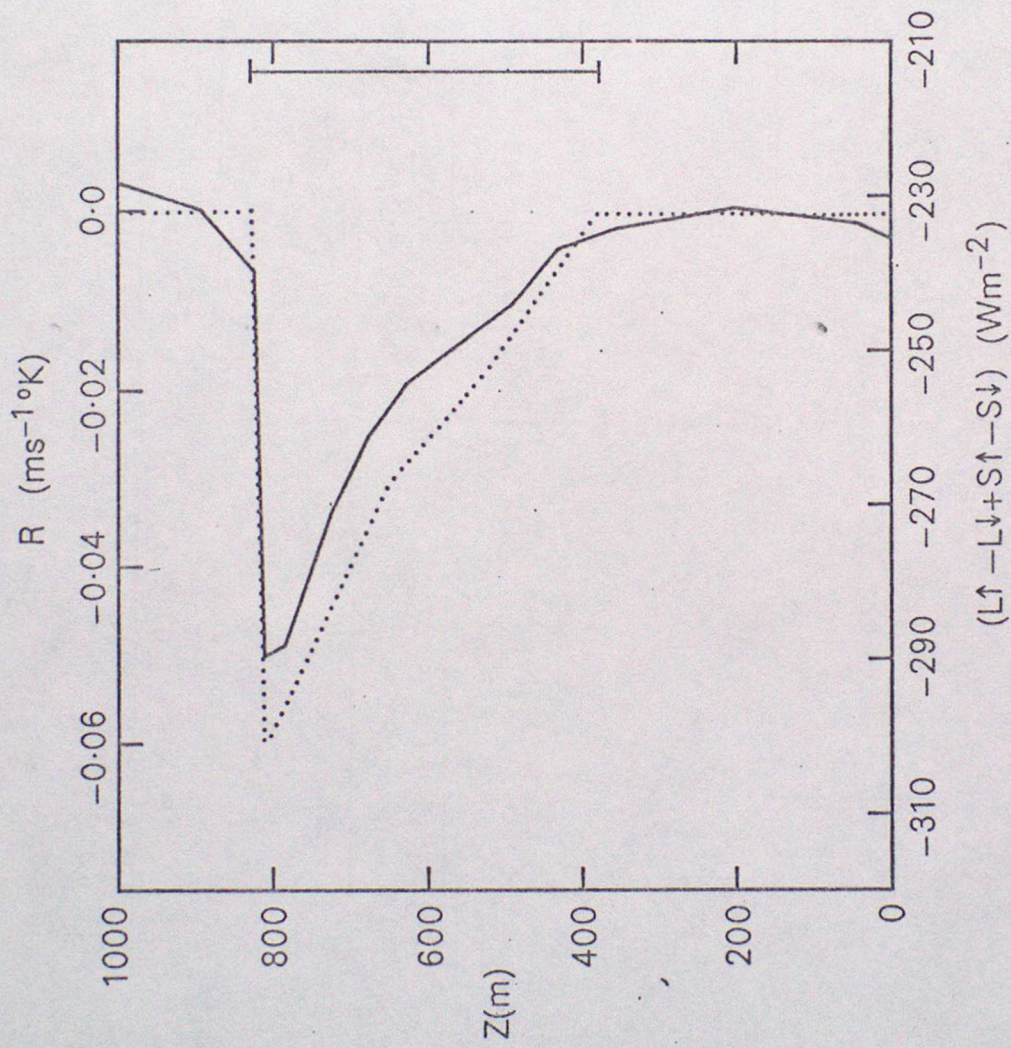


Fig 8 The computed net radiative flux as a function of height (full curve) and the representation used in the model (dotted line). The extent of the cloud layer is indicated by the vertical bar.

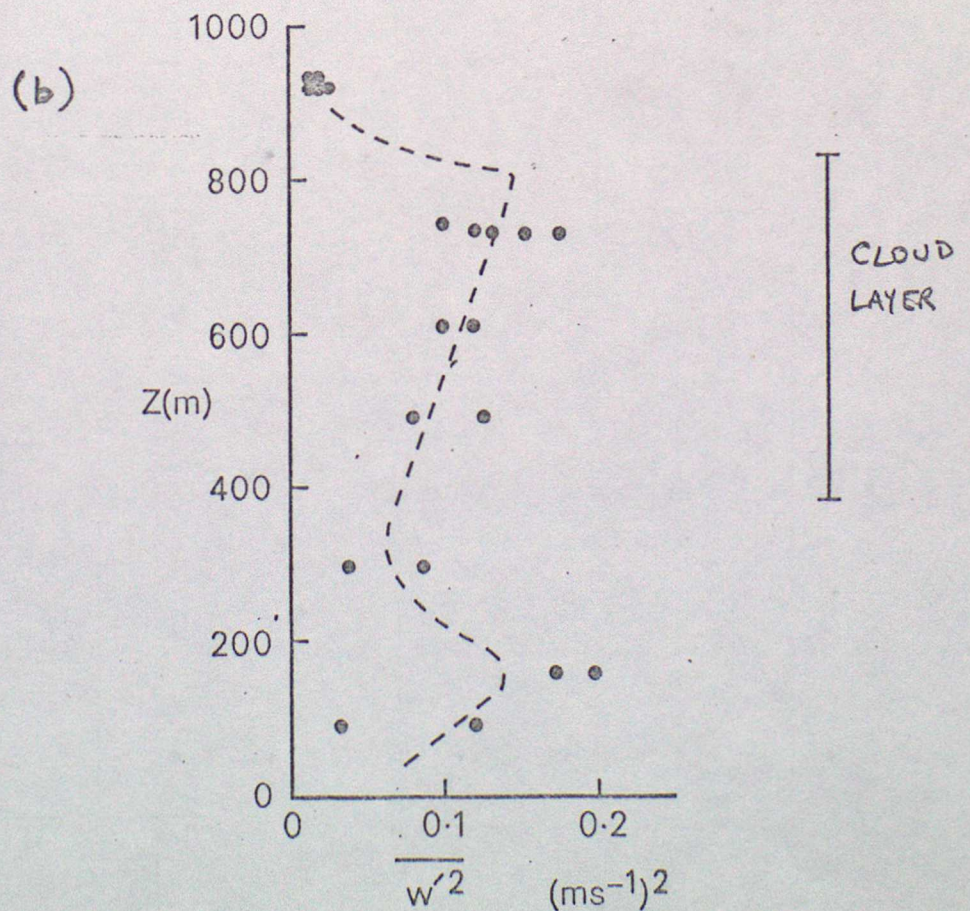
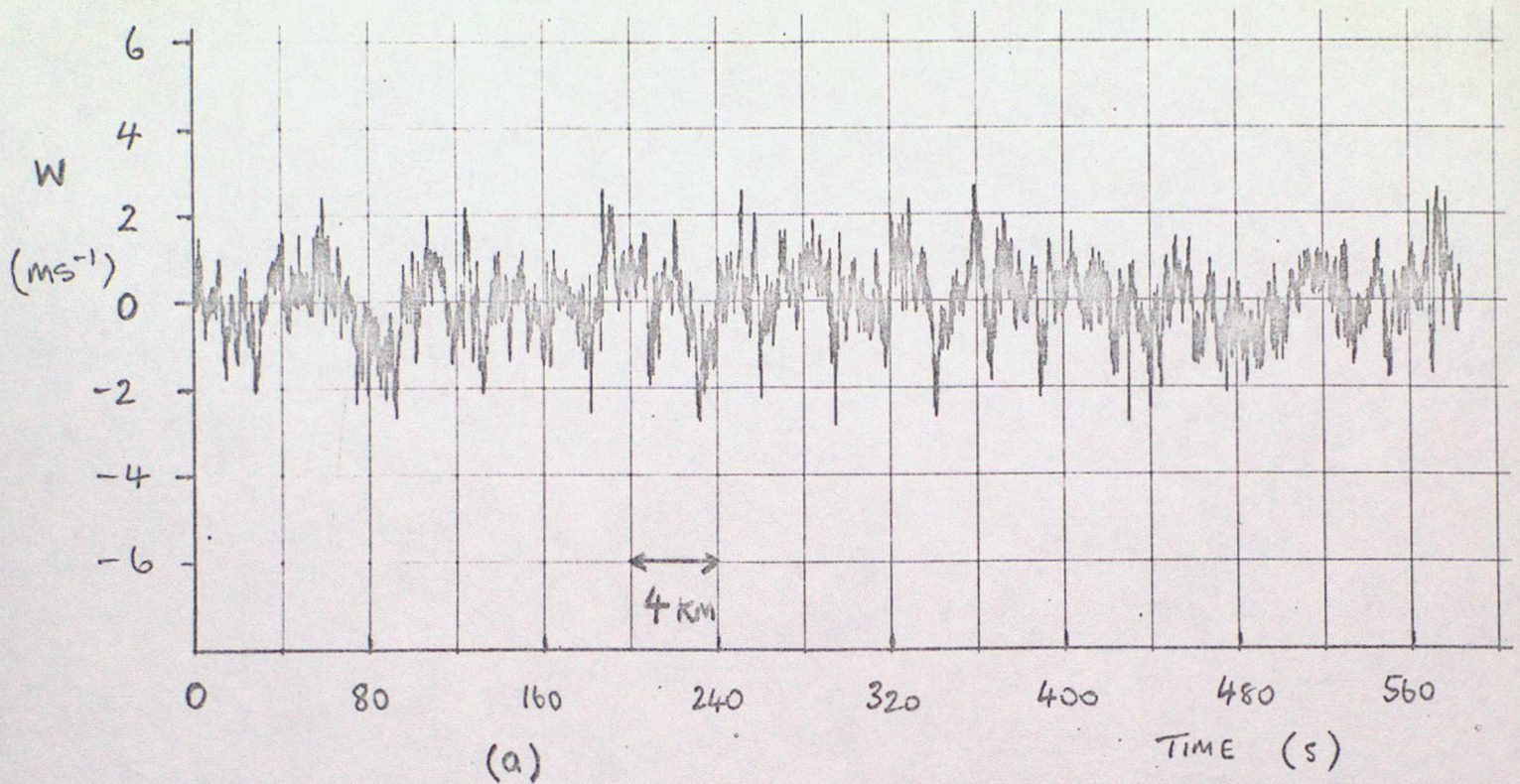


Fig 9 a) Vertical velocity trace at  $z = 850$  m, about 180 m below cloud top on 16 Nov 83, from the MRF C130.

b) Vertical velocity variance vs height for 22 June 83.

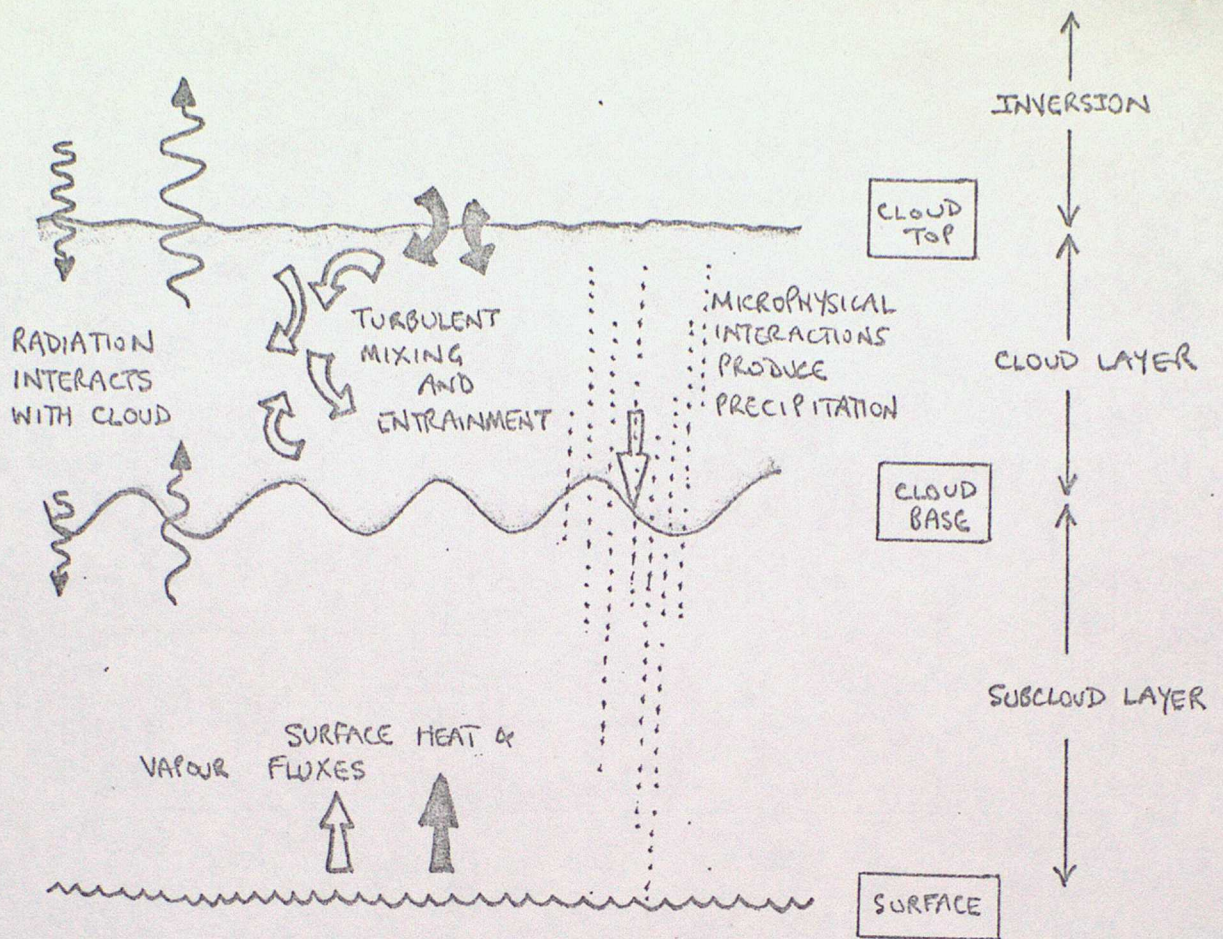


Fig 10 Summary of physical processes operating in a stratocumulus-topped boundary layer.

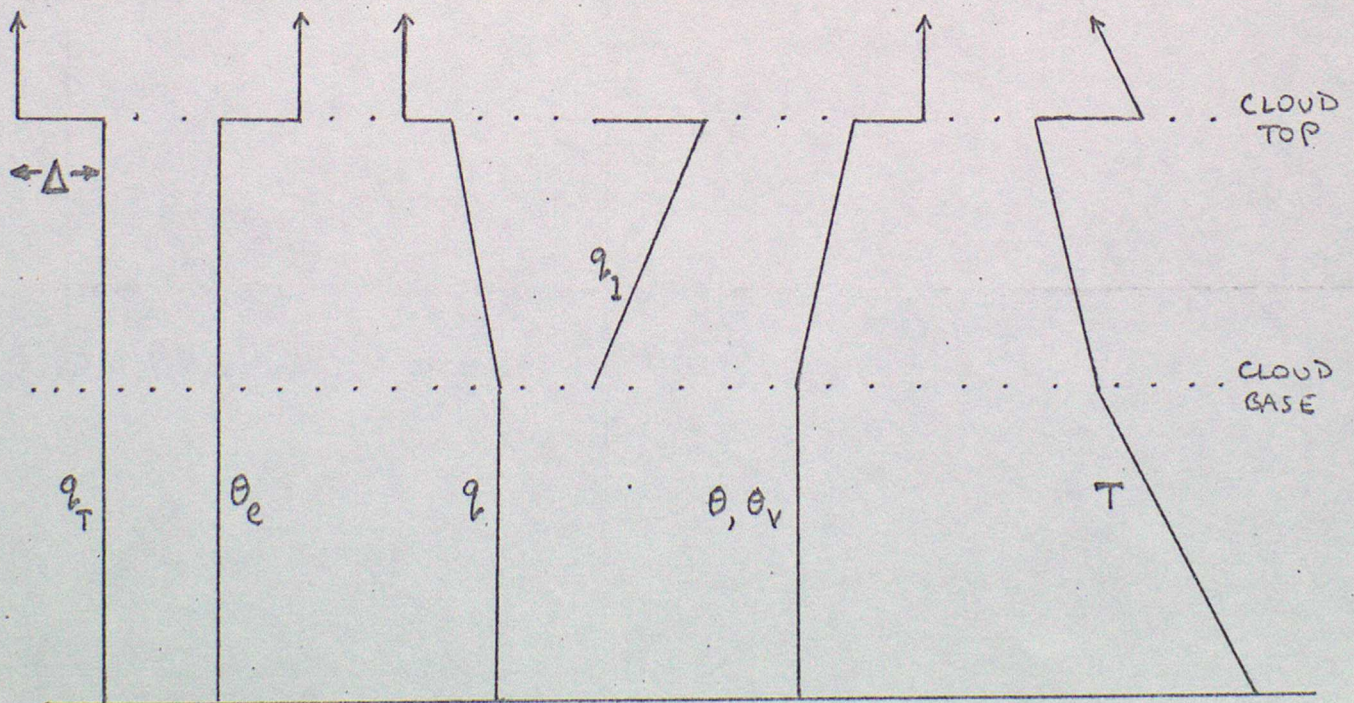


Fig 11 Appearance of vertical profiles in a typical mixed layer model.

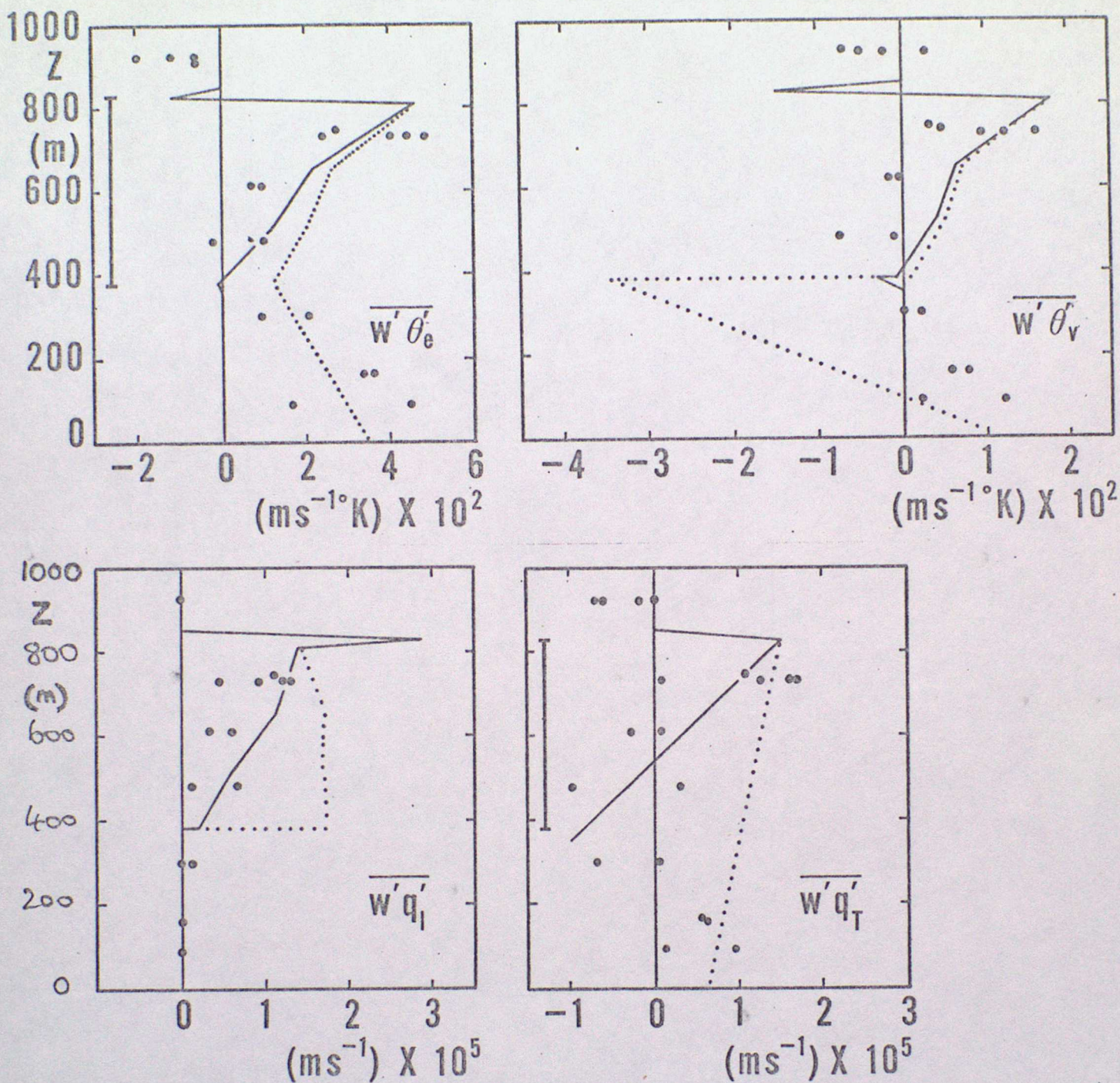


Fig 12

Examples of flux profiles predicted by a mixed layer model

- i)..... Assuming the mixed layer extends from cloud top to the surface
- ii)—— Assuming the mixed layer extends down from cloud top to just below cloudbase (350 m).

Observed values are also shown ( $\odot$ ).

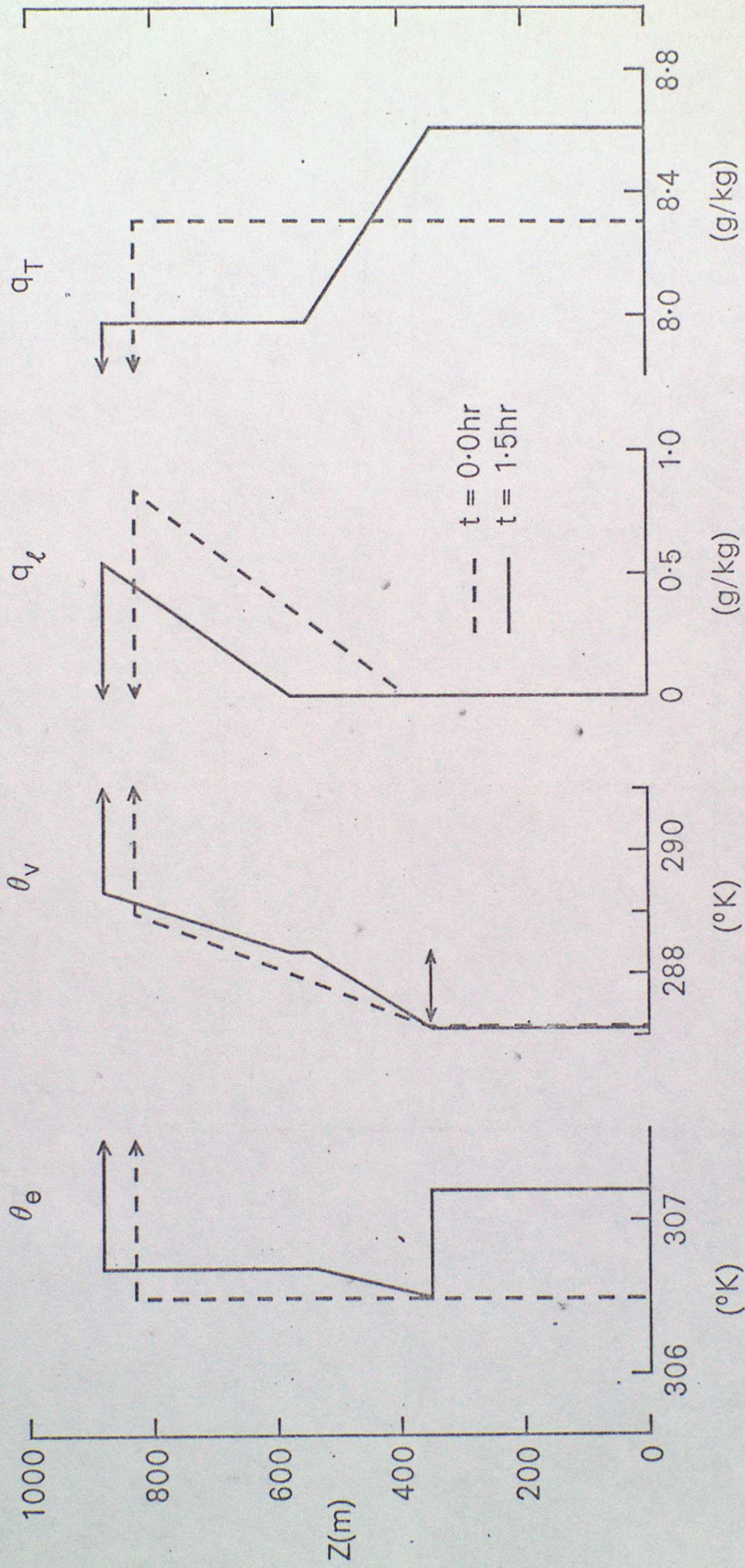


Fig 13 Evolution of mean profiles in  $1\frac{1}{2}$  hr assuming two independent mixed layers. Note the increase in  $\theta_v$  (arrowed) between the two layers tending to increase their separation. However the layers are conditionally unstable ( $\partial\theta_v/\partial z < 0$ ) and if water vapour flux convergence in the lower layer lowers the l.c. sufficiently, cumulus will form and rise into the elevated stratiform layer.

CLOUD PHYSICS INSTRUMENTATION

by S Nicholls

1. INTRODUCTION

In the past decade, the main emphasis in cloud physics research has swung away from laboratory based investigations of simple particle interactions to observational studies of real clouds. This revolution has come about because of the development of new measurement techniques. This lecture will describe some of the cloud physics instrumentation currently in use, concentrating on their basic principles of operation, giving examples of what can be measured and pointing out the limitations of each device.

The scope will be restricted to in situ techniques only; important remote methods e.g. radar, which have played a large role in cloud physics research will not be considered (these must often be calibrated using in situ measurements anyway). Methods suitable only for laboratory use will also be omitted. Finally, the lecture is biased towards those devices operated by M.O.15 which is an extensive subject of those currently available, covering a wide range of measurements.

These measurements may be divided into two broad areas:

- i. Microscale measurements in which individual particles are examined yielding shape, size, composition, number density information etc.
- ii. Integrated or bulk measurements which refer to a volume averaged property e.g. specific liquid water or ice content, rainfall rate, temperature or humidity mixing ratio, where the integrated effect of individual particles is of interest.

The different scales on which these measurements are made usually demands different measurement techniques.

Another important consideration is the platform from which the observations are to be made. Although measurements can be made from the ground, tethered balloons or towers, the height limitations, restricted sampling capability (waiting for the cloud to travel past fixed sensors) and the limited perspective gained from a fixed ground position mean that most observations are now made from aircraft. This immediately presents a number of problems:

- i. Exposure. How to measure an uncontaminated sample while moving at  $100 \text{ ms}^{-1}$  in something very large.
- ii. Response. If an average cloud droplet is characterised by a length scale of  $\sim 10 \mu\text{m}$ , its transit time relative to the aircraft is  $\sim 10^{-7} \text{ s}$ .
- iii. Artificial modification. The passage of a powered aircraft through a cloud might significantly alter the cloud structure either by the amount of turbulence generated in its wake or by the ejection of exhaust gases and particulates (eg Ref. 1 ).
- iv. Environment. Measurement techniques must be impervious to wetting. Icing conditions are particularly difficult.

These are largely overcome by carefully siting equipment in exposed locations (i), stringent criteria in instrument design (ii, iv) and by paying close attention to sampling strategy, flight planning and navigation (iii).

## 2. MICROSCALE MEASUREMENTS

Here we are essentially interested in single particle counters. The particle sizes which are of interest vary from  $\sim 0.1 \mu\text{m}$  to a few mm (all subsequent particle dimensions refer to particle radius or  $\frac{1}{2}$  maximum dimension for non-spherical particles) as shown in Fig. 1. Dealing with the smallest first:

### 2.1 CCN counters:

Recall that cloud droplets grow initially by condensation onto pre-existing cloud condensation nuclei (CCN). However only a small fraction of the total aerosol content act as CCN. This is because a small fraction become activated at very low supersaturations. These activated drops then take up the excess water vapour by additional condensational growth so that the supersaturation is maintained at very small values. Thus no further condensation nuclei are activated.

In more detail, recall that the equilibrium saturated vapour pressure over a solution droplet of radius  $r$ , denoted  $e'(r)$ , is given to a good approximation by the eqn in Fig. 2 where  $e(\infty)$  refers to the equilibrium s.v.p. over a plane, pure water surface under similar conditions. The 'curvature' term represents the increase in s.v.p. over a curved rather than a plane surface, the 'solution' term shows the reduction in s.v.p. caused by the solute. Together, these result in the typical variation shown in Fig. 2 (values for the constants  $a$ ,  $b$  may be found in Ref 2 p.62). At small  $r$  ( $r < r^*$ ), the solution effect dominates and a droplet can be in equilibrium at relative humidities less than 100%. Note that the droplet is stable if the RH is constant: if  $r$  is slightly increased, its equilibrium s.v.p. is also increased, so if the environmental RH remains constant, the droplet must evaporate back to its original size. Conversely, the RH must be increased in order for the droplet to grow. This may be continued until the RH is such that  $S = S^*$  ( $> 0$ ) when  $r = r^*$ . Once a droplet grows beyond  $r^*$ , its equilibrium s.v.p. is less than  $S^*$ , vapour diffuses towards the drop and it will continue to grow without any further increase in the environmental supersaturation. Growth will continue until the droplet population removes sufficient vapour to lower the RH again. Thus droplets which are smaller than  $r^*$  grow only in response to changes in RH and are termed 'haze particles'. A condensation nucleus is said to be activated when the drop formed on it grows to size  $r^*$ , it can then grow without the supersaturation exceeding  $S^*$  to form a cloud droplet.

Clearly,  $S^*$  depends on the properties of the condensation nucleus: decreasing the amount of solute increases the value of  $S^*$  as indicated in Fig. 2 (very small pure water drops need very high supersaturations to be stable). The number of nuclei which will become activated in incipient cloud formation therefore depends on the nature of the CCN and the degree of supersaturation achieved. Since the latter is also a function of the cloud dynamics, if we are to successfully model the growth of the droplet spectrum, we must know the number of nuclei which become activated as a function of supersaturation. This is known as an activation spectrum. Measurement difficulties stem from the fact that  $S$  is usually  $< 1\%$  in real clouds, so a reliable method of maintaining small constant supersaturations is required.

The most popular method is to use a thermal gradient diffusion chamber (TGDC) which uses the principle illustrated in Fig. 3. Two highly conducting, wet surfaces are maintained at slightly different temperatures. In steady state conditions, diffusion will maintain linear temperature ( $\theta$ ) and humidity mixing ratio ( $q$ ) gradients (eg  $\frac{\partial \theta}{\partial z} = K_{\theta} \frac{\partial^2 \theta}{\partial z^2} = 0$  and since  $K_{\theta}$  is not a strong function of  $\theta$ ,  $\frac{\partial \theta}{\partial z} = \text{constant}$ ). However,  $q_{SAT}$  varies non-linearly with  $\theta$  and if both plates are saturated,  $q > q_{SAT}$  in the centre (Fig. 3). In fact  $S$  varies parabolically with  $z$ ,  $S_{MAX} \propto \Delta \theta^2$  and  $S_{MAX} \propto 1/\theta$  (Ref 3). Small constant supersaturations can thus be produced by altering  $\Delta \theta$  eg if  $z = 1 \text{ cm}$ ,  $\theta = 20^\circ \text{C}$  and  $\Delta \theta = 3 \text{ K}$ ,  $S_{MAX} = 0.4\%$ .

If a sample is introduced into the chamber, some of the CCN will be activated and grow within a few seconds to several microns. They will then settle out, so the number of drops ( $r > \sim 1 \mu\text{m}$ )/unit volume in the centre of the chamber will initially increase as drops grow, then decrease as they fall out. Measuring the peak number of drops (which usually occurs after an elapsed time of several seconds) either directly or by light scattering techniques enables the number of activated nuclei to be determined (eg see Fig. 4).

### Limitations

- i.  $S$  must exceed 0.1%, otherwise drops do not grow sufficiently large sufficiently quickly to be distinguishable from haze drops and some drops may sediment out before others have had time to grow.
- ii. If the number of activated drops is very large ( $> \sim 10^3 \text{ cm}^{-3}$ ), the amount of water vapour might be depleted leading to undercounting.

An example activation spectrum obtained with a TGDC is also shown in Fig. 4.

### 2.2 Small particles, 1-20 $\mu\text{m}$ :

The majority of cloud droplets lie in this range.

2.2.1 Impact devices: These were virtually all that were available to determine the droplet spectrum until the early 1970's, although now largely superseded for most applications. These all involve the inertial capture of drops on suitably prepared surfaces followed by microscopic examination. Many different methods were used (see Ref 4) being based either around slides or continuous films exposed for a short (fractions of a second) time to the air-stream. Slides covered with soot or MgO record particle impacts as craters proportional to particle size while an oily coating traps droplets and arrests evaporation. A different method called replication uses a continuous tape coated with a  $\sim 70 \mu\text{m}$  thick layer of Formvar (plastic solution) in which particles are embedded. The tape then passes into a drying chamber to harden the plastic which also evaporates the encapsulated particles leaving behind a replica which can be examined later.

### Limitations

- i. All these methods suffer from the major disadvantage that the collection efficiency is usually strongly dependent on particle size.
- ii. Particles may break up on impact.
- iii. Craters are only proportional to particle size and require calibrating.

iv. Small samples are necessary to avoid the possibility of double impacts. Obtaining representative samples is therefore difficult.

v. Subsequent microscopic analysis is long and tedious.

2.2.2. PMS\* forward scattering probes (ASSP/FSSP)\*: Developed in the early 1970's by Dr R Knollenberg in the U.S., these devices have almost entirely superceded the impact methods. The basic principle of operation is to measure the forward scattering of light by single particles. Fig. 5 shows a schematic layout of the FSSP. Light from a SmW cw He-Ne laser ( $0.63\mu\text{m}$ ) is focussed to a diameter of  $\sim 200\mu\text{m}$  at the centre of the sampling aperture through which air passes in a direction perpendicular to the plane of the diagram. The collection optics accepts only light scattered between the angles of  $7^\circ$  and  $15^\circ$  ( $4^\circ$  and  $15^\circ$  for the FSSP). At this range of scattering angles, small water droplets scatter an intensity which is approximately proportional to  $r^6$ . Fig. 6 shows this intensity as a function of drop size computed from Mie Theory assuming spherical pure water drops. If the sampling volume is made sufficiently small so that it contains only one particle at a time; measurements of the scattered light enable water drops to be counted and sized automatically.

In practice, the scattered intensity depends upon.

- i. Particle size and shape.
- ii. Optical properties of the particle material.
- iii. Location of the particle within the beam.
- iv. Optical properties of the instrument (beam intensity, uniformity etc)

Particles are assumed to be perfectly spherical and composed of pure water. The effects of (iii) and (iv) are minimized by restricting the sampling volume. This is achieved in two ways. The scattered light is passed through a beam splitter to two detectors, one of which has an annular mask. In focus particles ie those within  $\sim \pm 2\text{mm}$  of the object plane form an image on the central dump spot, so only out of focus images will register. These are rejected. Also, the transit time of the particle through the beam is measured, if this is less than the average, the particle must have passed through the edge of the beam and is rejected. These two criteria define the sampling volume: approximately  $4\text{mm} \times 0.62 (200\mu\text{m}) \times 200\mu\text{m}$ , ie about  $10^{-4} \text{cm}^3$ . As particle concentrations are typically less than  $10^7 \text{cm}^{-3}$ , the volume will usually contain only a single particle.

#### Advantages

- i. Samples are relatively undisturbed.
- ii. Produces a drop size distribution ( $0.5 - 24\mu\text{m}$ ) in real time.
- iii. Short (0.1 - 10s) averaging time.
- iv. Good spectral resolution (15 bins approximately  $1\mu\text{m}$  wide).
- v. Data recorded and can be analysed immediately by computer.

---

\*PMS Particle Measuring Systems Inc., Boulder, Colo.  
ASSP Axially scattering spectrometer probe (superceded by the FSSP).  
FSSP Forward " " "

## Limitations

- i. Sampling volume/particle rejection is not defined with sufficient accuracy to enable integrated quantities e.g. liquid water content to be obtained directly from the spectra.
- ii. The sampled volume is an odd shape:  $\sim 200\mu\text{m}$  (across)  $\times 100\text{m}$  for a 1s averaged spectrum. This limits the spatial resolution.
- iii. Works for water drops only. Specular reflection from ice gives misleading counts and incorrect sizing.
- iv. Mie peaks at small radii ( $r < \sim 3\mu\text{m}$ , see Fig. 6) may lead to ambiguity when sizing small drops.

Some examples of data obtained using this device are shown in Fig. 7. A number of intercomparisons between these instruments and impact and bulk-measuring devices have recently been published (Refs 5,6 ).

### 2.3 Larger particles, $20\mu\text{m} - 4\text{mm}$

2.3.1 Impact devices: As 2.2.1. for droplets, these methods also work for larger particles. In addition foil impactors have been used for large particles ( $> \sim 100\mu\text{m}$ ) where the impact depressions in thin metal foil are measured (Ref 4 , p606), however the same disadvantage noted earlier remain.

2.3.2 PMS 2-D probes: Again, these have supplanted most earlier techniques for measuring particles in this size range. As the particles are much bigger than those measured by the FSSP, essentially geometrical optical techniques are employed. Two probes are used to cover the size range; the 'cloud' probe ( $12.5-400\mu\text{m}$ ) and the 'precipitation' probe ( $100\mu\text{m} - 4\text{mm}$ ), although both operate in a similar manner. A beam of light from a 2mW He-Ne<sup>laser</sup> passes through the sampling volume and illuminates a linear array of 32 photo-diodes, (Fig. 8). As the system is flown through the air (Fig. 8), particles will enter the beam and may shadow some diodes. If the level of illumination of any diode falls below 50% of its normal value, that diode will change its electronic state. By recording the state of the whole diode array many times during the particle's transit, a digital image may be built up of its shadow, (Figure 9).

The beam is magnified before it falls onto the diodes; the resolution of the instrument is determined by the magnification and the actual diode spacing. The image of the diode spacing in the sampling area of the cloud probe is thus designed to be  $25\mu\text{m}$ , and in the precipitation probe  $200\mu\text{m}$ .

If the frequency with which the diode array state is recorded ("clock" frequency) is set so that particles move  $25\mu\text{m}$  through the cloud-probe beam between pulses (or  $200\mu\text{m}$  through the precip-probe), then the record will maintain the shape of the shadow undistorted. With the aircraft flying at 100 m/s, this requires a clock frequency to the cloud-probe of 4 MHz (500 KHz to the precip-probe). Thus each probe records a 2-D 'plan' view of each particle. To convert this information to particle density, the sampling volume is required. This is essentially the product of the sampling area normal to the flow and the airspeed. The sampling area 'A' is given by  $A=F \times W$  where W is the diode array width and F the depth of field. Were it is not for diffraction effects, an object placed in a parallel beam of coherent light would cause a shadow which was itself rectilinearly propagating. The shadow's image would be brought to a sharp focus in the focal plane of a lens where~~ver~~ the shadowing object was situated. In other words,

illumination by laser light would produce an infinite theoretical depth of field; the actual depth of field would be limited only by the probe's physical aperture.

However, diffraction effects mean that the object's shadow is appreciably in focus only when the object is confined within a depth of field which is more limited, and size-dependent. In fact, Ref. 7 has shown that a reduction in intensity of at least 50% will be achieved if a spherical object of diameter  $D_{\mu\text{m}}$  is within  $\pm 7.5 \times 10^{-5} D/\lambda$  of the object plane ( $\lambda$  in  $\mu\text{m}$ ) and that the inferred size will be correct to within 10%. The depth of field must therefore be calculated for each image. It is limited by the physical aperture (i.e. distance between the probe ends) for particles whose radius exceeds  $80 \mu\text{m}$  (cloud probe: aperture 6.1 cm) and  $166 \mu\text{m}$  (precip. probe: 26.3 cm).

Bulk quantities e.g. liquid water content, radar reflectivity, rainfall rate may therefore be deduced. However for non-spherical particles assumptions must be made regarding the third dimension in volume calculations and also about density if particle mass is required.

Advantages: As FSSP.

Limitations:

- i. Discrete detector size,  $\lambda \times \lambda$  ( $\lambda = 25 \mu\text{m}$ : cloud probe,  $200 \mu\text{m}$  precip. probe) leads to counting problems for particles smaller than several  $\lambda$  in diameter. This causes severe undercounting of particles in the smallest categories.
- ii. The resolution of even quite large particles is poor due to the large 'pixel' size. Only particle shape tells you whether it is composed of ice or water.
- iii. The sampling volume is again dependent on measured particle dimensions. These are difficult to gauge for non-spherical particles.

Some examples of images obtained are shown in Fig. 10.

#### 2.4 Other methods:

2.4.1 High speed photography: Has been used but the major limitation is the available depth of field. Sampling volumes are therefore  $\sim 10^{-5} \text{ cm}^3$  which are unlikely to contain many particles although drops as small as  $\sim 1 \mu\text{m}$  may be detected. Analysis is also time consuming.

2.4.2 Holography: Developed by M.O.15, this technique overcomes the depth of field limitations of conventional photographic imaging. Highly coherent light from a pulsed laser is passed through a diverging lens illuminating the sampling volume (Fig. 11). Light scattered by particles interferes with the original beam in the plane of the film forming a set of fringes. When illuminated with a c-w laser, the hologram acts as a diffraction grating and an image is formed as shown. This reconstructed image may be altered by moving the hologram with respect to the source of illumination, thus successive planes in a 3-D volume can be scanned (Fig. 12) so that the effective depth of field is extremely large (several 10's of cm).

A high power Nd-YAG laser is necessary to provide sufficient light to expose the hologram, but a frequency doubling lithium iodate crystal is required because no sufficiently sensitive emulsion is available in the near IR ( $1.06 \mu\text{m}$ ). A very short pulse length (20 ns) effectively freezes the motion of the particles, even at aircraft speeds, and a short ( $\sim 2 \text{ ms}$ ) camera shutter speed eliminates daylight fogging of the film. The laser may be fired several times a second.

The use of divergent beams results in the real images being substantially magnified. This varies as the hologram is moved away from the illuminating source during reconstruction (decreasing with increasing distance). Further magnification is provided by the use of different wavelengths for recording and reconstruction (0.53/0.63  $\mu\text{m}$ ) and by using a CCTV camera and monitor (23x). Overall magnification factors up to several hundred may be obtained.

Particles from  $\sim 5\mu\text{m}$  to a few mm can be resolved by the system.

#### Advantages:

- i. Instantaneous, compact sample of about 0.5l volume.
- ii. Resolution of the images is much better than that of 2D probes making ice/water determination much easier and giving much better shape information.
- iii. Some information in the third dimension is available as different parts of the particle image may be brought into focus by moving the hologram.
- iv. The system records the actual relative positions of the particles in space so that positions and separations can be measured.

#### Limitations:

- i. Noise in the reconstructed images due to laser intensity variations in recording and film characteristics cause problems in detecting small drops and effectively eliminates the possibility of fully automated image processing.
- ii. The need for human pattern recognition means that analysis is fairly lengthy (n.b. it is not clear that processing of complex images from the 2-D probe is any better, although counting is much quicker).

Some examples of reconstructed images are shown in Fig. 13 and Ref 11.

### 3. BULK MEASUREMENTS

3.1 Liquid water content: As we have seen, sampling limitations or uncertainties about sampling volume preclude determining the liquid water content by integrating the droplet spectra even though the particles are known to be spherical and have a well defined density. Ice water or mixed ice and water content measurements are even more difficult. There is therefore a need for bulk condensed water measurements.

The most widely used device, designed primarily for airborne use, is the Johnson-Williams probe (other instruments working on similar principles also exist). The sensor consists of a short ( $\sim 2$  cm) length of heated wire (diam.  $\sim 0.5$  mm) exposed transversely to the airstream (Fig. 14). Impinging droplets are evaporated and cool the wire altering its electrical resistance. The heat balance of the wire is

$$\text{Electrical dissipation} = \text{Rate of loss of sensible heat} + \text{evaporative loss.}$$

The heat loss depends upon the ambient temperature and airspeed as well as the rate of accretion of drops. To compensate for the first two, a second heated wire is mounted longitudinally. Its heat loss also depends on ambient temperature and airspeed but is not as sensitive to water content. The difference between the power dissipated in the two wires is therefore related to the rate of accretion of water from which the liquid water content of the air may be obtained. The collection efficiency of the wire is clearly important. This is good for small drops ( $r < \sim 15\mu\text{m}$ ) although there is presently some discussion about its response to larger drops. The accuracy of a well maintained sensor is about  $\pm 5\%$  (Ref 8).

The response time is about 0.4s (Ref 9 ).

#### Limitations:

- i. The device saturates if  $q_l > \sim 3 \text{ g m}^{-3}$  when there is insufficient heat dissipated to evaporate all of the drops.
- ii. Sensitive to water drops only.
- iii. Needs frequent baselining (zero adjustment) in clear air.
- iv. Misreads in icing conditions when ice can form on the compensation wire mount.

An example of data from this device is shown in Fig. 7.

#### 3.2 Total water content:

Here the water in condensed phases is evaporated and the vapour density measured. This is useful because it is often the total water content which you wish to know rather than the proportion in different phases. The problem lies in designing an efficient evaporator, but with sufficient heat input these instruments can respond to water, ice and ice & water mixtures. Furthermore, fast response times are possible if Lyman- $\alpha$  hygrometers are used (eg Ref. 10).

3.3 Temperature: Although a basic thermodynamic variable, it is notoriously difficult to measure in cloud due to possible evaporative effects. This is especially true for aircraft where dynamic heating of up to several degrees can occur ie the air is no longer saturated and significant evaporative cooling is possible. Immersion thermometers (eg platinum resistance wires) are therefore carefully designed to try and keep the sensing elements dry, however, the degree to which this can be achieved is somewhat uncertain. Other techniques are therefore being investigated.

One method is not to measure dry bulb temperature at all, but to try to ensure the sensor stays wet. Problems are encountered here in ensuring that the shroud stays wet and also because of sensitivity to the chemical composition of the wetting agent.

Another possibility is to use a radiation thermometer. For this to work well, the chosen wavelength must lie in a band where the atmosphere absorbs very strongly (giving a low sensitivity to droplet shape, composition and concentration) and where sensitive detectors are available. M.O.15 are developing such a device based on the  $4.3 \mu\text{m}$   $\text{CO}_2$  absorption band where 80% of the signal originates from within 10m of the instrument. It is expected that a resolution varying between 0.1K (at  $30^\circ\text{C}$ ) and 0.6K (at  $-20^\circ\text{C}$ ) will be possible with a response time less than 0.1s.

#### 4. SUMMARY

Table 1 summarizes some of the characteristics of the instruments discussed above.

## 5. REFERENCES

Met O 15 instrumentation is described in detail in a number of internal reports. Those relevant to this lecture are:

Internal Report No.	Title	Author
8	Performance assessment of the Knollenberg Scattering spectrometer, Model ASSP-100.	W T Roach (1977)
22	A study of the Johnson-Williams liquid water content meter as fitted to the MRF Hercules.	D A Johnson (1979)
35	The PMS 2-D Optical Array Spectrometer System.	M Ouldridge (1982)
37	An introduction and guide to the M O 15 CCN counter.	M Kitchen (1982)
38	An introduction and guide to the PMS ASSP	R Brown (1982)
40	An introduction and guide to the Met O 15 holographic particle measuring system.	C N Taylor (1982)

1. Rangno, A L and P V Hobbs, 1983  
Production of ice particles in clouds due to aircraft penetrations. *J.Appl.Meteor*, 22, 214-232
2. Rogers, R R 1979  
A short course in cloud physics (International Series in Natural Philosophy). Pergamon International Library
3. Twomey, S. 1978  
Developments in Atmospheric Science Atmospheric Aerosols pp 169-172
4. Mason, B J 1971  
The Physics of Clouds. O.U.P.
5. Mossop, S C 1983  
Intercomparison of instruments used for measurements of cloud drop concentration and size distribution. *J.Appl.Meteor*, 22, 419-428
6. Pinnick, R G, Garvey D M and Duncan L D 1981  
Calibration of Knollenburg FSSP light scattering counters for measurements of cloud drops. *J.Appl.Meteor*, 20, 1049-1057
7. Knollenberg R G 1970  
The optical array: an alternative to scattering or extinction for airborne particle size determination. *J.Appl.Meteor*, 9, 86-123.

8. Kitchen M 1980  
Report on Johnson-Williams intercomparison experiments at the NRC icing wind tunnel, Ottawa, 22-24 Oct 1980. Unpublished M O 15 internal report.
9. Personne P, Brenguier J L Pinty J P and Pointin Y. 1982  
Comparative study and calibration of sensors for the measurement of the liquid water content of clouds with small droplets.  
J.Appl.Meteor, 21, 189-196
10. Ruskin R E. 1976  
Liquid water content devices.  
Atmospheric Technology, 8, 38-42
11. Conway B J, Caughey S J Bentley A N and Turton J D. 1982  
Ground-based and airborne holography of ice and water clouds.  
Atmos. Environment, 16, 1193-1207

Instrument	Ice/water	Size range (radius)	Sampling details	Limitations
TGDC CCN counter	water	-	~ 1 count/min	$0.1 < S < 5\%$
<u>Impactors</u> Oil MgO or soot Foil  Replication	both   both	$1\mu\text{m} \rightarrow$ $10\mu\text{m} \rightarrow$ $100\mu\text{m} \rightarrow$	Fraction of a )second exposure )time Few secs	Collection efficiency size. Particle shattering on impact. Small samples. Tedious analysis.
FSSP	water	$0.5-24\mu\text{m}$	$0.1\text{s}-10\text{s}$ average	Sampling volume uncertainty and shape. No ice crystals present. Sizing ambiguity at small radii.
cloud 2-D probes precip.	both	$12.5-400\mu\text{m}$ $0.1-4\text{mm}$	Each particle image recorded	Discrete detector size. Undercounting at small r Sampling volume uncertainty
Holography	both	$5\mu\text{m} \rightarrow$	Instantaneous $\sim 0.5\text{l}$ volume	Lengthy analysis Noise limits
Photography	both	$1\mu\text{m} \rightarrow$	Instantaneous $\sim 10^{-5}\text{cm}^3$	Small depth of field.
Johnson-Williams	water	smaller drops collected with higher efficiency	Response time $\sim 0.4\text{s}$	$e_d < 3\text{g}\mu\text{m}^{-3}$ . Insensitive to ice particles. Misreads in icing conditions.

Table 1 Summary

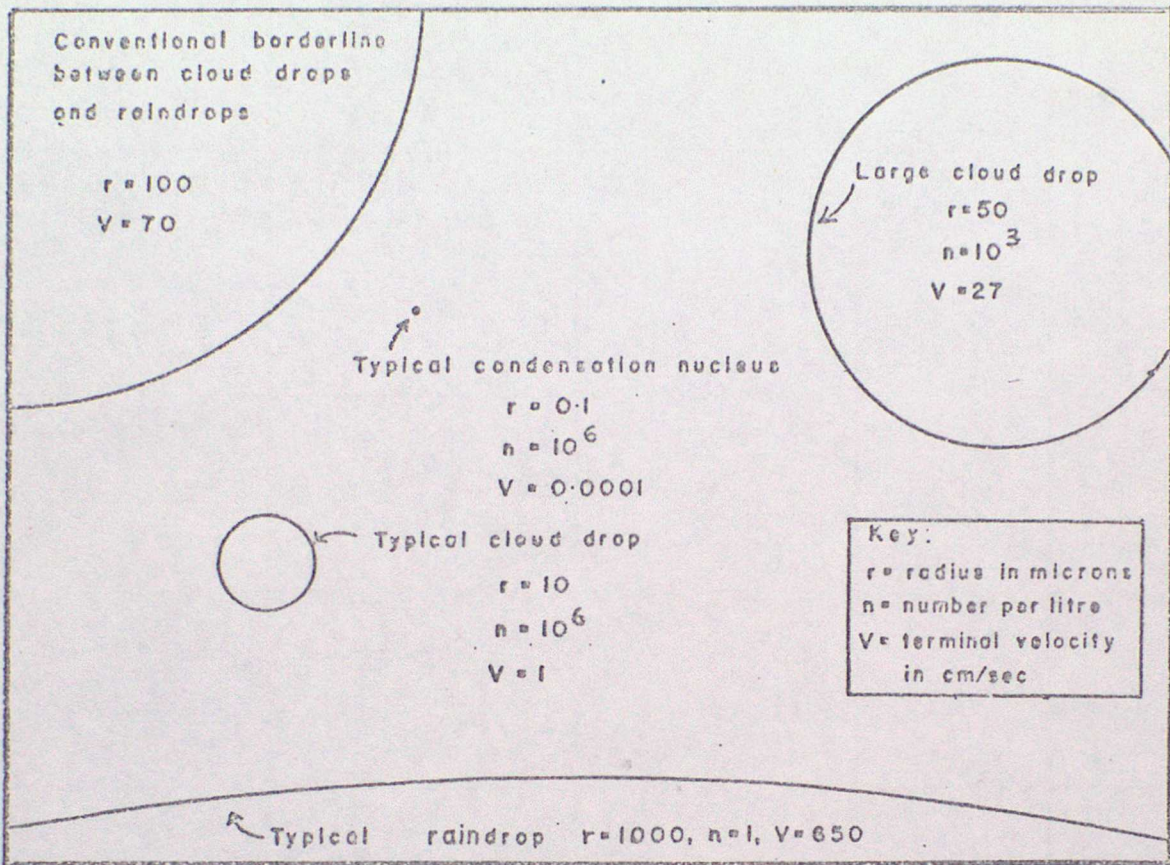


Fig 1 Relative particle sizes.

$$1 + S = \frac{e'_s(r)}{e_s(\infty)} = 1 + \frac{a}{r} - \frac{b}{r^3}$$

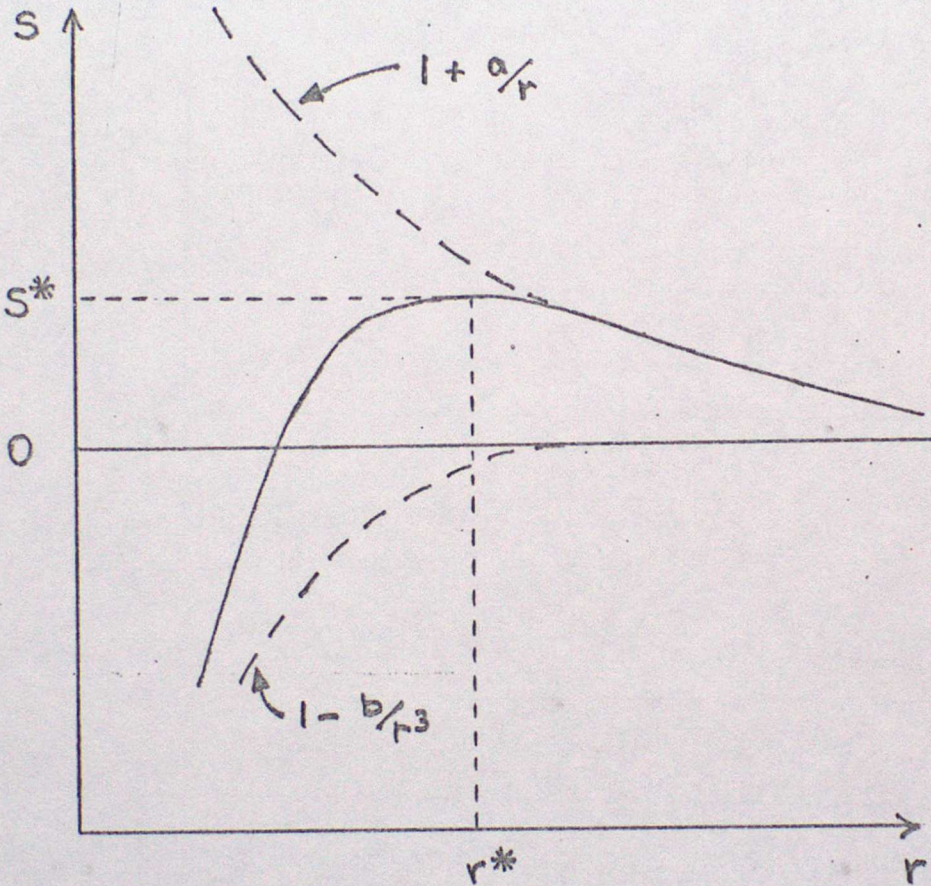
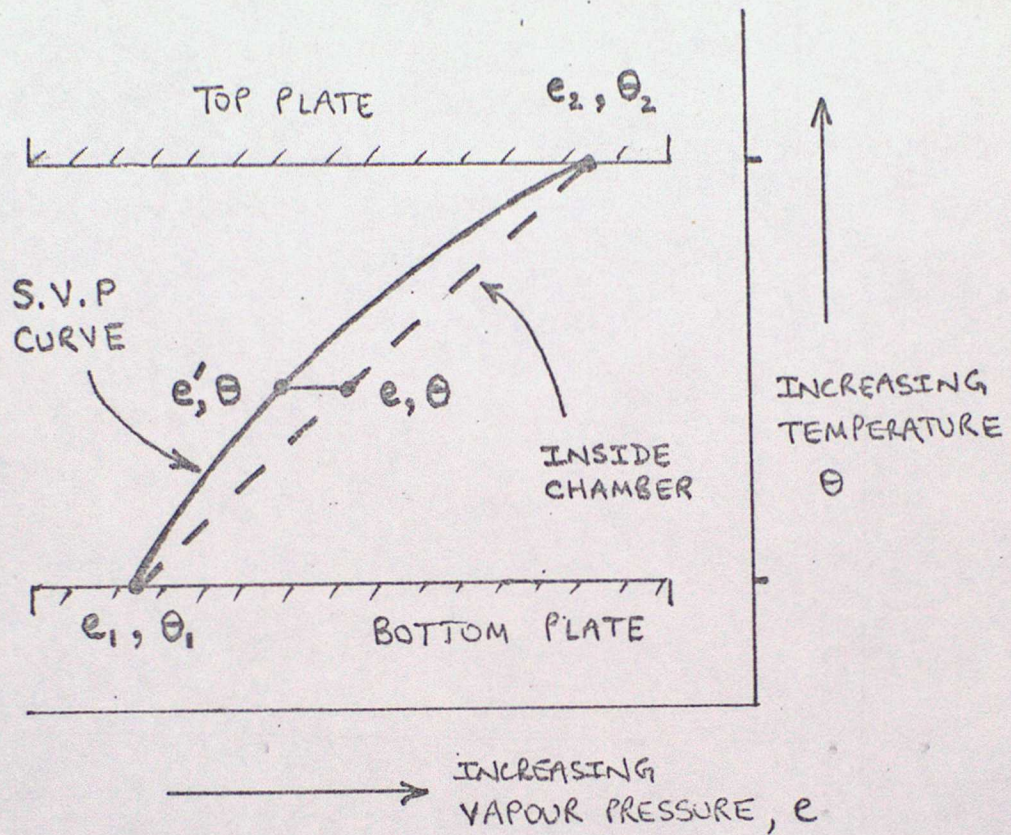


Fig 2 Equilibrium supersaturation as a function of solution droplet size.



SUPERSATURATION,  $S = e - e' / e'$

e.g. IF  $z = 1 \text{ cm}$ ,  $\theta = 20^\circ\text{C}$ ,  $\theta_2 - \theta_1 = 3^\circ\text{C}$   
 then  $S = 0.4\%$

Fig 3 Operating principle of the TGDC.

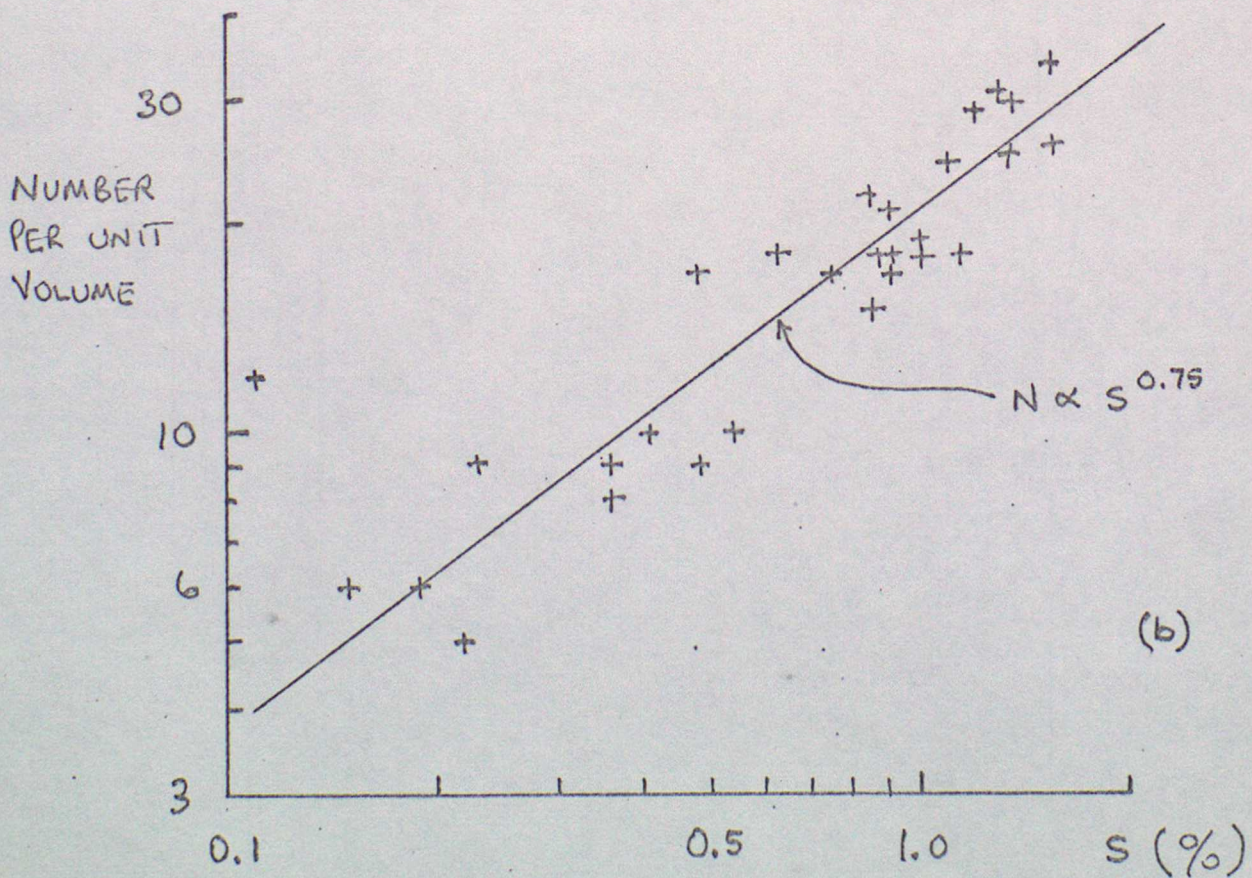
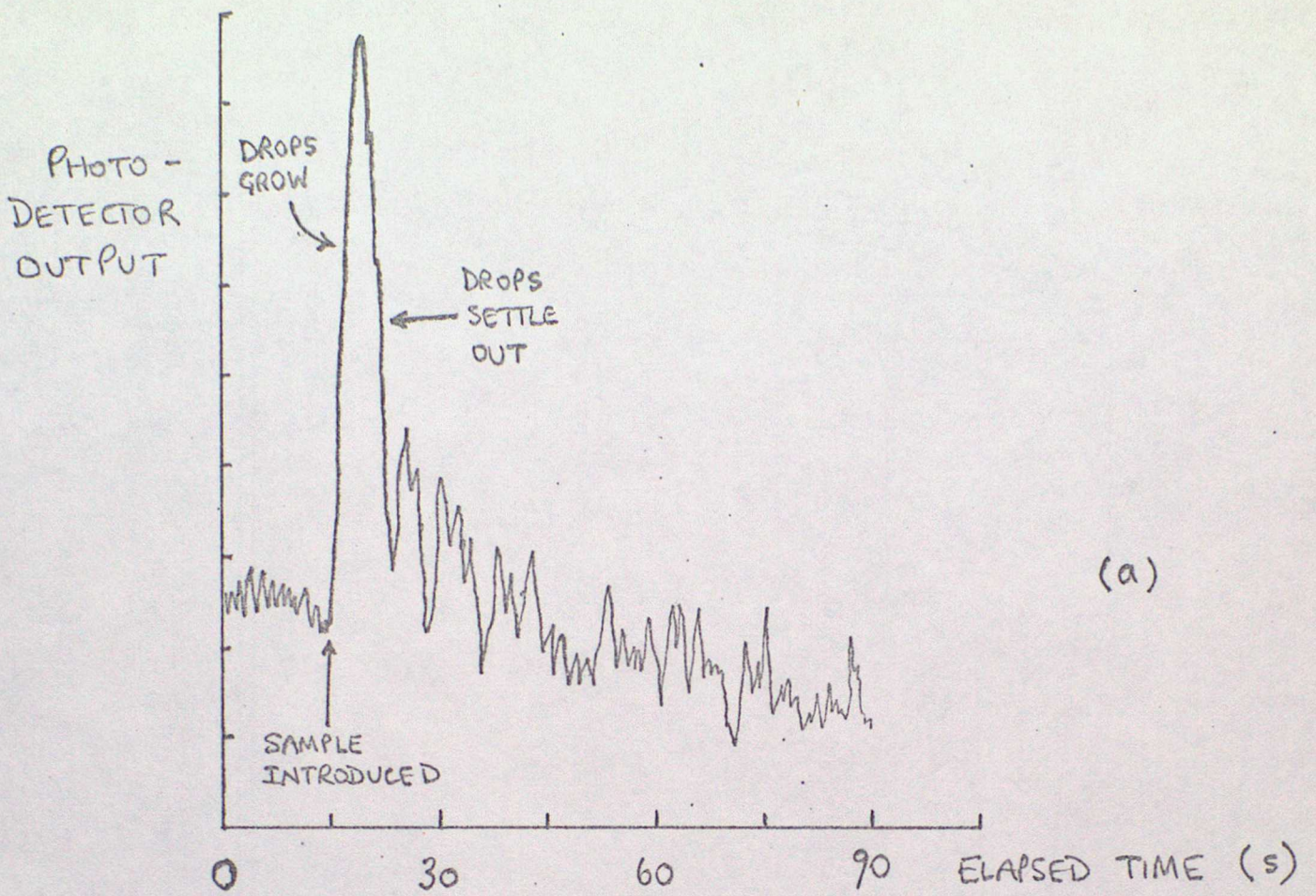


Fig 4 a) Example photodetector output from TGDC (proportional to number and size of drops) as a function of time.  
 b) An example of an activation spectrum measured with a TGDC.

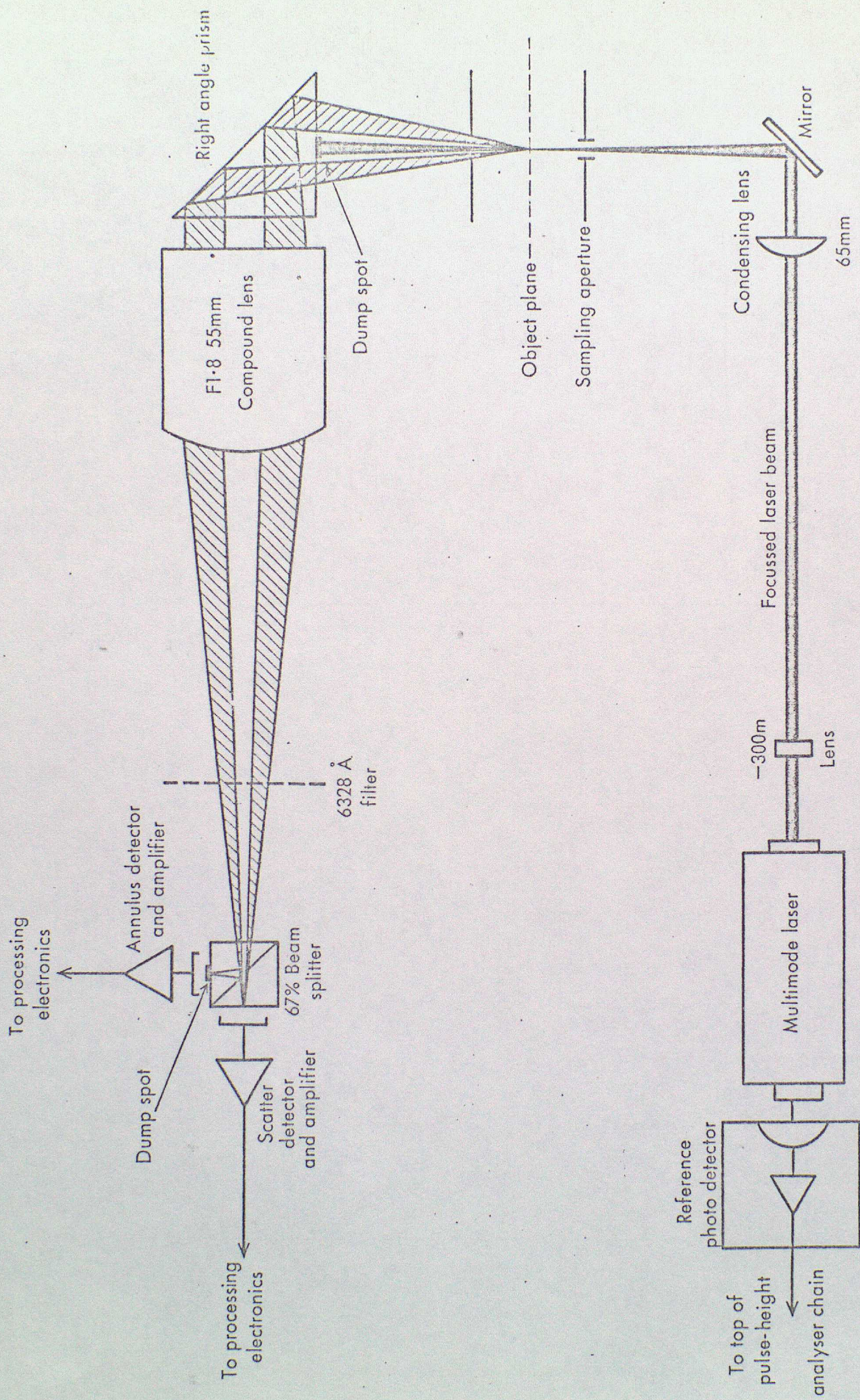


Figure 5. Forward scattering spectrometer probe optical and detector system

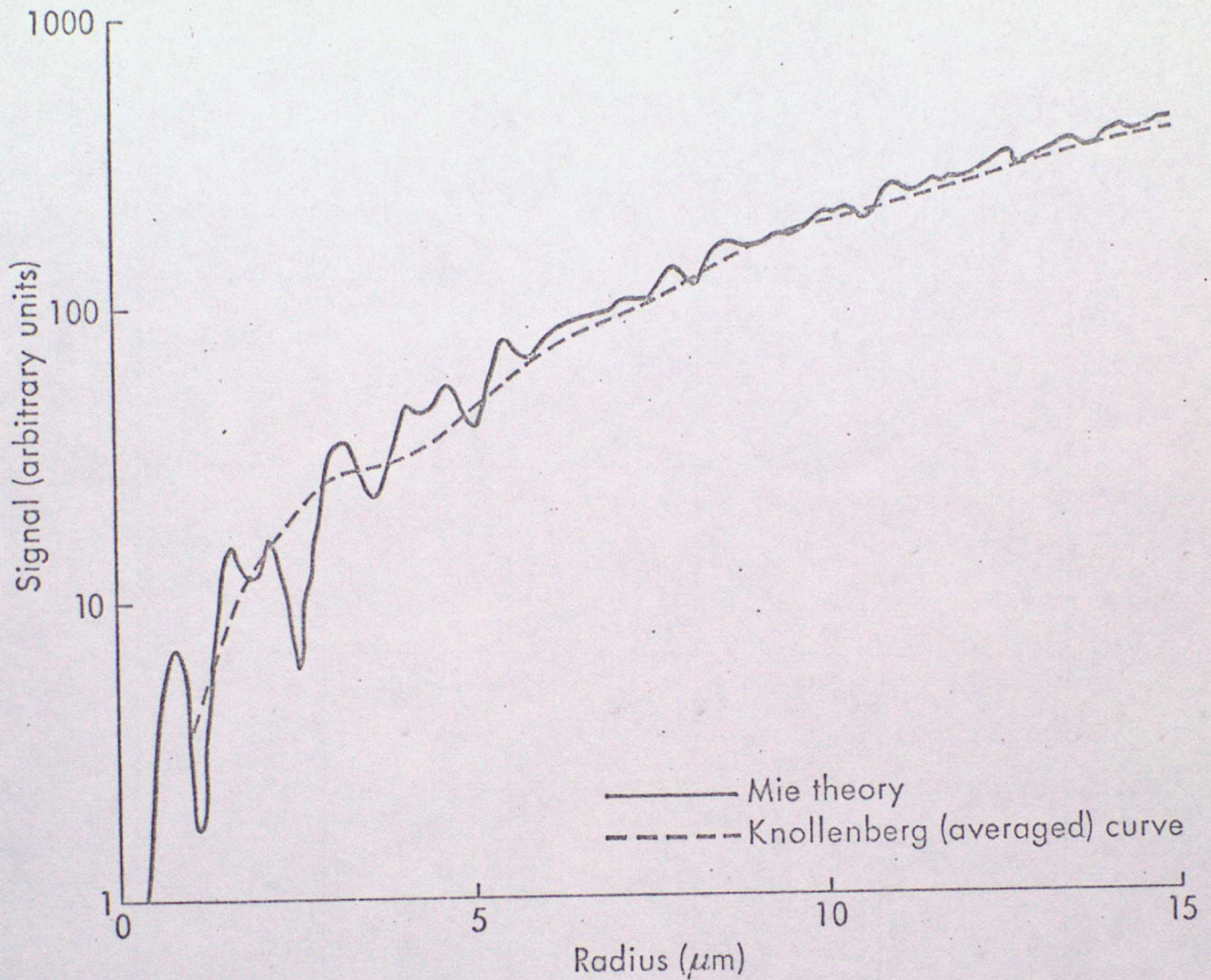


Fig 6 Intensity scattered into the range of angles  $7.1^{\circ}$ - $15.3^{\circ}$  from a spherical droplet of radius  $r$  at  $0.63 \mu\text{m}$ . Also shown is the makers calibration curve. (ASSP).

PLOT NO.4

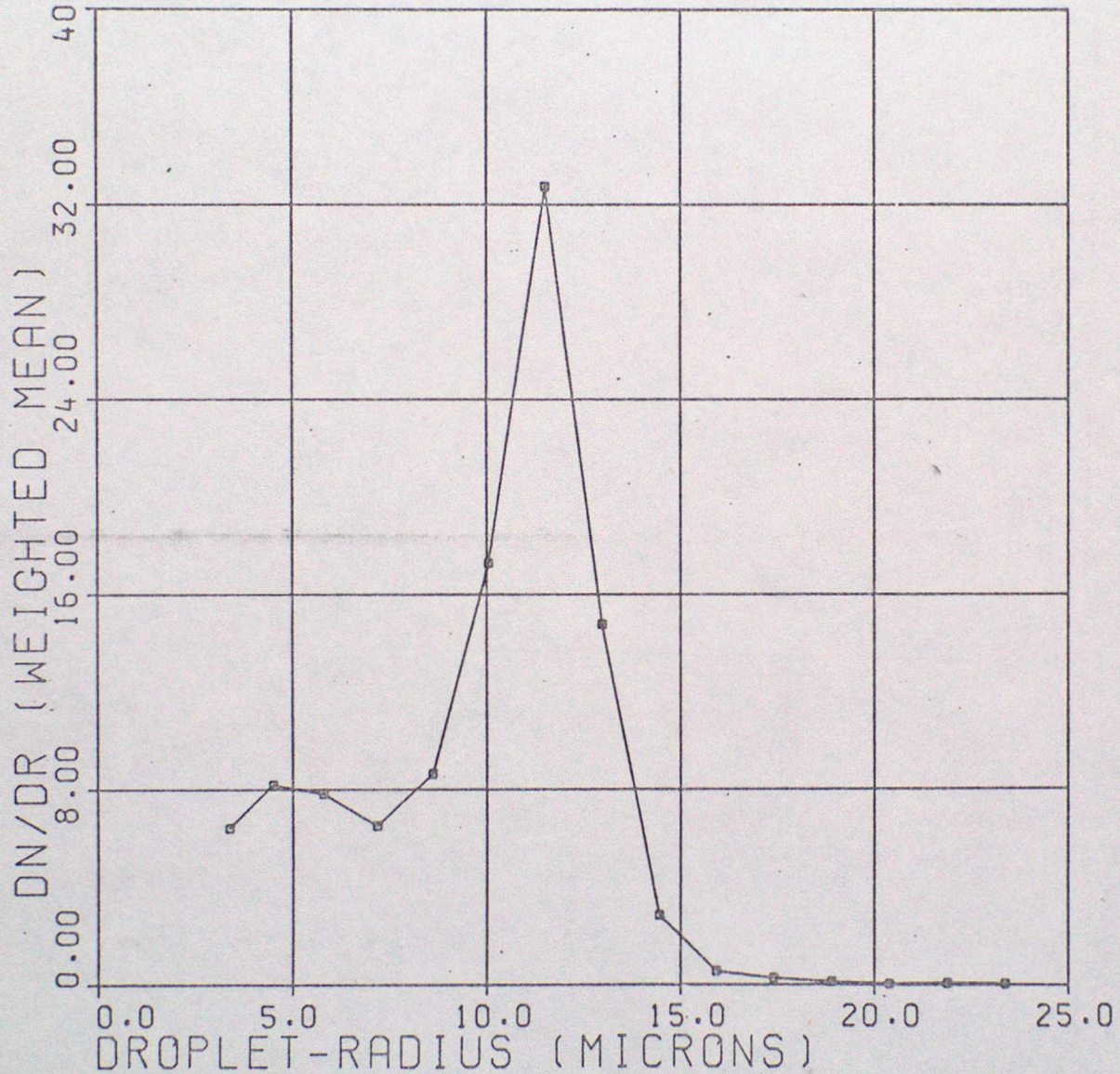
RUN 9.1

J/W COR APPLIED

H526B 22/7/82

ASSP MEAN DROPLET SIZE SPECTRUM

WEIGHTING FACTOR = CONTL (CM-3)



FIRST RECORD AT 143105 . LAST RECORD AT 143347

Fig 7 a Example averaged droplet spectrum measured by the ASSP in stratocumulus

PLOT NO.12 RUN6.2B

H528 29/7/82

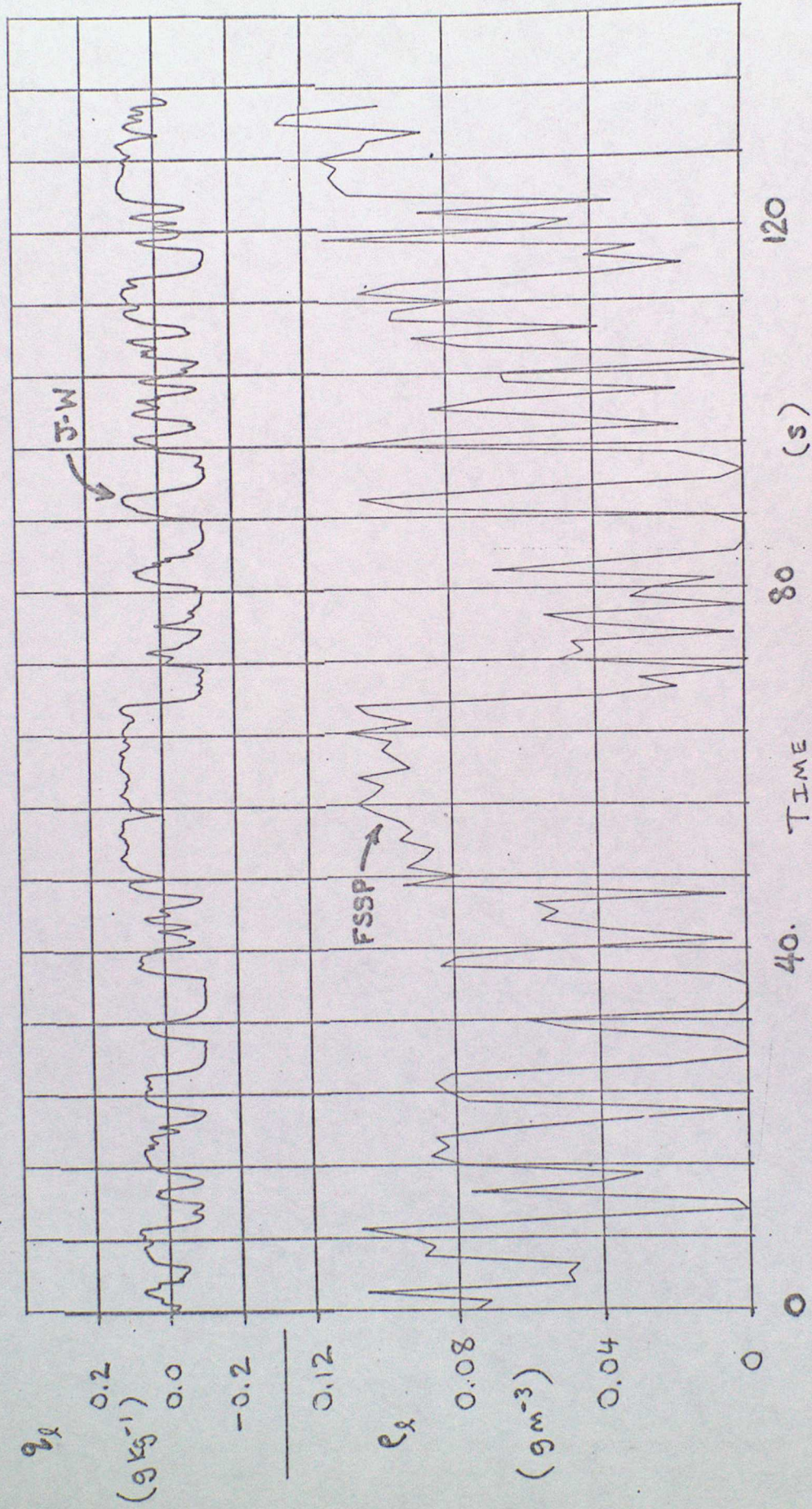


Fig 7 b A comparison of liquid water content measured by the FSSP (by integration of 1s averaged spectra) and the J-W probe (see section 3.1).

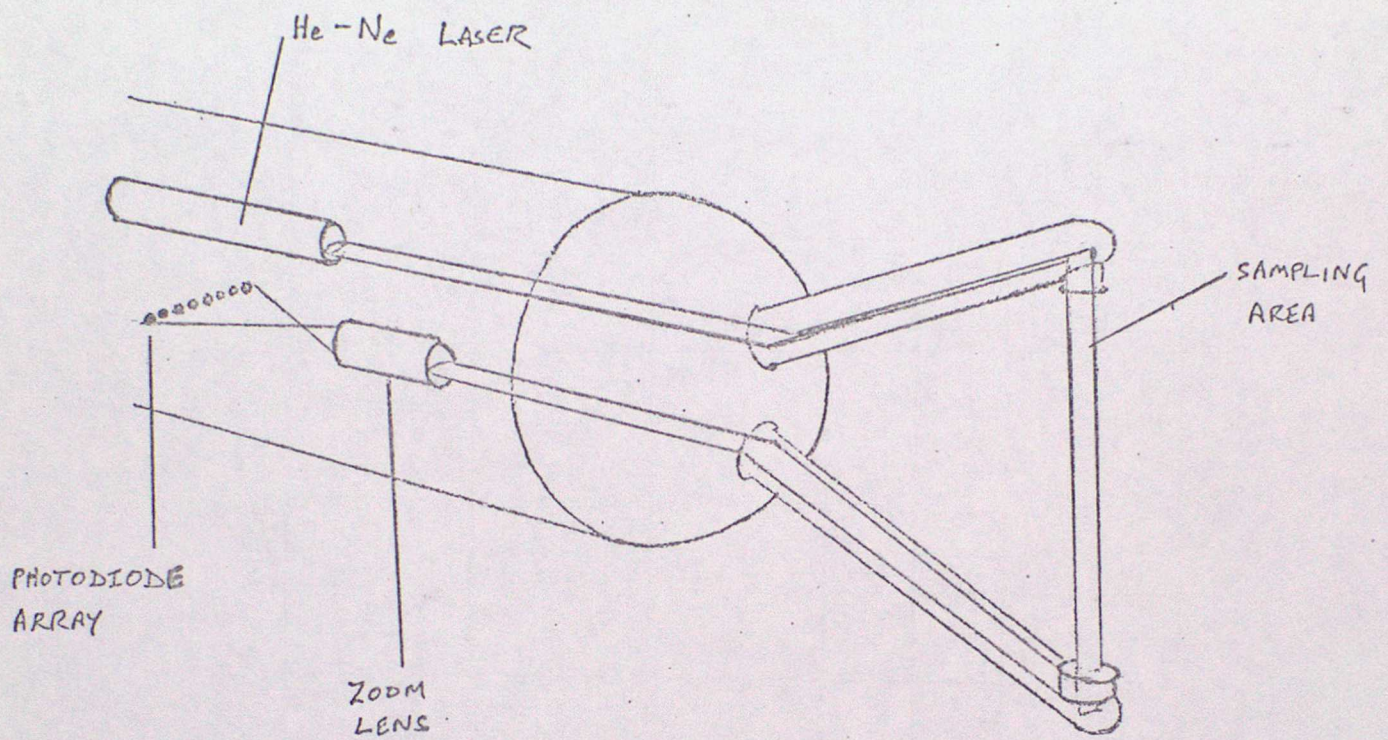


Fig 8 Optical layout of the PMS 2-D probes.

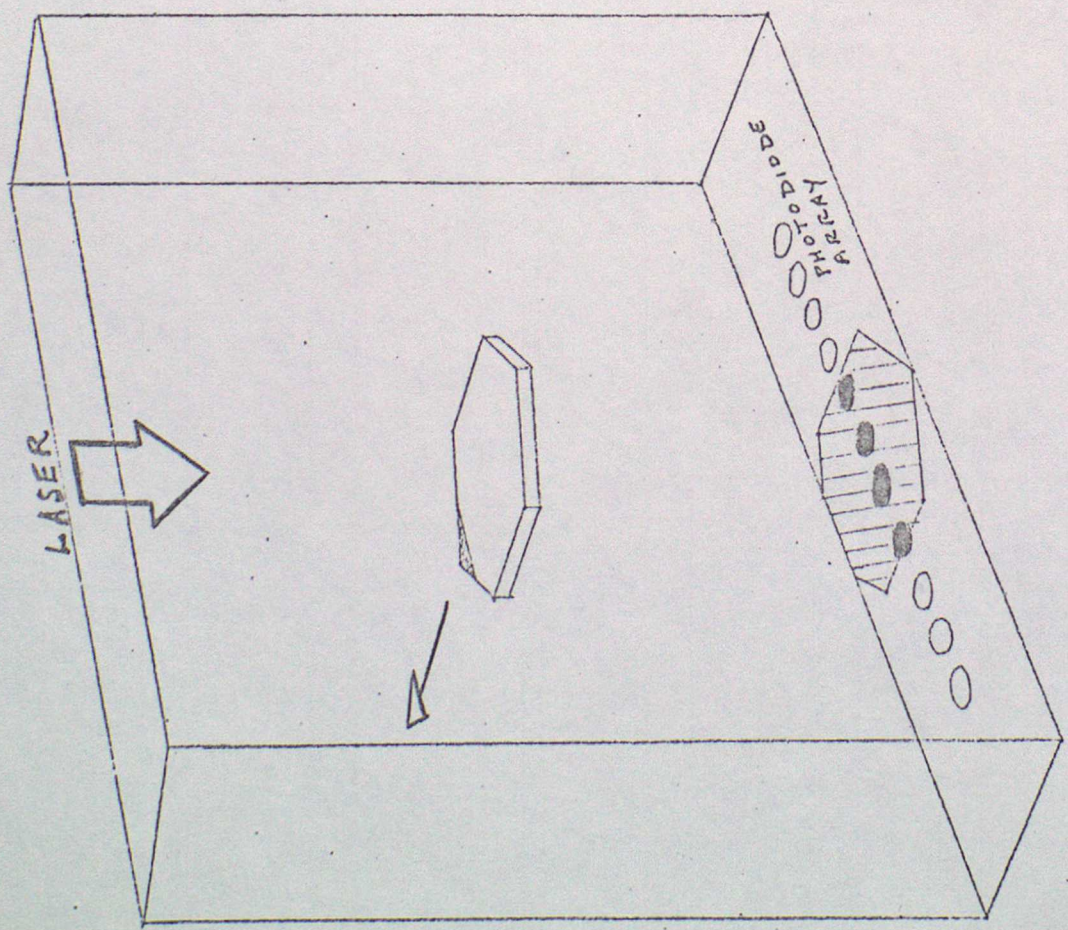
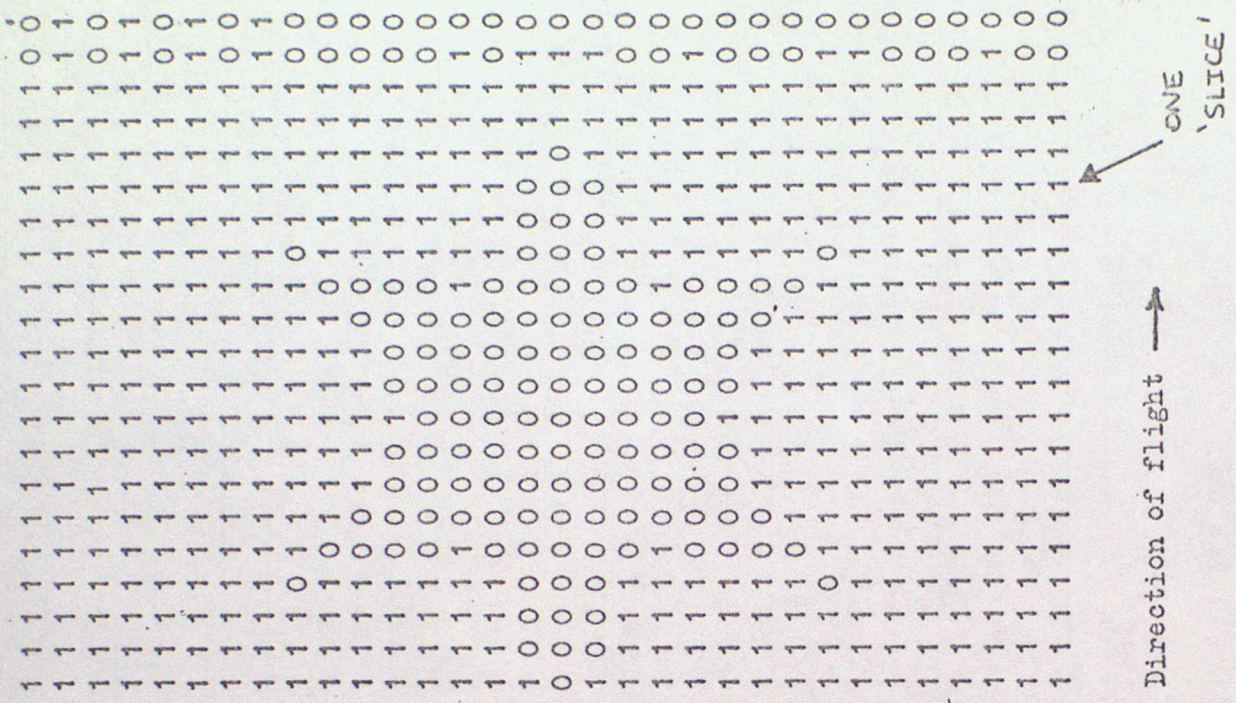


Fig 9 Formation of shadowgraph and digitized image in 2-D probes.

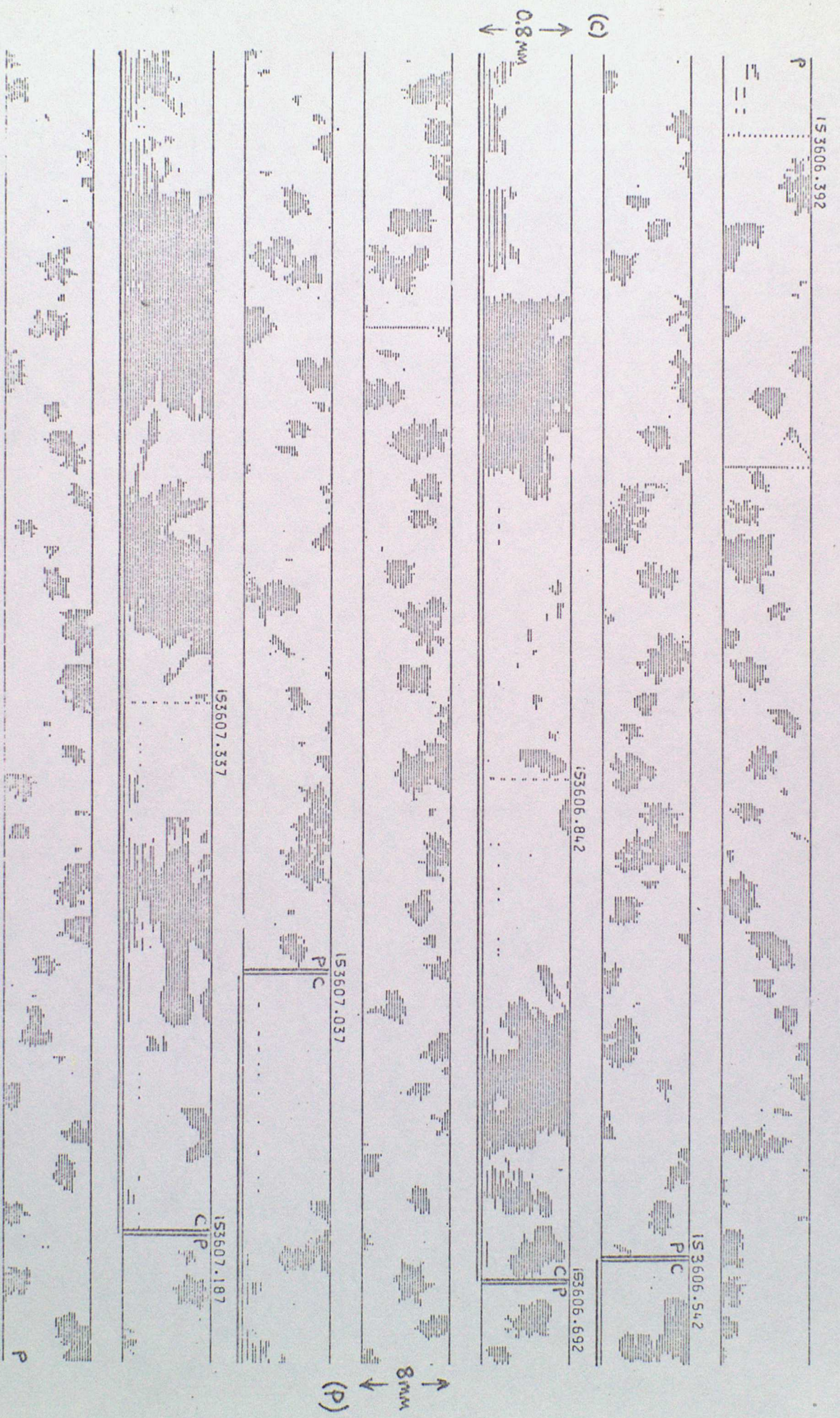


Fig 10

Example of 2-D cloud (C) and precip. probe (P) images from part of a flight on 21 Dec 1983 in precipitating Cu cong. The record is continuous with C and P data interleaved. C-probe data has a double underline. Length scales for both probes are indicated.

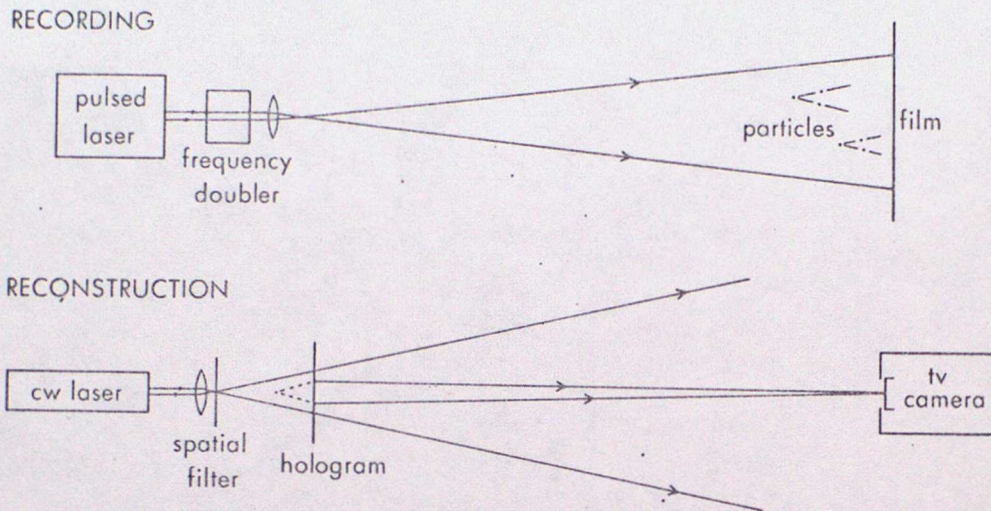


Fig 11 Operating principles of the holographic particle sizing system.

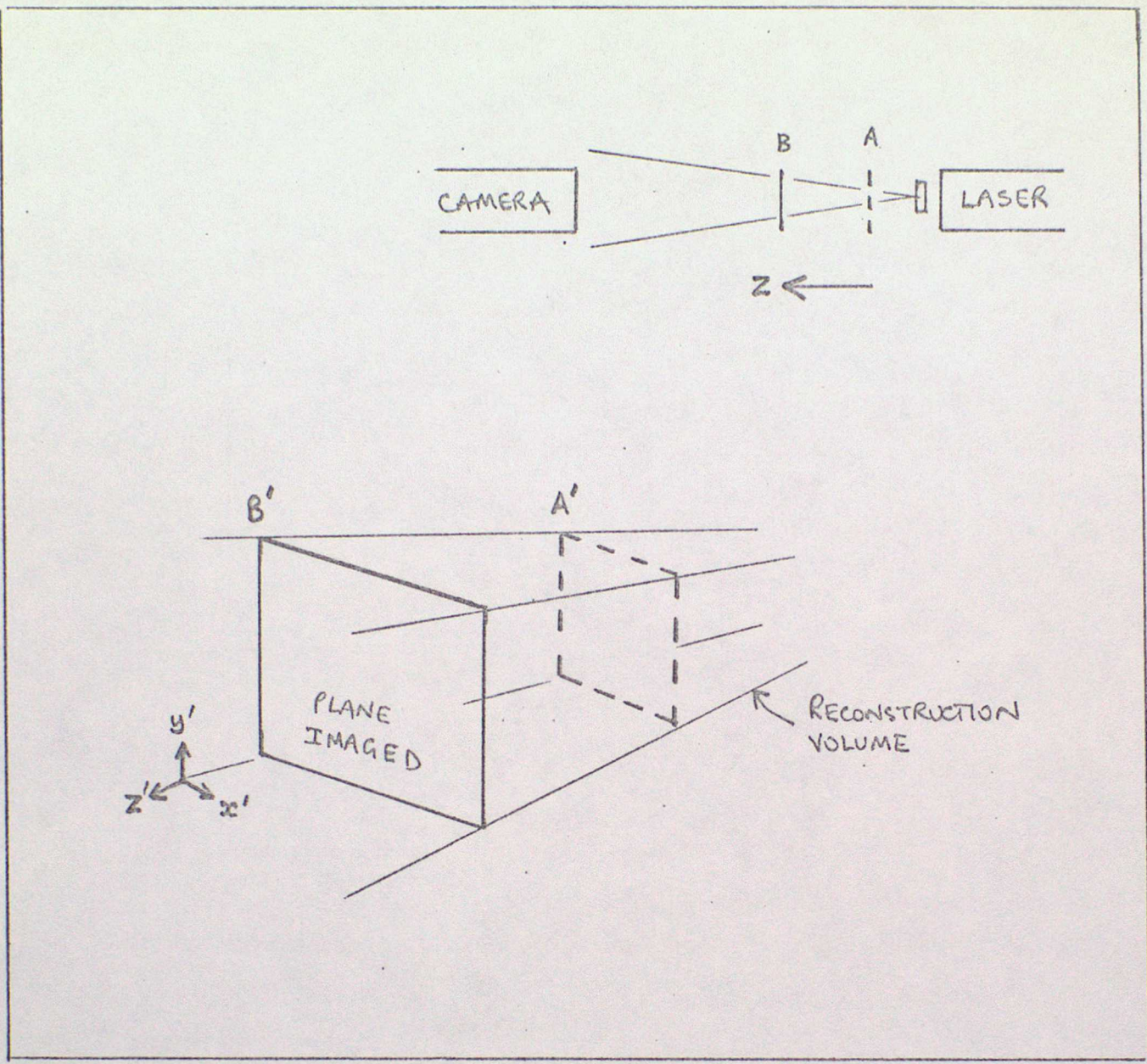
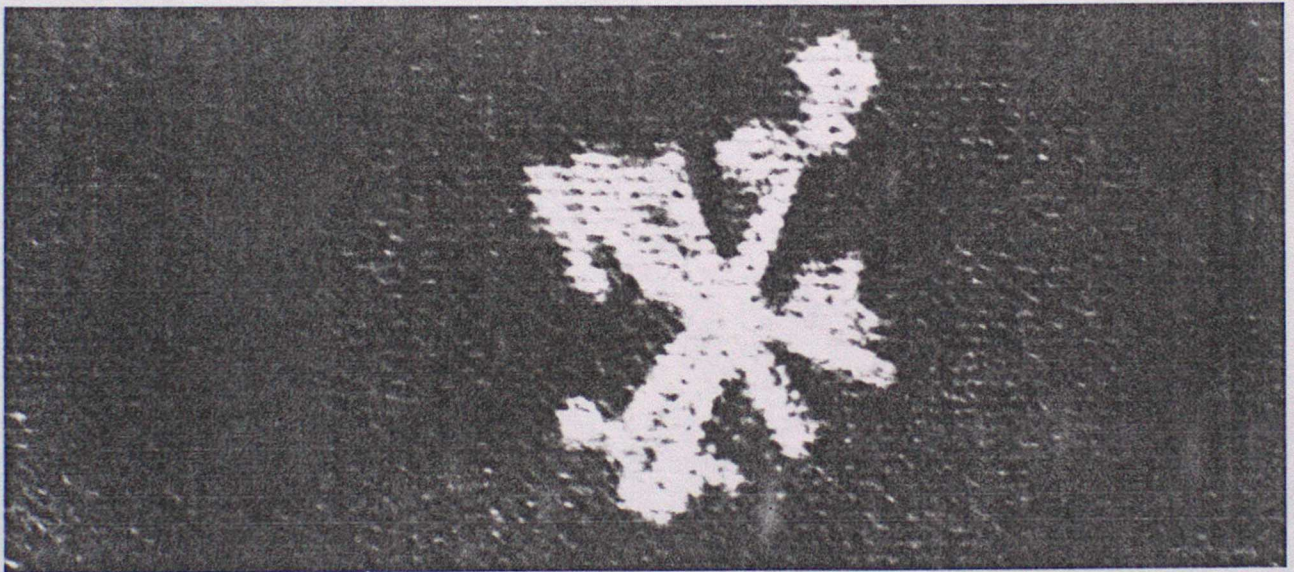
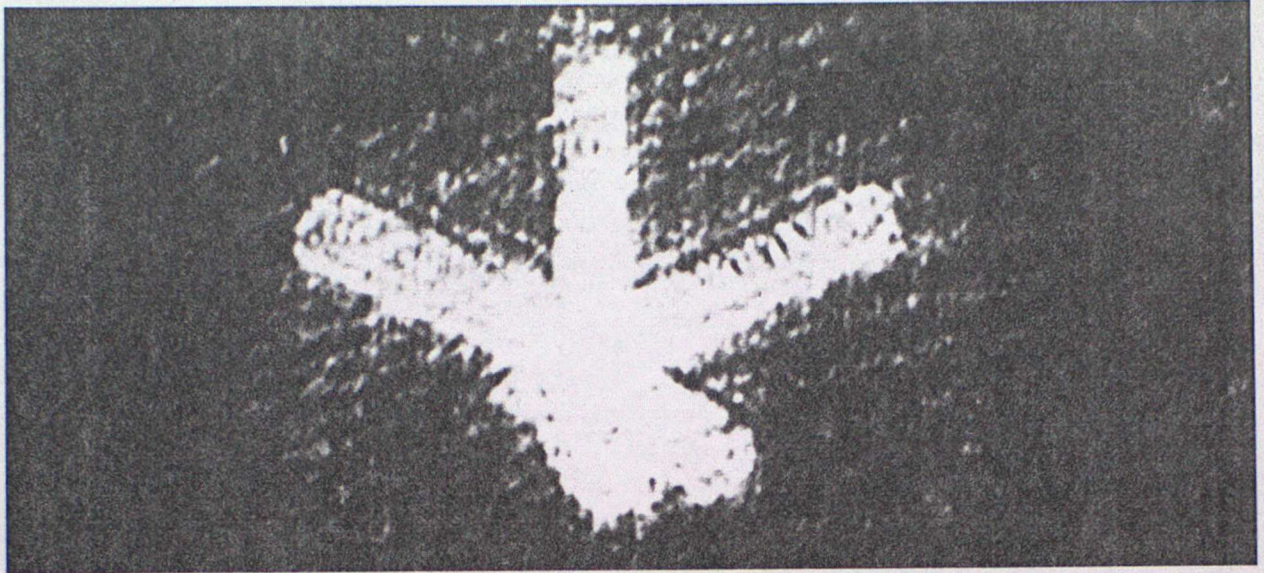


Fig 12 Successive xy planes are imaged as the hologram is moved in the z-direction.



0 500  $\mu\text{m}$

Fig. 13 Examples of reconstructed holographic images. These show ice crystals observed at the base of a Cs layer,  $T \approx 230\text{K}$ . (From Ref 11).

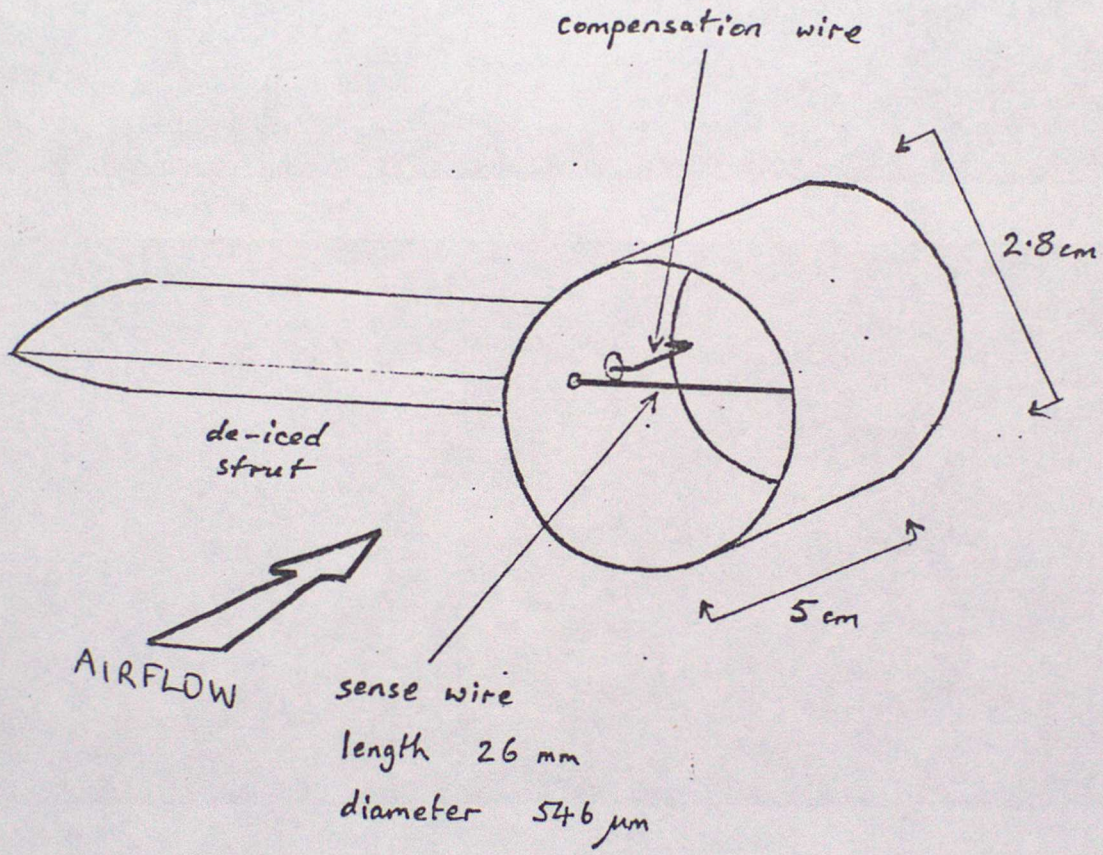
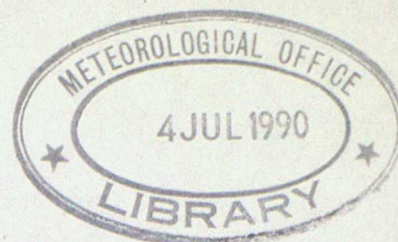


Figure 14. The Johnson-Williams sensor head.

## WEATHER MODIFICATION



### 1. Physical basis

Discussions of ways of deliberately changing the weather to benefit mankind has been going on for a very long time. However, it is only in the last few tens of years that practical means have become available which may make this possible. Here we consider for the most part techniques which affect the microphysical processes in clouds and which have been tried repeatedly in the field, often with considerable success to modify weather over areas from tens to thousands of square kilometers.

Clouds form when moist air is cooled below its dew-point and condensation takes place upon sub-microscopic hygroscopic particles. The cooling, of course, may be the result of radiation to space, of convective ascent of buoyant air masses originating as cool air moves over a warm surface, of meso-scale or synoptic-scale motions which produce widespread lifting, or of the mixing of two air masses at different initial temperatures and humidities.

As the cloud grows, the droplets increase in size and tend towards a single radius which increases with height above cloud base. Particularly if there are very large concentrations of condensation nuclei the resulting cloud is likely to be colloidally stable and no precipitation may result even if the cloud grows quite large. Such clouds often form, grow and evaporate over inland areas without producing any significant rain. However, if the concentrations of nuclei and droplets are relatively low and there are a few giant nuclei resulting in a few much larger than average droplets, both of which conditions are common in maritime air, the larger droplets will fall and grow by collecting the smaller ones in their path. Provided the cloud is deep enough, they will grow to sufficient size to fall to the surface as rain.

If the cloud grows tall enough to exceed the height of the freezing level the droplets will normally supercool, and indeed this supercooling can occur in natural clouds down to temperatures of  $-20^{\circ}\text{C}$ . Ultimately, however, and always before they reach a temperature of  $-40^{\circ}\text{C}$ , the droplets will freeze. Alternatively, ice crystals may form directly from the vapour upon freezing nuclei. As soon as ice particles of any form appear in the presence of supercooled water droplets, the cloud becomes colloiddally unstable because the saturation vapour pressure over ice is less than that of water at the same temperature and hence ice particles grow rapidly at the expense of the water droplets. As long as the concentration of ice particles is small in comparison to that of water droplets, the former will grow quite large by this process and commence to fall, collide with and collect the water-droplets and other smaller particles in their path. Again, provided the cloud depth is sufficient, the particles will grow large enough to precipitate to the surface.

These two natural precipitation processes are of immediate interest to the weather modifier because, by adding quite small concentrations of giant condensation nuclei or of ice nuclei to clouds where their absence or low natural concentrations prevents or renders inefficient the development of precipitation, it is often possible to augment the amount of precipitation which would otherwise occur.

There is another situation which is of interest from the viewpoint of weather modification. This is when a convective cloud becomes significantly supercooled but where its growth is limited by atmospheric stability conditions and where comparatively small increases in cloud buoyancy could result in considerable growth of the cloud giving greater precipitation. In such growth-limited supercooled clouds where the concentration of natural ice nuclei and resulting ice crystals is not excessive, the addition of very large numbers of artificial ice nuclei in the upper levels can result in complete glaciation of substantial regions of supercooled water. The release of the latent heat of

freezing can produce sufficient buoyancy to produce considerable cloud growth and significant increases in precipitation.

These mechanisms have all been explored with varying degrees of success and the results or typical experiments will be described briefly. It is important to realize that on average the increases that can be expected from precipitation enhancement techniques are relatively modest and are often well within the natural variability of the precipitation it is hoped to change. Hence quite sophisticated statistical techniques are essential to determine whether any changes in precipitation which are observed are associated with the modification treatment or merely part of the natural fluctuation.

## 2. Precipitation enhancement in warm clouds

In tropical or semi-tropical countries many of the potential rain-producing clouds are convective in nature and their tops often do not exceed the height of the freezing level. This is particularly true in conditions when little natural rain falls and there is the greatest interest in precipitation enhancement. Hence, the possibility of increasing rainfall by enhancing the efficiency of the collision-coalescence process is of considerable concern. When clouds develop whose tops do not significantly exceed the height of the freezing level, it may be possible to initiate or enhance the effectiveness of the precipitation process by seeding them with water droplets or hygroscopic particles. Only a limited number of experiments have been carried out to test the effectiveness of the technique because it is clear that large masses of seeding material are necessary. If seeding is to be carried out with  $10\ \mu\text{m}$  diameter salt particles of density  $2\ \text{g cm}^{-3}$  and each particle ultimately grows to a 2.5 mm diameter raindrop, it can readily be calculated that the original particles will increase in mass by a factor of nearly  $10^7$ . One mm of rain over an area of  $1\ 000\ \text{km}^2$  has a mass of  $10^9$  kg so that if it is to be induced by seeding it would be necessary to employ 100 kg of seeding material. The situation would be much more favourable if a "chain reaction" occurred, in which drops break up after first growing by coalescence to a large enough size and the fragments then serve as growth centres for new large droplets.

However, little evidence exists that such a process occurs extensively in natural clouds. In spite of these limitations, a few encouraging experiments have been carried out.

Braham et al carried out experiments in which up to 400 gallons of water was released from an aircraft into the tops of individual clouds. In each case the seeded cloud was chosen at random from a pair of essentially similar clouds and the differences studied between the behaviour of each cloud of the pair. In most cases both treated and untreated clouds produced rain at some time after they were first examined; however, the treated clouds rained much earlier than those untreated although the amount of rain they produced appeared the same.

Indian workers have carried out by far the greatest number of salt seeding experiments aimed at increasing precipitation from convective clouds. Biswas et al reported the results of long-term programmes. They used salt as a seeding material, ground to about  $10 \mu\text{m}$  diameter dispersed by blowers at a rate of about  $2.5 \text{ kg min}^{-1}$ . All experiments were randomized with upwind control areas and showed increases of up to 40% in precipitation associated with the seeding.

### 3. Precipitation enhancement in cold clouds (microphysical)

In the most commonly employed technique for seeding cold clouds (those rising above the height of the freezing level), moderate concentrations of ice forming nuclei have been introduced in order to enhance the efficiency of the microphysical process described earlier. As the simplest possible hypothesis of the effect of seeding, it might be assumed that one ice nucleus produces one raindrop. Depending upon the seeding material employed and the temperature level at which it is introduced or becomes effective, one gram of material may result in the production of  $10^{12}$  to  $10^{15}$  ice nuclei. Hence, if each nucleus results in the formation of a 2.5 mm diameter raindrop, less than 100 g, and possibly less than 0.1 g of material could suffice to produce 1 mm of rain over an area of  $1\,000 \text{ km}^2$ .

It would be impossible to review here the very many precipitation enhancement projects which have been carried out throughout the world in the past few decades but two well documented cases will be examined.

The first Israeli experiment commenced in 1961 and continued in all subsequent winter seasons until 1967. A cross-over design was employed in which either a northern area or a southern one was seeded on a random basis with a buffer zone in between never being seeded. Seeding was from an aircraft flying just off the coast, dispersing silver iodide smoke into the bases of the clouds which approached from the west. An increase in rainfall of 15%, significant at about the 5% level, was achieved over the whole target area with greater and more significant increases in the interior region of the northern area. In the second Israeli experiment, which ran from 1969 to 1975, the seeding line for the northern area was moved inland somewhat, allowing a control area to be available for statistical analysis. Using this control area in a preliminary analysis, Gagin and Neumann deduce that an increase of the order of 15%, significant at better than the 5% level, occurred in the northern target area. The increase was found to be greatest when cloud top temperatures were between -12 and -25 C.

A long-term randomized experiment was carried out in Tasmania between 1964 and 1970 over the catchment area of a hydroelectric authority. As reported by Smith et al there were 54 seeded and similar number of unseeded periods each of 10-18 days duration with the experiment running only on alternate years. Seeding with silver iodide smoke was carried out from aircraft either at cloud base or at the  $-5^{\circ}\text{C}$  level or above, depending upon cloud type. Results were analysed separately season by season. The authors concluded that seeding increased autumn rainfall by 20-40%, significant at the 2-4% level, that the winter rainfall increased by about 10%, significant at about the 0.1 level, but that any changes during spring or summer were not significant.

#### 4. Precipitation enhancement in cold clouds (dynamical)

It was noted very early in the experiments in which cumulus clouds were seeded that occasionally marked growth occurred. However, it is only comparatively recently that deliberate attempts have been made to cause such growth by massive seeding of convective clouds with a view to obtaining greatly enhanced precipitation. The physical principle on which the experiments are based is simply that when large quantities of supercooled water can rapidly be caused to freeze, the release of the latent heat of freezing will produce sufficient buoyancy to enable the cloud to grow much taller than would otherwise be the case. Greater cloud depth will in turn allow greater growth to take place on precipitation particles, longer cloud lifetime and more precipitation.

In the Florida Area Cumulus Experiment individual cumuli forming over an area of about  $10^4 \text{ km}^2$  were seeded by dropping pyrotechnic flares containing large quantities (100 - 1 000 g per cloud) of silver iodide into the upper levels of active supercooled clouds on days for which a simple numerical model suggested that such a procedure would result in significant cloud growth. It was claimed that significant increases in precipitation were obtained, particularly in cases where merging of adjacent clouds followed seeding. Woodley et al report the use of more efficient pyrotechnic devices in 1975 and give the results of further statistical analyses. For certain methods of analysis and certain categories of clouds (as defined by whether or not their radar echoes showed significant motion) positive, statistically significant effects are reported.

The North Dakota project was conducted in the summers of 1969-1972 and was intended to test the effects of seeding upon both rainfall and hail. The seeding rate was adjusted from 10 or 20 g or silver iodide for rain stimulation from small cumuli to continuous seeding rates exceeding  $1 \text{ kg hr}^{-1}$  for hail suppression if the project meteorologist judged a storm to be

approaching hail intensity. The experiment was randomized with 25% of days reserved as non-seeded days. The analysis suggested that on days on which a cloud model predicted dynamic growth would follow seeding there was a significant increase in frequency of rain events as well as an increase in actual rainfall in the target area.

5. Cold cloud precipitation enhancement (conclusion)

Of the many large-scale area experiments (order of  $10^3 - 10^4 \text{ km}^2$ ) in which moderate concentrations of artificial ice nuclei were dispersed in clouds, only a few have demonstrated at a satisfactory statistical significance level that seeding increased precipitation. The increases in precipitation were typically 10-20% when averaged over the target area for the full operating season. In many experiments no statistically significant increases were observed and in a few experiments there appear to have been decreases in precipitation following seeding.

These apparently contradictory results may well relate to the fact that clouds supercooled to the same extent but which have different microstructures and different ice budgets could be expected to respond in a different manner to a given seeding technique. The high colloidal stability of the winter stratiform clouds in Tasmania of the winter orographic clouds in central USA and the winter "continental" cumuli of Israel seem to render these clouds more favourable to seeding for microphysical effects than is true for maritime cumuli. These latter clouds have been found to produce naturally high ice particle concentrations at some stage in their life cycle and it may well be that the addition of additional ice nuclei would be detrimental, resulting in either no change in precipitation or possibly a decrease. It now seems that the water-ice budget of the clouds is probably one of the more crucial factors governing the release of precipitation. Thus it is in those cases when the process of ice nucleation and particle growth are slower than the rate at which moisture is released in clouds by the updraught that seeding can be expected to produce positive effects.

## 6. Artificial Dissipation of fog

Fogs are traditionally classified according to the cause of their formation; however from the standpoint of dispersal it is more relevant to classify them according to their constitution and temperature, since the method of modifying them depends upon these factors rather than the fog's origin. Ice fog is a suspension of small ice particles generally only occurring at temperatures less than  $-30^{\circ}\text{C}$ . Studies of this fog have been made and these have resulted in some practical recommendations for decreasing its occurrence by minimizing the production of moisture from human activities. However, no practical method has yet been found for modifying an ice fog once it has formed. Supercooled fog is composed of water droplets which remain unfrozen although their temperature is below  $0^{\circ}\text{C}$ . Provided the temperature is not too low and there is a relative absence of ice nuclei to stimulate freezing, such fogs are naturally stable. They can be modified quite readily by introducing artificial nuclei. The third type, warm fog, consists of water droplets at above freezing temperature. It is the most common type of fog and is difficult to disperse artificially: nevertheless, a number of methods have been developed which are successful.

Considerable effort has been devoted by many groups to the development of warm fog dissipation techniques based upon seeding with hygroscopic chemicals. The basic idea is that if hygroscopic substances in the form of either dry particles or solution droplets are released within a fog they absorb water vapour from the air, causing the fog droplets to evaporate. The hygroscopic particles themselves grow large enough to precipitate out of the system. Kunkel and Silverman have explored the best chemicals to be used for this purpose and have considered methods of encapsulation of the material. Theoretical models have been used to determine the optimum particle size and seeding strategy. Environmental considerations are also of major importance in hygroscopic seeding, since large quantities

of material may be necessary which ultimately is precipitated to the surface, and encapsulated urea has been put forward as the optimum choice. Successful development of a seeding agent and its use in small-scale field trials has not yet been followed by similar success over a large airport runway. Delivery of the seeding material at the right time and place to effect clearing more-or-less continuously of a runway some distance downwind from the seeding line has not proved reliable. More widespread seeding, which might be effective in clearing fog, is economically not practicable.

Another method that has been developed for clearing warm fog involves mixing of the relatively dry air often found above radiation fogs or stratus decks down into the fog or cloud layer. The method involves the use of the downwash from a large helicopter stationed just above the top of the fog. It has successfully created holes and clear lines in fogs up to 100-150 m thick. It has had operational success in special circumstances, such as helicopter rescue and supply operations in which the helicopter is able to land through holes in the cloud which it has cleared for itself.

At the present time the only major warm fog dissipation technique being used operationally is the thermal system in which sufficient thermal energy is used to evaporate the fog droplets and to raise the temperature of the air sufficiently to accommodate the additional water. Operational systems involve large, permanent, expensive installations, they consume large amounts of fuel and are practical for only the busiest and largest airports where fogs are common occurrences. In addition to two French installations a prototype system has been constructed in the USA, after extensive small-scale testing and engineering trials. A key attribute of this new system is the use of propellers to distribute the heated air.

Warm fog dissipation methods based upon the use of artificial electrification to increase the natural rate of coalescence and precipitation of fog droplets or the use of laser heating have not so far led to practical applications.

The dissipation of a supercooled fog is achieved by seeding it with material which produces ice crystals which, because of the difference in vapour pressure over ice and water at the same temperature, grow by deposition of vapour supplied by the fog droplets which thereby decrease in size. The reduction in fog droplet size itself increases the visibility but the main effect occurs when the ice crystals grow to such a size that they fall out. While the physics of the process has some similarities to that in which hygroscopic particles are used to clear warm fogs it is much more effective in that orders of magnitude less material is required to form effective ice nuclei than to form effective hygroscopic growth centres. A number of operational procedures for clearing supercooled fog have been developed, including seeding from an aircraft with dry ice or silver iodide or from extensive ground installations in which the expansion of propane gas produces sufficient cooling to generate large quantities of ice crystals. These methods of modifying supercooled fogs are in fairly wide use today, but are limited to the relatively few regions of the world where supercooled fog is a sufficiently important operational hazard. Operational clearing is conducted in France, Germany and Norway as well as in the USA and USSR.

#### 7. Hail suppression

Worldwide losses of agricultural production due to hail damage are estimated to be in excess of  $2 \times 10^9$  dollars annually. However, in contrast to other weather-related disasters such as drought, floods, hurricanes etc., hail losses tend to be very localized. The interest in hail suppression is worldwide as shown by the results of a survey conducted by WMO in 1972.

Hailstorms are complex meteorological phenomena which have extreme variability in time and space and this makes it very difficult to assess the results of any programmes aimed at their modification, several efforts in operational hail suppression have been carried out over the last three decades. However, because of the fundamental difficulty of evaluation, it has only been possible to provide a limited assessment of the effectiveness of such programmes.

Many hypotheses have been proposed for suppressing hail. Those which have received widest discussion are:

- (i) Enhancement of competition among hailstone embryos;
- (ii) Glaciation of the medium on which hailstones grow;
- (iii) Promotion of coalescence, followed by freezing; and
- (iv) Dynamic effects, e.g., destruction of cumulonimbus clouds by initiation of downdraughts.

Glaciation, meaning conversion of supercooled cloud water to cloud ice requires unrealistically large amounts of ice nucleating agents, and promotion of coalescence concepts need very large amounts of hygroscopic material. Dynamic effects, while potentially very important, have not been sufficiently studied to yield a useful working hypothesis. This leaves enhanced competition among hailstone embryos as the only hypothesis which is generally accepted as showing promise for success based on the current understanding of hailstorms. This hypothesis can be simply stated as follows:

"If the number of growing hailstone embryos can be increased by a large factor ( $\sim 100$ ), then the competition for the available water supply prevents any embryos from growing large and thus the resulting hailstones either melt before reaching the ground or are too small to cause any damage".

To implement this hypothesis it is necessary to increase the concentration of hail embryos in the hail growth zone. To produce this effect by means of seeding with ice nuclei requires the production of additional hail embryos to

compete with the natural embryos for the available supply of supercooled water in the hailstone growth region. The seeding agent must act when and where the embryos form, and this may be at some distance from the hailstone growth region.

The most favourable regions for rapid growth of large hailstones are those with moderate to strong updraughts ( $> 12 \text{ m s}^{-1}$ ), appreciable liquid water concentrations ( $> 2 \text{ gm}^{-3}$ ), and low temperatures ( $\leq -15^{\circ}\text{C}$ ). Embryo formation on the other hand is favoured by weaker updraughts, say  $5 \text{ m s}^{-1}$ . In much stronger updraughts, newly formed ice particles would be carried up to the cloud top before growing large enough to become hail embryos. Two types of embryos have been distinguished. One type results from the freezing of supercooled raindrops, the other from the growth of graupel. Which type predominates in a storm presumably depends upon cloud-base temperature, updraught speed, liquid water concentration, cloud droplet size spectrum and activity of the ice nuclei which are present. Analysis of hail suggests there is a higher percentage of frozen-drop embryos in the large stones compared with small stones.

Nearly all hail suppression projects rest upon the assumption that hail is due, at least sometimes, to a deficiency of natural ice nuclei in the atmosphere. Nevertheless, no correlation between hail occurrences and variations in the concentration of natural ice nuclei, which often vary by a factor of ten or more, has been noted. While it is still possible that there is a threshold concentration required to suppress hail, the threshold (if it exists) probably exceeds the maximum observed concentration of natural ice nuclei. Therefore, if hail processes are to be modified by addition of ice nuclei, the concentration of artificial nuclei must be larger than the typical concentration of natural ice nuclei by a large factor, of perhaps 1 000. Such changes have in fact been produced.

In cases where hail forms on graupel embryos, the concentration of graupel can, in principle, be increased by seeding early in the lifetime of new convective cells. A generalized concept of seeding new growth regions for this purpose has emerged independently in several hail projects, despite lack of precision in estimating the subsequent trajectories of such additional graupel particles and in ignorance of whether they in fact would enter the important regions to compete with the natural embryos.

Important questions have been raised about the required dispersion of the nuclei. For example, line sources (rockets, droppable pyrotechnics and airborne generators) offer an advantage over point sources (exploding shells). However, rockets and shells offer a chance for very rapid response to threatening situations. Also, problems of deactivation of nuclei by sunlight and by wetting in warm cloud have been raised, but these problems can be avoided when the seeding agent is injected directly. When airborne or ground-based generators are used, deactivation can be reduced by careful control of the chemical composition of the seeding agent.

The implementation of the seeding concepts in specific hailstorm situations requires very careful attention to the storm structure. In storms where each cell has a simple vertical structure and the hail embryos grow into hailstones near their place of origin, seeding in each new cell before the natural hail embryos appear offers a possibility of suppressing damaging hail. In more complex and persistent storms, where hail embryos may move in a continuous stream from the embryo growth region to a quite distinct hail growth region, more subtle techniques are likely to be required.

In spite of very intensive efforts by many groups in many countries seeding effects have not been clearly identified in the physical parameters of hailstorms. It is therefore still necessary to rely mainly on statistical evaluation of a hail suppression experiment to determine the likelihood that

the variations are not simply chance fluctuations. Crop damage is ultimately the most relevant parameter, but due to the great variations among crops and their different rates of maturing during the growing season, crop damage is not recommended as a primary response variable. The relation between the variables derived from hailstone number and sizes (e.g., mass or kinetic energy) and crop damage need to be better established.

In many regions where hail damage occurs, it is the same storms which produce much of the rainfall needed by agriculture. There is no observational evidence to show whether or not seeding for hail suppression increases or decreases rainfall in the defined target area or in nearby areas. However, this is a potential problem which needs further investigation and should be built into the design of future hail suppression experiments.

#### 8. Tropical cyclone moderation

Tropical cyclones contribute significantly to the annual rainfall of many areas, but they are also responsible for considerable damage to property and for a large loss of life. Therefore, the aims of any modification procedure should be to reduce the wind, storm surge and rain damage, but not necessarily the total rainfall.

Recent field experiments in tropical cyclone modification have been directed at reducing peak wind speed; a reduction of 10 to 15 percent in the maximum winds will result in a reduction of 20 to 30 percent in the maximum force of the winds. Research relating damage to wind speed suggests that a given percentage reduction in wind speed could reduce damage by an even higher percentage. The storm surge is a function of several parameters; the principal influences are the sustained wind speed and the slope of the ocean's bottom. This suggests that in most cases a reduction in the maximum wind speed will also reduce the storm surge. It seems reasonable to suppose therefore, that if the maximum surface wind speed

could be reduced by even 10 tropical cyclone damage could be reduced very significantly.

Tropical cyclone modification experiments have been conducted by the United States in the Atlantic Ocean. They are designed to cause a reduction in the maximum wind speeds through an alteration in the location of energy released near the storm's centre. A tropical cyclone draws most of its energy from latent heat released during the convective overturing of the atmosphere. At low levels, warm moist air spirals over the tropical sea toward the storm's centre. As this air flows into the storm, it acquires additional energy from the warm ocean. Most of this air flows upward into the eyewall, a band of clouds ringing the relatively calm eye, and into the surrounding rainband clouds. The rising air releases latent heat and thus furnishes most of the energy for driving the storm. The air, already turning slowly because of the rotation of the earth before it starts its inward spiral, gathers tangential speed through conservation of angular momentum as it draws nearer the storm's centre. This results in winds of destructive violence in the eyewall region before the air moves upward and then away from the storm's core at high levels.

The area of convective-scale ascent of air from the inflow to the upper tropospheric outflow layer is small compared to the total area of the tropical cyclone, the typical value of the ratio of the eyewall convective area to the total tropical cyclone area being less than 1 percent. This has important consequences for proposed experiments since only a very small region of the storm need be modified to produce a significant result. There is good reason to believe that the location and intensity of the convective-scale ascent can be modified through use of "dynamic seeding".

Dynamic seeding may provide a means of causing changes in the location of the major vertical mass transport. The additional heat release in the ascending convective currents increases cloud buoyancy and causes more vigorous and deeper ascending motion.

Observations of tropical storms suggest that in most of the areas radially outward from the eyewall there are clouds that can be made to grow rapidly by seeding. The growth of these seeded clouds provides the mechanism for shifting the major vertical mass transport to a larger radius. The reduction in the wind speeds comes naturally from this sequence of events. Thus, air flowing inward ascends in a new eyewall region before it reaches the tangential speeds that it would have achieved had it spiraled into the old eyewall. As there is no longer a bountiful supply of warm, moist air ascending in the old eyewall, it gradually weakens and dissipates.

Numerical model experiments suggest that creating a new eyewall, reducing maximum winds and dissipating the old eyewall are feasible objectives, and that the new eyewall may prove to be a stable circulation mode for at least a good portion of a day. Calculations show, for example, that if the inflowing air can be induced to rise in enhanced convective updraughts at a radius 80% larger than that of the pre existing eyewall, the maximum winds will be reduced 30%.

In 1969 Hurricane Debbie was seeded twice over a period of several hours according to the hypothesis described above, and reductions in peak wind of 15 and 31% were observed by aircraft at 3km. Nevertheless, wind speed variations of this magnitude occur naturally in tropical cyclones, and the hypothesis of deliberate modification is not easily proven. In particular measurements made during these experiments did not allow each of the links in the chain of events described earlier to be verified. Furthermore, while other experiments have been performed, only this single hurricane has so far been seeded over a period of several hours to the hypothesis described above.

### References

- Biswas, K.R., Kapoor, K.K. and Bh.V. Ramana Murthy, 1967:  
"Cloud seeding experiments using common salt", *J.Appl.Meteor.* 6, 914-923.
- Braham, R.R., L.J. Battan and H.R. Byers, 1957: "Artificial nucleation of cumulus clouds", *Meteor.Monog.* 2, 11, 47-85.
- Changnon, S.A., Jr., R.J. Davis, B.C. Farhar, J.E. Hass, J.L. Ivens, M. Jones, A. Klein, D. Mann, G.M. Morgan, Jr., S.T. Sonka, E.R. Swanson, C.R. Taylor and P.J. Van Blokland, 1977: "Hail suppression, Impacts and Issues", *Illionis State Water Survey, Urbana, Ill.*, 427 pp.
- Dennis, A.S. and A. Kozcielski, 1972: "Height and temperature of first echoes in unseeded and seeded convective clouds in South Dakota". *J.Appl.Meteor.* 11, 994-1000.
- Dennis, A.S., J.R. Miller Jr., D.E. Cain and R.L. Schwaller, 1975: "Evaluation by Monte Carlo tests of effects of cloud seeding on growing season rainfall in North Dakota". *J.Appl.Meteor.* 14, 959-969.
- Dyer, R.M., J.R. Thompson and C. Wisner, 1977: "Dispersal of supercooled stratus clouds by silver iodide seeding, Sixth Conference on Planned and Inadvertent Weather Modification Amer. Meteor.Soc. p. 184.
- Elliott, R.D., Pierre St. Amant and J.R. Thompson, 1971: "Santa Barbara pyrotechnic cloud seeding results". *J.Appl.Meteor.* 10, 785-795.
- Fletcher, R.D., 1971: "Operational applications of fog modification", Proc. Int. Conf. Weather Modification Canberra, Amer.Meteor.Soc., 255-258.

Foote, G.B. and C.A. Knight (Eds), 1977: Hail: A review of hail science and hail suppression. Meteo Monogr No. 38, Amer.Meteor.Soc., Boston, USA, 277 pp.

Gagin, A. and J. Neumann, 1974: "Rain simulation and cloud physics in Israel". Weather and Climate Modification (W.N. Hess, Ed.) New York, Wiley p. 454-494.

Gagin, A. and J. Neumann. 1976: "The second Israeli cloud seeding experiment - the effect of seeding on varying cloud populations". Second WMO Scientific Conference on Weather Modification, Boulder, Colorado, 2-6 Aug 1976. WMO. No. 443, 195-204.

Grant, L.O. and A.M. Kahan 1974: "Weather modification for augmenting orographic precipitation". Weather and Climate Modification (W.N. Hess Ed.) New York, Wiley p. 282-317.

Kunkel, B.A. and B.A. Silverman, 1970: A comparison of the warm fog clearing capabilities of some hygroscopic materials, J.Appl.Meteor., 9, 634-638.

Langmuir, I., 1948: "The production of rain by a chain reaction in cumulus clouds at temperatures above freezing". J.Meteor. 5, 175-192.

Plank, V.G., 1971: The fog clearing capabilities of helicopters, Proc. Int. Conf. on Weather Modification, Canberra, Amer.Meteor.Soc. 245-250.

Rosenthal, S.L. 1971: A circularly symmetric primitive-equation model of tropical cyclones and its response to artificial enhancement of the convective heating functions, Monthly Weather Review, 99, 414-426.

Schaefer, V.J., 1946: "The production of ice crystals in a cloud of supercooled water droplets". Science, 104, 457-459.

Silver, B.A. and B.A. Kunkel, 1970: A numerical model of warm fog dissipation by hygroscopic particle seeding, J.Appl.Meteor 9, 627-635.

Simpson, J. and A.S Dennis, 1974: "Cumulus clouds and their modification". Weather and climate Modification (W.N. Hess Ed.) New York, Wiley, p. 229-281.

Simpson, J. and W.L. Woodley, 1975: "Florida area cumulus experiments 1970-1973 rainfall results". J.Appl.Meteor., 14, 734-744.

Smith, E.J., L.G. Veitch, D.E. Shaw and A.J. Miller, 1979: "A cloud seeding experiment in Tasmania". J.Appl.Meteor., 18, 804-815.

World Meteorological Organisation, 1975: Typhoon modification, Proceedings of the WMO Technical Conference, Manila, 15-18 October 1974, 142 pp.

World Meteorological Organisation 1977: "Areal extent of seeding effects in relation to the Precipitation Enhancement Project". P.E.P. Report No. 6, pp. 56.

World Meteorological Organisation, 1977: Report on the meeting of experts on the present status of hail suppression, Geneva, Switzerland, 12 pp.